Annual Report
Jahresbericht

2020

Walther–Meißner–Institut
für Tieftemperaturforschung

Bayerische Akademie der Wissenschaften

Contact:

Prof. Dr. Rudolf Gross
Walther–Meißner–Institut für Tieftemperaturforschung
Bayerische Akademie der Wissenschaften
and
Lehrstuhl für Technische Physik – E23
Technische Universität München

Address:

Walther–Meißner–Str. 8
D - 85748 Garching
GERMANY

Phone: +49 – (0)89 289 14249
Fax: +49 – (0)89 289 14206
e–mail: Rudolf.Gross@wmi.badw.de
www: http://www.wmi.badw.de

Secretary's Office and Administration:

Emel Dönertas

Phone: +49 – (0)89 289 14202
Fax: +49 – (0)89 289 14206
e–mail: Emel.Doenertas@wmi.badw.de
Sekretariat@wmi.badw.de

Andrea Person

Phone: +49 – (0)89 289 14205
Fax: +49 – (0)89 289 14206
e–mail: Andrea.Person@wmi.badw.de
Verwaltung@wmi.badw.de

Preface

Dear colleagues, friends, partners, and alumni of the Walther-Meißner-Institute (WMI),

due to the Covid-19 pandemic, the past year certainly was quite unusual with many unexpected turns of events. While writing this opening words, the dark clouds of the Corona virus pandemic are still there and counteract the inspiration we are drawing from science. Despite these adverse circumstances, for the WMI the year 2020 was one of the most successful within the past decade. Apart from our big success in research and pushing ahead strategic developments, the most important achievement was the fact that we did not have to suffer from any Covid-19 infections at WMI. Therefore, our ***Annual Report 2020*** can provide you a very positive look back on our last year's activities. As every year, it also contains relevant statistical data, an overview of our teaching and public engagement activities, and information on recent developments in infrastructure and experimental facilities.

The best piece of good news is the start of our new scientific director, Prof. Stefan Filipp, who joined WMI in June 2020 from the IBM Research Laboratory in Zurich. At the same time, he was appointed professor for Technical Physics at TUM (see page 11-12). We are very happy to have one of the world-leading experts on quantum computing on board. With his arrival, also the new governance structure of WMI with a managing board of up to three scientific directors headed by a managing director has been successfully implemented. We firmly believe that it will strengthen the position of WMI and become a future success story.

Due to the success of WMI in applying for third party funding, we could invest the record amount of more than 6 Mio. € in 2020 to improve the technological infrastructure of WMI and to set up new experimental facilities. Among other things, a fully automated UHV deposition system for qubit fabrication (see page 63-64), a cryogen-free dilution refrigerator with large cooling power, huge sample space and large number of microwave lines (see page 65-66), and two optical cryostats already have been taken into operation. Two further dilution fridges for experiments on quantum systems, a UHV MBE/PLD system for the fabrication of quantum materials and a new helium liquefaction system already have been ordered und will be delivered in 2021. It goes without saying that the additional work load was tremendous. I would like to thank all the team members who contributed to writing the successful proposals, carrying out the European-wide tenders, clarifying all the technical details in the purchasing process, and preparing the technical infrastructure for the installation of the new equipment. This great success would not have been possible without your strong commitment and persistence.

The year 2020 also was very successful regarding the continuation of the ongoing long-term projects and the acquisition of new research projects. After starting in January 2019, the Cluster of Excellence **«Munich Center for Quantum Science and Technology» (MCQST)** rapidly has developed into a success story. For example, a joint TUM/LMU Master's Course in Quantum Science & Technology has been started in record time. Moreover, the spokespersons of MCQST have been the key drivers in writing a strategy paper with the aim to initiate the Munich Quantum Valley. Meanwhile, the Munich Quantum Valley has been formally implemented by signing a Memorandum of Understanding and our State Government has announced a 300 Mio. € support for the next five years (see page 21-27). The start of the Munich Quantum Valley will certainly be very fruitful for the WMI research activities in quantum science & technology. In the EU Quantum Flagship project **«Quantum Microwave Communication and Sensing» (QMiCS)**, which is coordinated by WMI, a 6.6 meter long quantum local area network (QLAN) cable connecting two dilution refrigerators at millikelvin temperatures has been set up during the past year despite the Covid-19 related restrictions. (see page 28-28). Furthermore, three new EU projects have been started in 2020 and two new BMBF projects

with a total funding volume above 6 Mio. € already have been granted and will start in February 2021 (see page 21-27). We have been particularly pleased to welcome State Minister Bernd Sibler at WMI in July 2020 and to be able to directly inform him on our ambitious research efforts in quantum science & technology (see page 13-14). In this context it is important to note that the persistent support of the Bavarian Ministry for Science and Arts and, of course, the generous financial support from the German Research Foundation, the BMBF, the EU and other funding agencies is the key to our success.

Despite the unfavorable circumstances due to the Covid-19 pandemic, our research activities could be successfully continued and resulted in a number of high level publications (see page 89). The high impact of our research work is documented by more than 2 300 citations of WMI publications in 2020 (ISI Web of Science). I would like to thank the scientific, technical and administrative staff of WMI for its outstanding performance! As in previous years, WMI also was active in organizing symposia, workshops and conferences to increase its international visibility (see page 103). Unfortunately, some have to be cancelled or could be held only as virtual online events.

An important ingredient for our success is the training of students. In 2020, 6 bachelor, 7 master and 3 Ph.D. students completed their theses at WMI, while 14 master and 21 Ph.D. students as well as 2 habilitation candidates are still ongoing (see page 93). Even more important is the recruitment of outstanding, scientifically independent group leaders with complementary research interests and technical expertise. WMI has a long tradition in fostering young talents, an effort that is strongly supported by its Scientific Advisory Board. Although we are always a little bit sad about loosing excellent junior researchers, we are also pleased to see that WMI provides a good platform for them to make the next career step. In this sense, we are particulary happy that Mathias Weiler, who worked since 2014 as a junior group leader at WMI, received a W3 professorship at TU Kaiserslautern and already started there in October 2020 (see page 113). Fortunately, a promising new postdoc, Nadezhda Kukharchyk, joined WMI from the Saarland University in November 2020 supported by a Junior Researcher START Fellowship of the Excellence Cluster MCQST. She sets up experiments aiming at the study of quantum memories based on rare-earth ions.

Attracting the best students and young scientists is only possible due to the extensive teaching efforts of the WMI scientists as well as the inspiring and collaborative atmosphere offered by WMI to young talents. In the same way as in previous years, the lectures and seminars offered by WMI have been attended by a large number of students and evaluated very positively. In 2020, WMI could even get a prestigious teaching award (Goldene Kreide) of the Physics Department (see 114).

Finally, I would like to thank all colleagues, guests, students, postdocs and cooperating partners, who contributed to our progress within the past year, and last but not least all our friends and sponsors for their interest, trust and continuous support. I hope that our Annual Report 2020 inspires your interest in WMI.

Garching, December 2020

Rudolf Gross

© Walther-Meißner-Institute

Contents

© Walther-Meißner-Institute

The Walther–Meißner–Institute

General Information

The ***Walther-Meißner-Institute for Low Temperature Research (WMI)*** was originally operated by the Commission for Low Temperature Research of the ***Bavarian Academy of Sciences and Humanities (BAdW)***. Between 2013 and 2015, the Bavarian Academy of Sciences and Humanities with its more than 300 employees was reorganized. With the passing of the new statutes in October 2015, the 36 Commissions (Research Groups) of the Academy — they were originally set up in order to carry out long-term projects, which are too ambitious for the lifetime or capacity of any single researcher, or which require the collaboration of specialists in various disciplines — were abolished. The research program of BAdW is now implemented in Academy Institutes (such as the Walther-Meißner-Institute, the Leibniz Supercomputing Center or the Bavarian Research Institute for Digital Transformation) and Academy Projects. The Academy Institutes and Projects are managed by the Institute and Project Committees and supervised by the Institute and Project Advisory Boards, respectively. In this way a clear separation between the managing bodies of the institutes/projects (responsible for the implementation of the research programs) and the corresponding supervisory bodies (responsible for the quality control) was established. To this end, also the Commission for Low Temperature Research was dissolved and replaced by the WMI Committee and the WMI Advisory Board in 2015.

The historical roots of WMI go back to ***Walther Meißner***. He founded the Commission for Low Temperature Research in 1946 when he was president of BAdW (1946 – 1950). The first research activities then were started in 1946 in the Herrsching barracks. After the retirement of Walther Meißner in 1952, Heinz Maier-Leibnitz, who followed Walther Meißner on the Chair for Technical Physics of the Technical University of Munich (TUM), became the new head of the Commission for Low Temperature Research. In 1967, the commission moved to the Garching research campus after the construction of the new «*Zentralinstitut für Tieftemperaturforschung*» (ZTTF) was completed (director: Prof. Heinz Maier-Leibnitz, technical director: Prof. Franz Xaver Eder). Until 1972, the theory group of the Institute Laue Langevin was hosted at the ZTTF with prominent members such as Peter Fulde. In 1980, Prof. Dr. Klaus Andres became the new director of the ZTTF again associated with the Chair for Technical Physics (E23) at TUM. In 1982, the ZTTF was renamed into Walther-Meißner-Institute for Low Temperature Research (WMI) on the occasion of the 100. anniversary of Walther Meißner's birth.

In 2000, Prof. Dr. Rudolf Gross followed Klaus Andreas on the Chair for Technical Physics (E23) at TUM and as the new director of WMI. He significantly reoriented and extended the scientific focus of WMI by starting new activities in the field of quantum science and technology, as well in magnetism, spin dynamics and spin electronics. Even more importantly, he newly established the materials technology for superconducting and magnetic materials (both in form of thin films and single crystals) and a clean room facility, allowing for the fabrication

of solid-state nanostructures. These measures had been very successful and allowed WMI to play a leading role in several coordinated research projects in the field of quantum science and technology (e.g. Collaborative Research Center 631 on Solid-State Quantum Information Processing (2003-2015), Cluster of Excellence Munich Center for Quantum Science and Technology (since 2019)) as well as in nanosciences (e.g. Cluster of Excellence Nanosystems Initiative Munich (2006-2019)). To accommodate the new activities, starting from 2000 the so far unused basement of the WMI building was made available for technical infrastructure (airconditioning, particulate airfilters, pure water system etc. for clean room) and additional laboratory space. Fortunately, in 2008 WMI succeeded in getting extra money from the state government within the so-called *«Konjunkturpaket II»* to establish the new *«WMI Quantum Science Laboratory»* in the basement of the building, providing about 150 m^2 additional laboratory space particularly suited for low temperature facilities and ultra-sensitive studies on solid state quantum systems. The WMI Quantum Science Laboratory was fully operational early in 2011 and meanwhile hosts several mK systems and sophisticated experimental techniques for the study of solid state based quantum systems and circuits. In 2016, the Bavarian Ministry for Science and Arts granted more than 6 Mio. Euro for redevelopment measures regarding the technical infrastructure, safety requirements and energy efficiency. An important part of the building project implemented in 2017/18 was the reconstruction of the entrance area and the main staircase, providing now direct access to the new WMI Quantum Laboratories in the basement of the WMI building as well as additional communication areas and meeting rooms in the ground floor. Moreover, it included the replacement of all windows and doors, the upgrade of the technical infrastructure for cooling water, air conditioning, liquid nitrogen and helium storage, as well as the complete redevelopment of the mechanical workshop and various safety measures.

With the availability of additional laboratory space and the success of the WMI in Germany's Excellence Initiative (2006-2018), Excellence Strategy (starting from 2019), and other third-party funded research projects, the research activities, the number of staff and obviously the related administrative tasks at WMI were strongly growing. Therefore, Rudolf Gross proposed in 2017 to start the appointment procedure for his successor at an early stage to guarantee sufficient temporal overlap. Moreover, due to the strong increase of staff, research projects and administrative tasks he proposed to change the governance structure of WMI from a single director to a board of up to three directors headed by a managing director. This change of governance structure has been supported by the Scientific Advisory Board of WMI and the decision-making bodies of BAdW. Meanwhile, it is implemented in the new rules of order of WMI valid since 18th October 2019. Already in June 2020, Prof. Dr. Stefan Filipp started as the second scientific director of WMI with strong focus on superconducting quantum computing.

As already mentioned, it is a long tradition that WMI hosts the Chair for Technical Physics (E 23) of TUM with the director of the WMI being a full professor at the Faculty of Physics of TUM. However, in general WMI has established tight links to research groups of both Munich universities, joining technological and human resources in the fields of experimental and theoretical solid-state and condensed matter physics, low temperature techniques, materials science as well as thin film and nanotechnology. Noteworthy, the WMI supplies liquid helium to more than 25 research groups at both Munich universities and provides the technological basis for low temperature research.

Important Discoveries

The WMI looks back on a long history of successful research in low temperature physics. In the following we list some important discoveries as well as experimental and technical developments made at WMI:

© Walther-Meißner-Institute

- **1961: discovery of flux quantization in multiply connected superconductors**

  (R. Doll, M. Näbauer, *Experimental Proof of Magnetic Flux Quantization in a Superconducting Ring*, Phys. Rev. Lett. **7**, 51-52 (1961)).
- **1986: discovery of an anomalous temperature dependence of the penetration depth in UBe_{13}**

  (F. Gross, B.S. Chandrasekhar, D. Einzel, K. Andres, P.J. Hirschfeld, H.R. Ott, J. Beuers, Z. Fisk, J.L. Smith, *Anomalous Temperature Dependence of the Magnetic Field Penetration Depth in Superconducting UBe_{13}*, Z. Physik B - Condensed Matter **64**, 175-188 (1986)).
- **1992: discovery the intrinsic Josephson effect**

  (R. Kleiner, F. Steinmeyer, G. Kunkel, and P. Müller, *Intrinsic Josephson Effects in $Bi_2Sr_2CaCu_2O_8$ Single Crystals*, Phys. Rev. Lett. **68**, 2394-2397 (1992)).
- **2002: development of dilution refrigerators with pulse tube refrigerator precooling**

  (K. Uhlig, *$^3He/^4He$ Dilution Refrigerator with Pulse Tube Precooling*, Cryogenics **42**, 73-77 (2002)).
- **2010: first demonstration of ultrastrong light-matter interaction**

  (T. Niemczyk, F. Deppe, H. Huebl, E. P. Menzel, F. Hocke, M. J. Schwarz, J. J. Garcia-Ripoll, D. Zueco, T. Hümmer, E. Solano, A. Marx, R. Gross, *Circuit Quantum Electrodynamics in the Ultrastrong-Coupling Regime*, Nature Physics **6**, 772-776 (2010)).
- **2010: development of dual path method for state tomography of propagating quantum microwaves**

  (E.P. Menzel, M. Mariantoni, F. Deppe, M.A. Araque Caballero, A. Baust, T. Niemczyk, E. Hoffmann, A. Marx, E. Solano, R. Gross, *Dual-Path State Reconstruction Scheme for Propagating Quantum Microwaves and Detector Noise Tomography* , Phys. Rev. Lett. **105**, 100401 (2010)).
- **2012: first realization of path entanglement of propagating quantum microwaves**

  (E. P. Menzel, R. Di Candia, F. Deppe, P. Eder, L. Zhong, M. Ihmig, M. Haeberlein, A. Baust, E. Hoffmann, D. Ballester, K. Inomata, T. Yamamoto, Y. Nakamura, E. Solano, A. Marx, R. Gross, *Path Entanglement of Continuous-Variable Quantum Microwaves*, Phys. Rev. Lett. **109**, 250502 (2012)).
- **2013: discovery of the spin Hall magnetoresistance** (jointly with partners at Tohoku University and TU Delft)

  (H. Nakayama, M. Althammer, Y.-T. Chen, K. Uchida, Y. Kajiwara, D. Kikuchi, T. Ohtani, S. Geprägs, M. Opel, S. Takahashi, R. Gross, G. E. W. Bauer, S. T. B. Goennenwein, E. Saitoh, *Spin Hall Magnetoresistance Induced by a Non-Equilibrium Proximity Effect*, Phys. Rev. Lett. **110**, 206601 (2013)).
- **2013: first demonstration of strong magnon-photon coupling**

  (H. Huebl, Ch. Zollitsch, J. Lotze, F. Hocke, M. Greifenstein, A. Marx, R. Gross, S.T.B. Goennenwein, *High Cooperativity in Coupled Microwave Resonator Ferrimagnetic Insulator Hybrids*, Phys. Rev. Lett. **111**, 127003 (2013)).
- **2017: first experimental observation of the spin Nernst effect**

  (S. Meyer, Yan-Ting Chen, S. Wimmer, M. Althammer, S. Geprägs, H. Huebl, D. Ködderitzsch, H. Ebert, G.E.W. Bauer, R. Gross, S.T.B. Goennenwein, *Observation of the spin Nernst effect*, Nature Materials **16**, 977-981 (2017)).
- **2019: first demonstration of remote state preparation in the microwave regime**

  (S. Pogorzalek, K. G. Fedorov, M. Xu, A. Parra-Rodriguez, M. Sanz, M. Fischer, E. Xie, K. Inomata, Y. Nakamura, E. Solano, A. Marx, F. Deppe, R. Gross, *Secure Quantum Remote State Preparation of Squeezed Microwave States*, Nature Communications **10**, 2604 (2019)).

Present Research Activities

The research activities of the Walther-Meißner-Institute are focused on low temperature condensed matter and quantum physics (see reports below). The research program is devoted to both **fundamental** and **applied research** and also addresses **materials science, thin film and**

nanotechnology aspects. With respect to **basic research** the main focus of the WMI is on

- quantum phenomena and quantum coherence in solid state systems,
- superconductivity and superfluidity,
- magnetism, including spin transport, spin dynamics, spin mechanics and spin caloritronics,
- circuit quantum electrodynamics and circuit electro-nanomechanics,
- ordering and emergent phenomena in correlated quantum matter,
- and the general properties of metallic systems at low and very low temperatures.

The WMI also conducts **applied research** in the fields of

- superconducting quantum circuits for quantum computing,
- solid-state quantum information processing and quantum communication systems,
- superconducting and spin-based devices,
- multi-functional and multiferroic materials,
- and the development of low and ultra-low temperature systems and techniques.

With respect to **materials science, thin film and nanotechnology** the research program is focused on

- the synthesis of superconducting and magnetic materials,
- the single crystal growth of oxide materials,
- the thin film technology of complex superconducting and magnetic heterostructures, including multi-functional and multi-ferroic material systems,
- and the fabrication of superconducting, magnetic and hybrid nanostructures.

The WMI also develops and operates systems and techniques for low and ultra–low temperature experiments. A successful development have been dry mK-systems that can be operated without liquid helium by using a pulse-tube refrigerator for precooling. In the early 2000s, these systems have been successfully commercialized by the company VeriCold Technologies GmbH at Ismaning, Germany, which was taken over by Oxford Instruments in 2007. Currently, in a collaboration with Oxford Instruments such dry dilution refrigerators are used to establish a so-called cryolink, allowing for quantum communication in the microwave regime between two superconducting quantum processors over an about 10 m distance. WMI also operates a helium liquifier with an annual capacity of above 180.000 liters and supplies both Munich universities with liquid helium. To optimize the transfer of liquid helium into transport containers, WMI has developed a pumping system for liquid helium which has been commercialized in collaboration with a company.

To a large extent the research activities of WMI are integrated into national and international research projects such as Clusters of Excellence, Collaborative Research Centers, Research Units, or BMBF and EU projects. The individual research groups of WMI offer a wide range of attractive research opportunities for bachelor and master students, Ph.D. students and postdoctoral fellows.

Experimental Facilities and Resources

The WMI is equipped with state of the art facilities for the preparation and characterization of superconducting and magnetic materials as well as for various low and ultra–low temperature experiments. The main experimental and technological resources of WMI are listed in the following.

© Walther-Meißner-Institute

Materials Preparation and Fabrication of Nanostructures

- Laser Molecular Beam Epitaxy (L-MBE) system for oxide heterostructures (equipped with in–situ RHEED, Omicron AFM/STM system, atomic oxygen/nitrogen source, infrared-laser heating system, metallization). The L-MBE systems is connected to a UHV magnetron sputtering systems for metals (e.g. Nb, Al, NiPd, ...) and an electron beam deposition system via a UHV transfer chamber
- Plassys MEB550 S4-I UHV electron beam evaporation and sputtering system for qubit fabrication
- molecular beam epitaxy (MBE) system for metals
- UHV cluster tool (Bestec GmbH) consisting of two magnetron sputter deposition systems for superconducting and magnetic heterostructures, respectively, and a load lock
- UHV magnetron sputtering system (Mantis Deposition GmbH) for large-area deposition of superconducting thin films and heterostructures
- Oxford Instruments Plasmalab 80 Plus reactive ion etching (RIE) system with ICP plasma source
- ion beam etching (IBE) system equipped with a LN_2 cooled sample holder
- automated critical point dryer Leica EM CPD 300
- polishing machine for substrate preparation
- ultrasonic bonding machine
- 50 m^2 class 1000 clean room facility
- maskless lithography UV Direct Laser Writer, PicoMaster 200 UV of the company 4PICO, The Netherlands
- 100 kV nB5 Electron Beam Lithography System by NanoBeam Limited, UK, with 6 inch laser stage
- optical lithography (Süss maskaligner MJB 3 and projection lithography)
- four-mirror image furnace for crystal growth

Characterization

- 2–circle x–ray diffractometer (Bruker D8 Advance, sample temperature up to 1 600°C)
- high resolution 4–circle x–ray diffractometer with Göbel mirror and Ge monochromator (Bruker D8 Discover)
- Philips XL 30 SFEG scanning electron microscope with EDX analysis
- UHV room temperature AFM/STM system
- two Raman spectroscopy systems (1.5 to 300 K, in-situ sample preparation)
- tip-enhanced Raman spectroscopy (TERS) system
- SQUID magnetometer (Quantum Design, 1.5 to 700 K, up to 7 T)
- several high field magnet systems (up to 17 T Tesla) with variable temperature inserts
- 7 T split coil magnet systems with optical access and variable temperature insert
- 3D vector magnet (2/2/6 Tesla) with variable temperature inserts
- experimental set–ups for the measurement of noise including low noise SQUID amplifiers and signal analyzers
- high-frequency network analyzers (up to 40 GHz) and various microwave components (sources, mixers, circulators, attenuators) for the determination of high frequency parameters
- ultra-sensitive microwave receiver for state tomography of quantum microwaves (dual path method with FPGA signal processing)
- high-frequency cryogenic probing station (up to 20 GHz, $T > 4$ K)
- magnetooptical Kerr effect (MOKE) system
- broadband ferromagnetic resonance (FMR) system

Low temperature systems and techniques

- several ^{3}He/^{4}He dilution refrigerator inserts for temperatures down to 10 mK
- WMI cryogen-free mK-cooler based on a dilution refrigerator with pulse-tube precooling and equipped with a large number of microwave lines and cold electronics (e.g. amplifiers, circulators, attenuators, directional couplers) for ultra-sensitive experiments on solid state quantum systems
- Oxfod Instruments cryogen-free dilution refrigerator (model VDR 400-10) with a base temperature of about 10 mK equipped with a 3D vector magnet (1/1/6 Tesla)
- Oxfod Instruments cryogen-free dilution refrigerator (model TRITON-15-300) with a base temperature of about 10 mK equipped with a standard bucket tailset
- Oxford Instruments cryogenic link with supporting structure and superconducting microwave link
- Bluefors cryogen-free dilution refrigerator system (model BF-XLD 1000) with a base temperature below 10 mK and, in particular, with large cooling power (about 1 mW at 100 mK) and sample space
- "wet" dilution refrigerators based on liquid helium precooling and equipped with a large number of microwave lines and cold electronics (e.g. amplifiers, circulators, attenuators, beam splitters) for time-domain microwave experiments on solid state quantum systems
- experimental set–ups for the measurement of specific heat, magnetization, thermal expansion as well as electrical and thermal transport properties as a function of temperature, magnetic field and pressure

© Walther-Meißner-Institute

Stefan Filipp Joins WMI as a New Scientific Director

Rudolf Gross

The Walther-Weißner-Institute cordially welcomes Prof. Dr. Stefan Filipp as a new scientific director.

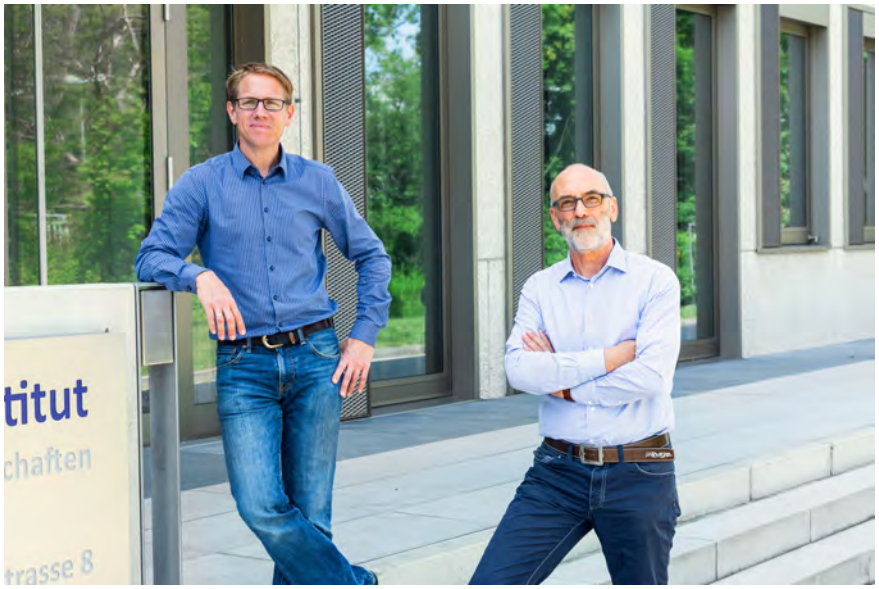

Figure 1: Rudolf Gross (left) and Stefan Filipp (right) in front of the WMI building (photo: Kai Neunert).

Prof. Stefan Filipp has been appointed professor for Technical Physics at the Physics Department of the Technical University of Munich and became a new scientific director at the Walther-Meißner-Institute. He started in June 2020 and joins forces with Rudolf Gross and his team to make WMI an international top player in quantum science and technology. He also became a Core Principal Investigator in the Munich Center for Quantum Science and Technology (MCQST). With the arrival of Stefan Filipp the new governance structure of WMI with a managing board of up to three scientific directors headed by a managing director has been implemented.

Stefan Filipp is one of the key players in the field of quantum computing and will allow Germany to take a leap ahead. He is interested in quantum phenomena since long. Already during his physics studies he was fascinated about quantum phenomena and inspired by the experiments of his Austrian fellow countryman Anton Zeilinger. However, already at a very early stage he was not only concerned about understanding and explaining quantum physics but rather captivated by the idea of making use of quantum phenomena. In applications such as quantum computers he sees a huge potential allowing us to achieve something really new and provide mankind new tools for solving urgent problems.

At the beginning of his career, Stefan Filipp was strongly interested in theoretical physics. In 2002, he completed his Master's degree at Uppsala University in Sweden as part of an Erasmus program, where he studied the so-called geometric quantum phases. After coming back to Vienna, he also received a degree in engineering (Dipl.-Ing. in Technischer Physik) from the Vienna University of Technology in 2003. For his Ph.D. he joined the group of Prof. Helmut Rauch at the Atomic Institute. Although he planned to continue in theoretical physics it became immediately evident that it was hardly possible to deal solely with theory at an experimental institute. Therefore, suddenly a neutron interferometer became part of Stefan Filipp's daily life and he realized beautiful experiments on new aspects of the quantum geometric phase based on neutron interferometry. In 2006, he submitted his doctoral thesis to the Vienna University of Technology. It was awarded the Victor Hess prize from the Austrian Physics Society (Österreichische Physikalische Gesellschaft). From 2006 to 2008, he continued to perform experiments on geometric phases using ultra-cold neutrons at the Atomic Institute.

In the next career step he switched from neutrons to photons, being convinced that quantum optics is the better approach to realize practical quantum information processing systems. His search for more promising and seminal research objects led him to Andreas Wallraff's group at the ETH Zurich, where he worked as a postdoc between 2008 and 2014. This was the time when the first experiments in circuit quantum electrodynamics were done, where individual quantum bits, realized by superconducting circuits, and single microwave photons are strongly coupled. Andreas Wallraff started these experiments as a postdoc in Robert Schoelkopf's group at Yale, one of the pioneers in superconducting quantum circuits besides John Martinis at Santa Barbara, Yasunobo Nakamura at NEC, and Hans Mooij at TU Delft. In this early stage of superconducting quantum technology, there were only about ten groups worldwide that worked in the area – one also at Walther-Meißner-Institute. Now, with the hype on quantum computing, there are quite a few more, and industry has jumped on the train as well in the meantime.

Figure 2: The scientific directors of WMI are joining forces to push quantum mechanics towards applications (photo: Jan Greune/MCQST.

IBM was one of the first industrial players recognizing the potential of quantum technology. Therefore, IBM was setting up a group with Mattias Steffen and Jerry Chow, who came from the Schoelkopf and Martinis groups, to build functioning quantum computers. In 2014, Stefan Filipp moved to the IBM T.J. Watson Research Center in New York, USA, to join the IBM effort in quantum computing based on superconducting circuits. Later on, in 2015, he came back to Europe to the IBM Research Laboratory in Zurich. There he handled the technical management of the team fabricating and characterizing superconducting quantum circuits.

We are very happy that we could convince Stefan Filipp to join WMI as a new scientific director. As one of the world-leading experts in superconducting quantum computing he will not only strengthen our activities on superconducting quantum circuits but also will allow WMI to play an important role in the development of superconducting quantum computers. Without any doubt, he also will become an important player in our excellence clusters MCQST.

Dear Stefan, a very warm welcome to WMI. We are looking forward to join forces to make quantum technology a big success!

State Minister Bernd Sibler Visits WMI

Rudolf Gross, Stefan Filipp

The scientific directors of WMI, Rudolf Gross and Stefan Filipp, welcomed Bavarian State Minister of Science and Arts, Bernd Sibler, on the Garching research campus on 23rd July 2020. They provided him an overview of the current and future research priorities of the institute and its role in the field of quantum technologies. In particular, they informed him on the cutting-edge research of WMI on quantum devices and circuits required for the realization of quantum computers.

Figure 1: Rudolf Gross (left) shows a quantum chip to State Minister Sibler (right) in one of the WMI thin film labs (photo: Stefan Obermeier).

Figure 2: State Minister Sibler (left) and WMI director Rudolf Gross (right) in front of a real "Bavarian Quantum Machine" (photo: Stefan Obermeier). .

Quantum computers based on superconducting circuits are operated at low temperatures, a research field in which WMI is performing pioneering work since decades. WMI develops novel methods for the generation of temperatures close to absolute zero, advanced thin film technology for superconducting and magnetic materials, and recipes for the realization of superconducting and magnetic nanodevices. During a lab tour, Rudolf Gross and Stefan Filipp informed State Minister Sibler on the current research efforts in the design, fabrication, and characterization of superconducting quantum circuits. All these efforts strengthen the role of the WMI in the worldwide strongly growing research field of quantum science and technology, particularly in the field of quantum computing.

«The Walther-Meißner-Institute is one of the internationally visible lighthouses in the Bavarian research landscape», State Minister Sibler pointed out during his visit. «I am very pleased that progress and innovation in the field of quantum science and technology are strategically planned and implemented at WMI since almost two decades. The state-of-the-art basic research but also the development of core technologies at WMI are path-breaking and will be the basis for future efforts in building useful quantum computers», he added.

Figure 3: From left to right: Stefan Filipp, Rudolf Gross and Bernd Sibler in front of the new low temperature machine funded by MCQST (photo: Stefan Obermeier). .

Figure 4: From left to right: Bernd Sibler, Stefan Filipp and Birgit Schmid debate on cool quantum technology at a hot summer day (photo: Stefan Obermeier). .

«The continuous support by the State Ministry of Science and Arts together with the long-term research strategy of WMI is the key to our success», the two directors of WMI let Minister Sibler know. «As one of the spokespersons of MCQST, I am particularly happy that we can show the new extra-large low temperature machine, which has been partly funded by MCQST and will host a future Bavarian quantum computer», Rudolf Gross pointed out. Stefan Filipp confirmed that «this new machine will boost the WMI activities and will allow WMI to take a leading position within Europe».

Building and Reconstruction Measures

Infrastructure and Reconstruction Measures

Rudolf Gross, Achim Marx

The reconstruction measures and building activities for accommodating new equipment and technical infrastructure are continuously ongoing. Although this is perturbing, these measures are unavoidable and demonstrate that WMI is attracting considerable funding for new equipment and research projects. Also in 2020, several laboratories and office space had to be renovated and reorganized to adapt them to the needs of the new scientific director Stefan Filipp and his group.

Figure 1: Gas handling cabinet of the Bluefors XLD 1000 system (left) and heat exchangers for the cooling system of the two compressors (right) located in a technical room in the basement of WMI.

Moreover, two large pieces of equipment partly financed by the Cluster of Excellence MCQST – a UHV thin film deposition systems of the company Plassys (see report on page 63) and a cryogen-free dilution refrigerator with high cooling power and large sample space of the company Bluefors (see report on page 65) – were delivered and installed in 2020.

The installation of the UHV system and dilution refrigerator required a major adjustment of the technical infrastructure. For the UHV thin film deposition system, this included the installation of the cabinet and connection lines for pure gases, as well as the placement of the roughing pumps in the basement underneath the thin film laboratory. For the dry dilution refrigerator, which is operated with two 8 kW compressors for the two pulse tube cryocoolers, the cooling water and electrical supply had to be upgraded. The compressors together with the gas handling cabinet of the dilution refrigerator have been placed in the basement underneath the respective laboratory room.

Supported by the Cluster of Excellence

MCQST, WMI also could purchase two low temperature systems for optical experiments. These systems also have been installed and taken into operation in 2020. They will considerably extend the experimental techniques of WMI. They will be partly used also by our partners within MCQST.

Experiments with superconducting qubits are quite sensitive to stray magnetic fields. Although stray fields can be shielded, this is increasingly demanding with the rapidly growing complexity of superconducting quantum circuits. Therefore, it is optimum to disentangle laboratories for qubit experiments from those employing high magnetic fields. To this end, in 2020 we started to move several high magnetic field systems to new laboratories. This is accompanied with a renovation of the respective laboratories and an upgrade of the high magnetic field setups.

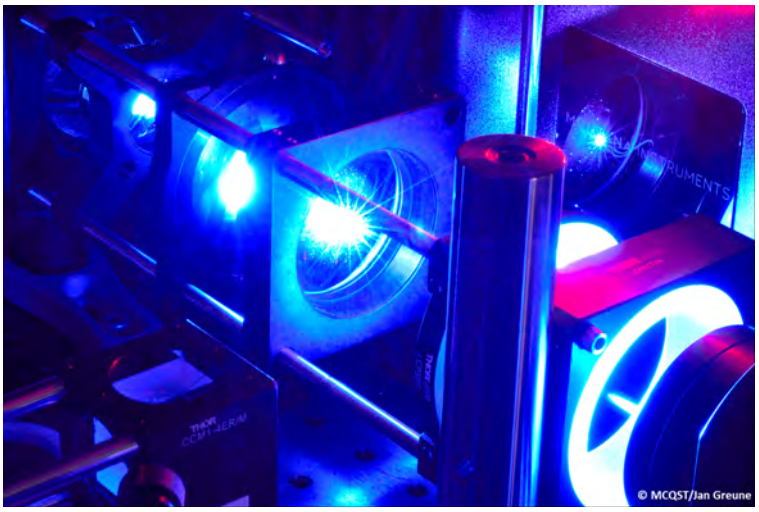

Figure 2: Optical part of the Montana Instruments optical cryostat.

In 2020 we also could receive funding for a new helium liquefier, which meanwhile already has been ordered. Therefore, the next major rebuilding activity is already at the horizon. It will be related to the installation of the coldbox of the liquefier in the main building and the compressor in the annexe building. This will go along with major reconstruction measures of the associated technical infrastructure and building parts. The installation of the new helium liquifier together with the helium gas recovery system will guarantee the save and cost efficient and supply of liquid helium to about 30 research groups at TUM, LMU and MPG for the next two decades.

Joint Research Projects

Research Activities in Quantum Science and Technology

Rudolf Gross

The Walther-Meißner-Institute (WMI) plays a key role in several coordinated research programs, centers, graduate schools and initiatives in the field of Quantum Science and Technology (QST) already since about two decades. Starting with the Collaborative Research Center 631 on «Solid-state Based Quantum Information Processing» (2003 – 2015), our effort in QST have been continued within the Cluster of Excellence «Nanosystems Initiative Munich» (2006 – 2019). In these research programs, WMI was providing the spokesperson and the coordinator of the quantum-related research area over the full funding period. Moreover, WMI was participating in several EU projects such as «Circuit and Cavity Quantum Electrodynamics» (CCQED) or «Quantum Propagating Microwaves in Strongly Coupled Environments» (PROMISCE).

At present, WMI is involved in the Cluster of Excellence

- **«Munich Center for Quantum Science and Technology» (MCQST)**,

where it provides one of the three spokespersons, and the EU projects

- **«Quantum Microwave Communication and Sensing» (QMiCS)**
- **«Neuromorphic Quantum Computing (Quromorphic)**
- **«Molecular Quantum Simulations (MoQS)**
- **«Quantum Science and Technologies at the European Campus (QUSTEC)**
- **«Magnetomechanical Platforms for Quantum Experiments and Quantum Enabled Sensing Technologies» (MaQSens)**.

The EU Quantum Technology Flagship Project QMiCS is coordinated by F. Deppe of WMI (see page 28–28). QMiCS sets up a quantum microwave local area network cable over a distance of several meters. This architecture is then used to implement quantum communication protocols such as teleportation between two superconducting quantum nodes. In the project MaQSens a radically new technology platform for experiments in macroscopic quantum physics and for quantum enabled sensing is developed.

Moreover, WMI is a founding institution of the graduate programs

- **Ph.D. School of Excellence «Exploring Quantum Matter» (ExQM)** and
- **International Max Planck Research School «Quantum Science and Technology» (IMPRS-QST)**

as well as of the

- **Munich Quantum Center (MQC)**.

The latter was founded in 2014 as a 'virtual center' and gets continuous financial support from both Munich universities since 2019 to promote QST activities in the Munich area. The

IMPRS-QST recently has been evaluated very positively and will be funded for a second six-year period until 2028.

In the following we briefly summarize some important developments within the already ongoing projects and provide basic information on currently planned research efforts in the field of quantum science and technology.

A. Munich Center for Quantum Science and Technology (MCQST)

The first seven-year funding period of the Cluster of Excellence *«Munich Center for Quantum Science and Technology» (MCQST)* started on 1st January 2019. The cluster joins groups from the Ludwig-Maximilians University Munich (LMU), the Technical University of Munich (TUM), the Max Planck Institute of Quantum Optics (MPQ), the Walther-Meißner-Institute (WMI) and the German Science Museum (DM). It is coordinated by the three spokespersons Immanuel Bloch (LMU Munich and MPQ), Ignacio Cirac (MPQ and TUM) and Rudolf Gross (TUM and BAdW). It combines more than 50 Principal Investigators and more than 300 scientists in the Munich research area working across the different disciplines of Quantum Science and Technology (QST), including Physics, Computer Science, Mathematics, Materials Science, Electrical Engineering and Chemistry. MCQST is structured in seven interconnected Research Units covering the entire range from fundamental science, through technology and material development to applications (see Fig. 1).

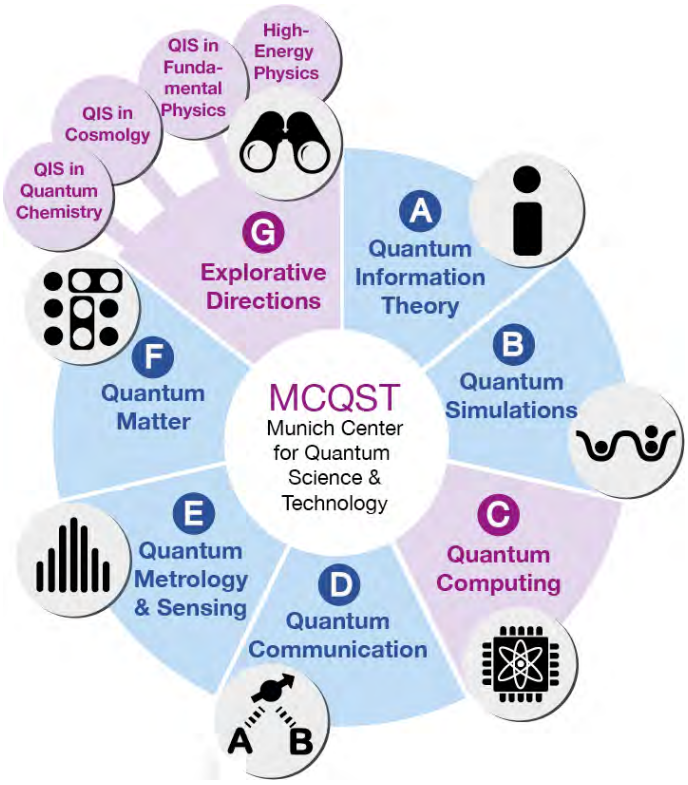

Figure 1: Schematic of the focus Research Units A-G of MCQST, connecting fundamental science and technological applications. Purple fields/circles indicate either topics to be strengthened (RU-C) or new, explorative fields of research (RU-G) that will significantly extend the reach of the MCQST and connect Quantum Information Science (QIS) to other fields of science.

MCQST had a very busy and successful start-up phase in the past two years. This included a lot of administrative work (e.g. finalizing the statutes and legal contracts among the participating institutions, ramping up the support programs and public outreach activities, etc.) but fortunately also a lot of successful research-related activities. A comprehensive overview of the MCQST scientific activities and programs including outreach and equal opportunity measures, press releases, etc. can be found on the MCQST web site **www.mcqst.de**. We note that

WMI actively contributes to the scientific output of MCQST. Already 14 MCQST-related publications of WMI are listed in the Web of Science. Several of the WMI publications have been highlighted in press releases, e.g. our articles in Physical Review Letters on *Multiple echoes as a result of a strong link between spins and microwave photons* and *Observation of the magnon Hanle effect in antiferromagnetic insulators*.

In the following we only address a few new developments and some aspects which are particularly relevant for WMI.

A.1. Start of the new Master's Program in Quantum Science & Technology

Figure 2: Curriculum of the new Master's Program «Quantum Science & Technology (QST)» jointly offered by TUM and LMU.

An important educational objective of MCQST was to establish an interdisciplinary **Master's Program «Quantum Science & Technology (QST)»** for top students from all over the world. Such a program is urgently required to make the new generation of scientists, engineers and entrepreneurs well trained for the QST revolution to come. Therefore, MCQST made a considerable effort to establish a joint QST Master's Program between the two Munich universities (TUM, LMU) as soon as possible. Despite the fact that two universities and several faculties have been involved, MCQST succeeded in getting the new Master's Program accepted in record time. The program started in the winter semester 2020/21 with more than 60 students, although there was very little time for advertisement. This is a great success. The QST Master's Program links students in physics, mathematics, chemistry, information science and engineering to the MCQST graduate program. It provides a broad education in QST, fosters interdisciplinary collaboration from an early stage and provides students skill sets in QST relevant for both academia and industry.

A.2. START Fellowship for Nadezhda Kukharchyk

To support young talents on their transition from postdocs to independent researchers, MCQST is offering **Junior Researcher START Fellowships**. With a total budget of 300.000 € for a funding period of two years, the fellows have the opportunity to start their own scientific projects in one of the Research Units of MCQST. The funds are flexible and may be spent for instrumentations, staff, consumables, traveling as well as for the fellows' own salary.

In 2020, one of the prestigious START Fellowships was granted the Dr. Nadezhda Kukharchyk. She joined WMI in November 2020 and is already setting up her experiments, aiming at the study of quantum memories based on rare-earth ions.

A.3. MCQST supports acquisition of large-scale equipment

In 2020, WMI could purchase a cryogen-free dilation refrigerator with large cooling power and sample space (see report on page 65) as well as a UHV deposition system for fully-automated fabrication of superconducting quantum circuits (see report on page 63). Although a significant part of the cost has to be covered by WMI, the acquisition of this high-tech equipment would not have been possible without the generous support of MCQST. Both systems considerably extend the capabilities of WMI in the fabrication and experimental study of circuits and components required for the realization of superconducting quantum computers. Thereby, they considerably strengthen the experimental facilities of the MCQST Research Unit C on Quantum Computing. They are also of key importance for new BMBF projects starting in 2021 (see below).

B. The Munich Quantum Valley Initiative

In August 2020, the spokespersons of MCQST – **Immanuel Bloch**, **Ignacio Cirac** and **Rudolf Gross** – started an initiative to establish the Munich Quantum Valley. In a strategy paper, written with support of Max-Planck Vice President **Klaus Blaum** and FhG Research Director **Raoul Klingner**, they point out that the larger Munich area with its excellent research institutions as well as its active industrial, high-tech and venture capital environment is ideally suited to establish a unique European center for quantum science and technology. By such a center Bavaria can be placed at the very forefront of a research field with high scientific and future economic relevance. On the basis of the Munich Quantum Valley, other Bavarian sites can be integrated into an efficient network, making the Munich Quantum Valley an important nucleus and pillar of a national and European quantum strategy.

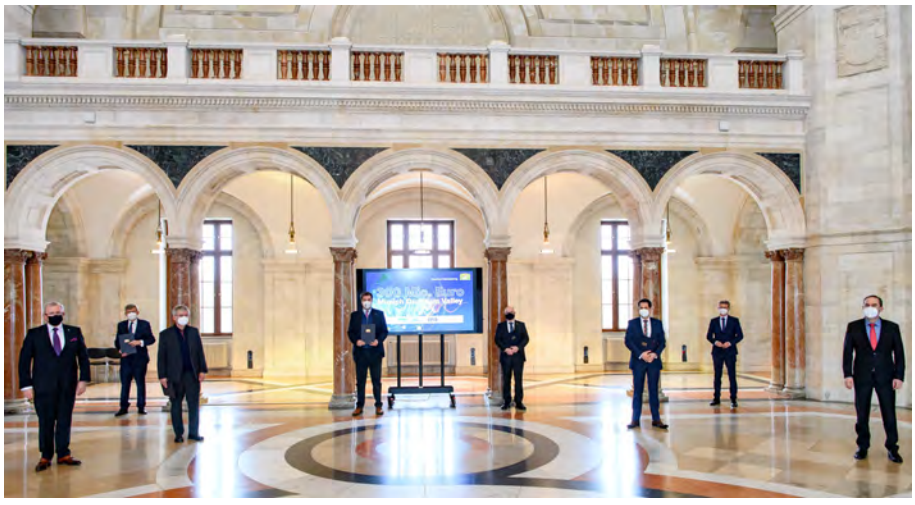

Figure 3: Green light for the Munich Quantum Valley: Reimund Neugebauer, Bernd Huber, Thomas O. Höllmann, Markus Söder, Martin Stratmann, Thomas F. Hofmann, Bernd Sibler und Hubert Aiwanger (from left to right) after signing the Memorandum of Understanding to support the Munich Quantum Valley.

The Munich Quantum Valley Initiative is supported by an alliance of the non-university research institutions Max-Planck Society, Fraunhofer Society for the Advancement of Applied Research and Bavarian Academy of Sciences and Humanities, together with Germany's leading universities, the Technical University of Munich (TUM) and the Ludwig Maximilian University of Munich (LMU). The relevance and usefulness of the Munich Quantum Valley for positioning Bavaria within the national and European research agenda

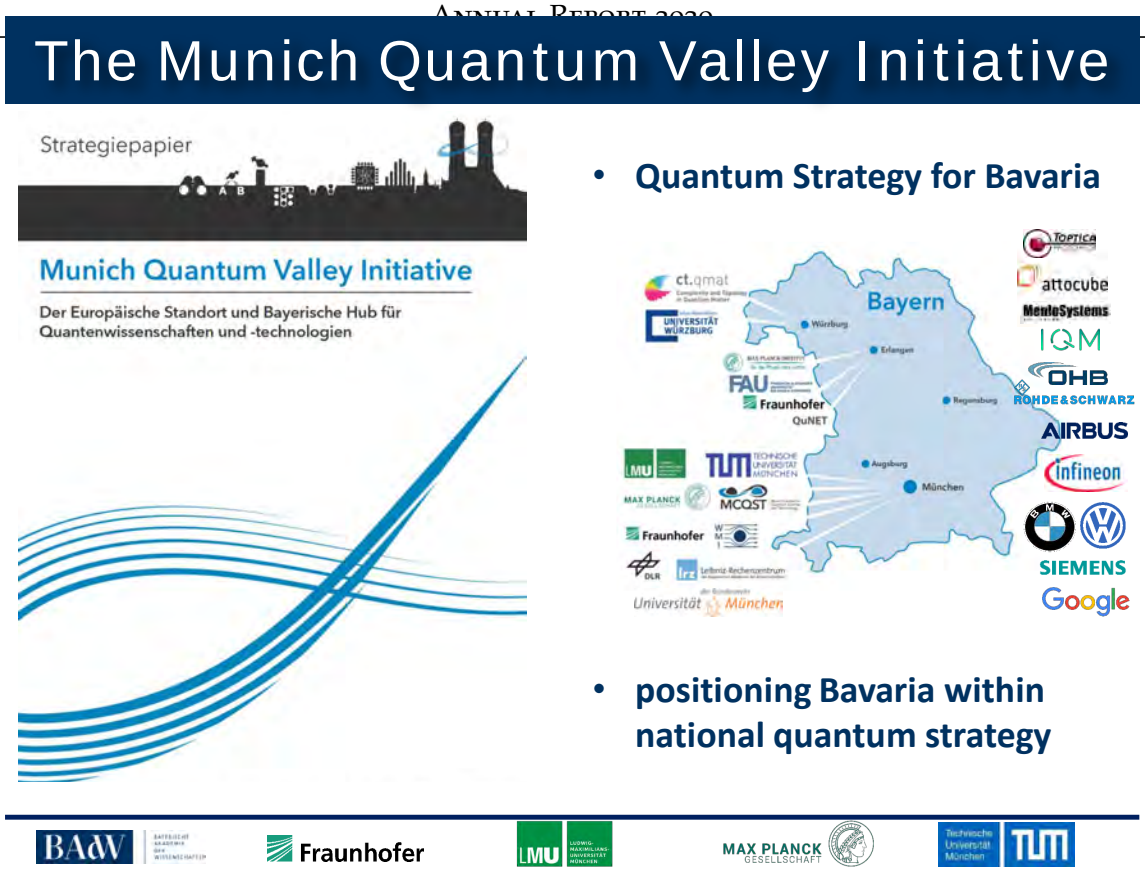

Figure 4: Left: title page of the strategy paper «Munich Quantum Valley Initiative». Right: possible networking partners from industry and academia within Bavaria.

in QST was recognized by the Bavarian state government. Financial support of quantum science and technology was immediately included into the Bavarian **«Hightech Agenda Plus»**. Meanwhile, the Memorandum of Understanding has been signed by Prime Minister Söder and the presidents of the five involved research organizations. For the next two years, a budget of 120 Mio. € is already allocated and a total budget of 300 Mio. € is planned for the next five years. In this way Munich and Bavaria as a whole can be developed into a leading international center with the potential to attract the best researchers and open up new opportunities for Bavaria as a business location in this innovative field.

To implement the Munich Quantum Valley, the following three-point plan has been proposed in the strategy paper:

1. Foundation of a **Center for Quantum Computing and Quantum Technology** to foster networking with industry, to develop priorities in QST research and development, and to coordinate the allocation of funding with the following priorities:
   (a) Support of basic science and development of basic quantum technologies within so-called lighthouse projects.
   (b) Development, realization and operation of quantum computers based on a long-term institutional funding to guarantee international competitiveness.
   (c) Technology transfer to industry and start-ups.
2. Establishment of a **Quantum Technology Park** to provide the technological infrastructure for the development and fabrication of quantum devices required for basic research and the industrial application of quantum technologies. In particular, the technology park shall provide expensive high-tech infrastructure to start-up companies.
3. **Qualification and Education** of the next generation of quantum experts in natural and computer sciences as well as engineering. This includes training and re-education of

skilled employees in industry.

Historically, point 1) goes back to an earlier proposal for a Bavarian Quantum Computing Center made by Gerhard Abstreiter, Rudolf Gross and Dieter Vollhardt already in March 2019. A version detailed by Rudolf Gross has been handed over to Prime Minister Söder in October 2019 and a further update was provided by Stefan Filipp and Rudolf Gross in March 2020. In these concept papers also the need for a quantum technology park was emphasized. The latter was triggered by the fact that the start-up company IQM, co-founded by the former WMI Ph.D. student Jan Goetz, could not rent the required high-tech equipment for qubit fabrication in the Munich area.

The Munich Quantum Valley Initiative paper points out that Germany is internationally well-positioned in basic research and also can build on companies with broad experience in the development and integration of quantum technologies as well as their transfer into novel products. Therefore, Germany is in a good starting position to shape the forthcoming quantum revolution and to profit from it. However, there is also considerable need to catch up regarding courageous and decisive actions in order to be able to act at the top of international research and, in particular, innovative business fields. Here, the Munich Quantum Valley can make a significant contribution by implementing a national and European strategy, which aims at acting on eye level with the leading international centers.

C. New BMBF Projects Have Been Granted to WMI

Within the program **«Quantentechnologien – von den Grundlagen zum Markt»**, the BMBF announced the new calls **«Anwendungsbezogene Forschung in der Quantensensorik, -metrologie sowie -bildgebung»** and **«Quantenprozessoren und Technologien für Quantencomputer»**. As WMI is active in these fields, we participated in both calls and submitted proposals together with our project partners in 2020. Both proposals have been successful and granted in December 2020. The projects will start in February 2021.

Within the call «Anwendungsbezogene Forschung in der Quantensensorik, -metrologie sowie -bildgebung» WMI is participating in the coordinated project **«Quantum Radar Team (QUARATE)»**. The idea for this projects has been developed by WMI. We are very happy that our industrial partner Rohde & Schwarz GmbH took over the coordination of the project, demonstrating the growing interest of industry in quantum technologies. Further partners are DLR and TUM. The project aims at using quantum microwaves to demonstrate a quantum advantage in the signal-to-noise ratio in radar applications. The project joins a multi-disciplinary team of experts from industry, electrical engineers, and quantum physicists. The key goal is to demonstrate a leap in technology and to transfers the quantum microwave technology developed at WMI into industrial applications.

Within the call «Quantenprozessoren und Technologien für Quantencomputer» WMI is coordinating the project **«German Quantum Computer based on Superconducting Qubits (GeQCoS)»**. Project partners are the Forschungszentrum Jülich GmbH, the

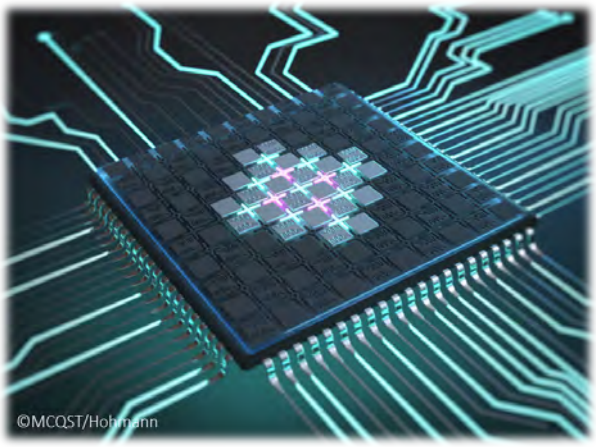

Karlsruher Institut für Technologie, the Friedrich-Alexander-Universität Erlangen-Nürnberg, the Fraunhofer Gesellschaft zur Forderung der angewandten Forschung e.V, and Infineon Technologies AG. Although the complexity and performance of superconducting quantum computers is continuously increasing, an architecture suitable for handling practical problems still requires fundamental improvements. Therefore, the project addresses on the one hand the improvement of the gate fidelity and on the other hand the reduction of the algorithmic depth by reducing the number of required gates by an increased connectivity. The key goal is the development of a 9-qubit processor with improved components and architecture.

D. New EU Projects

With the arrival of the new scientific director Stefan Filipp in June 2020, also new EU projects have been partly transferred from his former place IBM Research in Zurich to WMI. This includes the following projects:

- *Quantum Optimal Control* within the EU H2020 ITN *Quantum-enhanced Sensing via Quantum Control (QuSCo)*.
- *Quantum Neural Networks* within the EU FET Open project *Neuromorphic Quantum Computing (Quromorphic)*.
- *Parametric Multi-Qubit Gates* within the EU MSCA Cofund Action *Quantum Science and Technologies at the European Campus (QUSTEC)* set up by the European Grouping of Territorial Cooperation (EGTC) Eucor – The European Campus.

The EU Quantum Flagship Project QMiCS

F. Deppe, K. G. Fedorov, A. Marx, M. Partanen, M. Renger, R. Gross [1]

Since 2018, the European Union (EU) fosters the development of quantum technologies via the Quantum Flagship program (**www.qt.eu**). One of the 20 projects funded in the first call, *"Quantum microwave communication and sensing (QMiCS)"* (www.qmics.wmi.badw.de) is coordinated by Frank Deppe from the Walther-Meißner-Institute (WMI). The project logo is shown in Fig. 1. Scientific project partners are Aalto University (Finland), École Normale Superieure der Lyon (ENSL, France), Instituto de Telecomunicações (Portugal), Universidad del País Vasco / Euskal Herriko Unibertsitatea (UPV/EHU, Spain), and VTT (Finland). Active industry partners are Oxford Instruments Nanotechnology Ltd. (OINT, United Kingdom) and TTI Norte S.L. (Spain). QMiCS explores continuous-variable quantum microwaves. Its three main goals are a 6.6 meter long quantum local area network (QLAN) cable connecting two dilution refrigerators at millikelvin temperatures, a proof-of-principle quantum illumination experiment, and a roadmap to real-life applications of quantum microwaves.

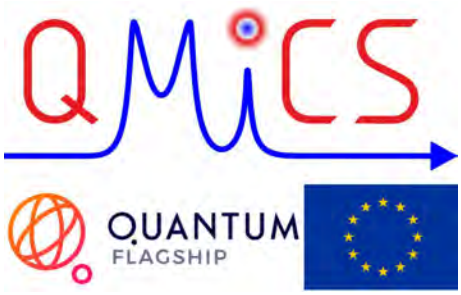

Figure 1: Logos of QMiCS (top), the Quantum Flagship (bottom left), and the EU (bottom right).

Scientifically, 2020 has brought significant progress. WMI has shown the absence of a standard quantum limit in parametric amplification of broadband signals [1] and first steps towards microwave quantum key distribution [2] (see reports on page 33-34 and page 31-32). Other partners could advance microwave single photon detection, which is required for the illumination experiments. A qubit-based microwave photon counter resolving up to three 10 GHz-photons has been demonstrated by partner ENSL [3] and a graphene-based on-chip bolometer from partner AALTO [4] has reached an energy resolution of $h\times 30$ GHz. In addition to science, advancing quantum microwave technology is an equally important part of QMiCS. Here, key tasks have progressed significantly. Partner TTI has just finished the development of improved high-electron-mobility transistor (HEMT) amplifiers for the frequency bands around 600 MHz and 6 GHz. These devices will be tested soon by other partners. Regarding the QLAN cable, half of the millikelvin link has been successfully assembled and tested by OINT and WMI (see report on page 49-50) for details. Currently, WMI is about to insert three low-loss coaxial NbTi microwave cables into the full link followed by final mechanical and thermal tests.

All in all, despite slight delays for all partners due to the omnipresent Europe-wide CoViD-19 restrictions, QMiCS has been moving ahead steadily in 2020. This judgment has been confirmed during the successful and constructive midterm review meeting in May 2020. All partners are well prepared to attack the pending challenges in 2021.

References

[1] M. Renger, S. Pogorzalek, Q. Chen, Y. Nojiri, K. Inomata, Y. Nakamura, M. Partanen, A. Marx, R. Gross, F. Deppe, and K. G. Fedorov. Submitted for publication, arXiv:2011.00914 (2020).
[2] F. Fesquet. *Microwave quantum key distribution*. Master's thesis, Technische Universitä München (2020).
[3] R. Dassonneville, R. Assouly, T. Peronnin, P. Rouchon, and B. Huard, Phys. Rev. Applied **14**, 044022 (2020).
[4] R. Kokkoniemi, J. Girard, D. Hazra, A. Laitinen, J. Govenius, R. E. Lake, I. Sallinen, V. Vesterinen, M. Partanen, J. Y. Tan, K. W. Chan, K. Y. Tan, P. Hakonen, and M. Möttönen, Nature **586**, 47–51 (2020).

[1]We acknowledge support by the German Research Foundation under Germany's Excellence Strategy (EXC-2111 – 390814868), the Elite Network of Bavaria through the graduate program ExQM, and the EU Flagship project QMiCS (Grant No. 820505).

Basic Research

Beyond the Standard Quantum Limit of Parametric Amplification

M. Renger, S. Pogorzalek, Q.-M. Chen, Y. Nojiri, M. Partanen, A. Marx, R. Gross, F. Deppe, K. G. Fedorov [1]

In quantum technology, low-noise amplification of weak quantum signals is a crucial requirement of countless protocols in quantum information processing. This task is commonly accomplished with linear phase-preserving amplifiers, which increase the amplitude in both signal quadratures without altering the signal phase. This amplification process is of particular relevance for tomography of quantum microwave states due to the low energy of microwave photons, compared to the thermal background environment. State tomography is essential for experimental protocols such as secure quantum remote state preparation [1] and quantum teleportation [2]. However, fundamental laws of quantum physics imply that any phase-preserving amplifier needs to add at least half a noise photon in the high-gain limit, a bound known as the standard quantum limit (SQL). In the following, we theoretically and experimentally demonstrate that this limit can be overcome by employing non-degenerate parametric amplification of sufficiently broadband signals and find a quantitative criterion for the required signal bandwidth [3].

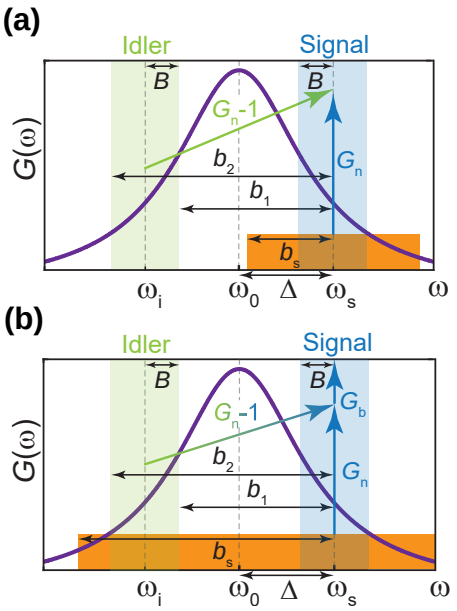

Figure 1: (a) Spectrum of parametric amplification of narrowband signals with bandwidth b_s. The purple solid line shows a Lorentzian gain function. Blue-shaded and green-shaded regions represent measurement bands with full bandwidth $2B$ around the signal and idler modes, respectively. For input signals with $b_s \leq b_1$, the idler adds at least vacuum fluctuations to the output. (b) Spectrum of parametric amplification process for broadband signals. If $b_s \geq b_2$, each mode in the signal bandwidth corresponds to a correlated input mode on the idler side, resulting in amplification with the total gain $G_b = 2G_n - 1$ and absence of the SQL.

We use the quantum efficiency η to characterize the noise performance of our amplifiers. The quantum efficiency is defined as the ratio between vacuum fluctuations in the input signal and fluctuations in the output signal. For narrow-band signals, the SQL implies that $\eta \leq G_n/(2G_n - 1)$, where G_n is the parametric power gain. To investigate the dependence of the maximally achievable quantum efficiency on the signal bandwidth b_s, we start from the input-output relation of the non-degenerate parametric amplifier [4],

$$\hat{c}(\omega) = \int_{\mathcal{I}} d\tilde{\omega} \left[M(\omega,\tilde{\omega})\hat{a}(\tilde{\omega}) + L(\omega,\tilde{\omega})\hat{a}^{\dagger}(\tilde{\omega}) \right] + \hat{f}(\omega)\,. \tag{1}$$

Here, $\hat{a}(\tilde{\omega})$ and $\hat{a}^{\dagger}(\tilde{\omega})$ represent the input signal and idler modes, $\hat{c}(\omega)$ is the amplified output mode and $\hat{f}(\omega)$ is an uncorrelated noise mode. The coefficients $M(\omega,\tilde{\omega})$ and $L(\omega,\tilde{\omega})$ represent the linear signal and idler amplitude gain and $\mathcal{I}$ denotes the set of all input modes. We calculate the noise spectral density of $\hat{f}(\omega)$ and apply the Heisenberg uncertainty principle to Eq. 1. The evaluation of the integral results in two threshold values for the single-side signal bandwidth b_s. The first one is $b_1 = 2\Delta - B$ and the second one is $b_2 = 2\Delta + B$, where Δ represents the detuning of the signal reconstruction frequency ω_s from the resonance frequency ω_0 of the amplifier and B is the single-side reconstruction bandwidth. Non-degenerate narrowband amplification is then determined by $b_s \leq b_1$ and illustrated in Fig. 1(a). In this case,

[1] We acknowledge support by the German Research Foundation under Germany's Excellence Strategy (EXC-2111 – 390814868), the Elite Network of Bavaria through the graduate program ExQM, and the EU Flagship project QMiCS (Grant No. 820505).

the input signal is amplified with a power gain G_n and the idler mode adds at least vacuum fluctuations to the signal, resulting in the SQL. In the nondegenerate broadband case, $b_s \geq b_2$, the input signal covers the idler sideband, as shown in Fig. 1(b). As a result, the idler acts as an additional signal port and no longer adds uncorrelated noise, implying a total broadband gain $G_b = 2G_n - 1$ and the absence of the SQL.

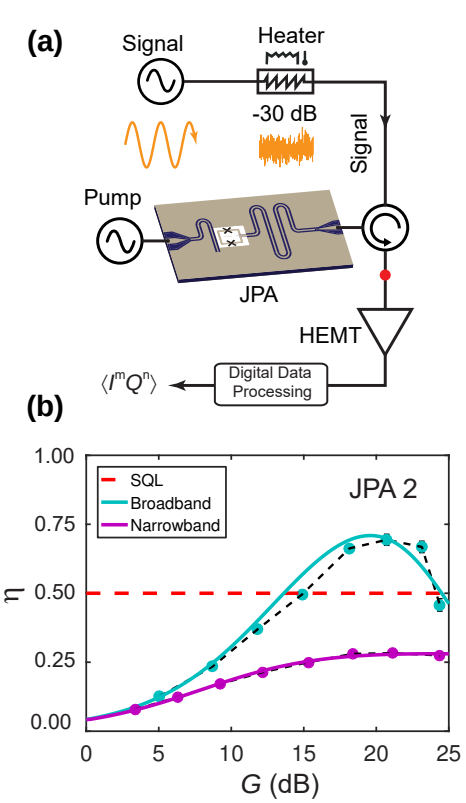

Figure 2: (a) Illustration of the experimental setup. The amplification chain consists of a non-degenerate Josephson parametric amplifier and a cryogenic HEMT amplifier. The red dot labels the signal reconstruction point. (b) Experimental quantum efficiency of JPA 2 for broadband (cyan dots) and narrow-band (purple dots) input signals. The red dashed line represents the SQL, the solid lines are theory fits.

As depicted in Fig. 2(a), our experimental setup to verify this prediction consists of a flux-driven Josephson parametric amplifier (JPA) serially connected to a cryogenic high-electron-mobility transistor (HEMT) amplifier [3]. A coherent input signal can be applied via a microwave input line. A heatable 30 dB attenuator allows us to generate thermal states as broadband input signals. To measure the quantum efficiency for broadband amplification, we perform Planck spectroscopy for varying G_b. A similar experiment with coherent input states enables us to extract the quantum efficiency for amplification of narrow-band signals. The experiment is performed with two different JPAs to verify reproducibility. The measurement results are displayed in Fig. 2(b) for JPA 2. There, we show the dependence of η on the gain G, where $G = G_b$ and $G = G_n$ for broadband and narrow-band amplification, respectively. For both JPAs, we find a gain region where we clearly exceed the SQL for the amplification in the case of broadband signals. For JPA 2, we achieve a maximum efficiency $\eta = 0.69 \pm 0.02$, which substantially exceeds the SQL. The maximum in Fig. 2(b) is determined by the optimal trade-off between gain-independent HEMT noise $n_H = 11.3$ and gain-dependent JPA noise $n_J(G)$. Under the assumption that n_J results from fluctuations in the pump signal, it can be shown that it obeys a power law dependence as a function of G. We use these results to obtain the fits to the measured quantum efficiencies shown in Fig. 2(b), which successfully reproduces the maximum as well as the low-gain behavior.

In summary, we have verified that for parametric amplification of broadband input states, an idler mode may also carry information about the signal and does not add extra noise to the output [3]. Possible applications include high-efficiency broadband dispersive qubit readout, parity detection, or quantum amplitude sensing.

References

[1] S. Pogorzalek, K. G. Fedorov, M. Xu, A. Parra-Rodriguez, M. Sanz, M. Fischer, E. Xie, K. Inomata, Y. Nakamura, E. Solano, A. Marx, F. Deppe, and R. Gross, Nat. Commun. **10**, 2604 (2019).
[2] R. Di Candia, K. G. Fedorov, L. Zhong, S. Felicetti, E. P. Menzel, M. Sanz, F. Deppe, A. Marx, R. Gross, and E. Solano, EPJ Quantum Technol. **2**, 25 (2015).
[3] M. Renger, S. Pogorzalek, Q. Chen, Y. Nojiri, K. Inomata, Y. Nakamura, M. Partanen, A. Marx, R. Gross, F. Deppe, and K. G. Fedorov. Submitted for publication, arXiv:2011.00914 (2020).
[4] C. M. Caves, Phys. Rev. D **26**, 1817–1839 (1982).

Microwave Quantum Key Distribution

K. G. Fedorov, F. Fesquet, M. Renger, Y. Nojiri, Q. Chen, M. Partanen, A. Marx, F. Deppe, R. Gross [1]

Quantum communication based on continuous-variables (CV) is a field of intense research investigating various topics, such as quantum key distribution (QKD), quantum teleportation, dense coding, and free-space quantum communication. Historically, the majority of the previously mentioned implementations have been performed in the optical domain. Nowadays, the field of quantum communication in the microwave domain also enjoys rapid progress [1, 2]. This development is motivated by the tremendous progress in the field of quantum information processing with superconducting circuits. In particular, the development of superconducting multiqubit processors operating at gigahertz frequencies has been highly successful. Here, we promote the approach of quantum communication directly in the microwave regime based on propagating squeezed states. Since these states have the same frequency and are generated by technology platforms already used for superconducting quantum computers, there is no frequency mismatch between communication and data processing units. Therefore, this approach is expected to be useful for short and medium distances in future quantum local area networks, where superconducting waveguides can be used. Already at this level, it might be important to protect the communicated information from potential eavesdroppers. Furthermore, quantum microwave communication can already be considered in certain open-air scenarios [3], where the questions of security become of the paramount importance.

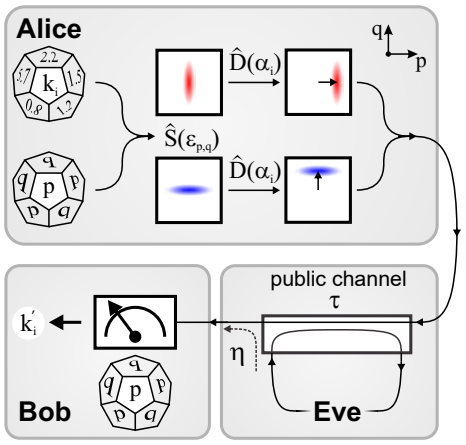

Figure 1: Scheme of a QKD protocol based on displaced squeezed states. Alice starts by generating a random continuous-variable number k_i corresponding to Alice's key element. She randomly chooses among one of two possible encoding bases, p or q, which results in vacuum states squeezed along one of the quadratures with the squeeze factor $\varepsilon_{p,q}$. Every key element k_i is encoded via a displacement amplitude α_i. The resulting displaced squeezed state is sent through the public channel with transmissivity τ. This channel can be coupled to a potential eavesdropper Eve, which induces extra photon noise η as a result of interaction with the signal. In the end, Bob receives a state which he measures in a random basis, p or q, in order to obtain an estimate k_i' of the original key element. The protocol must be repeated multiple times in combination with further (here not discussed) information reconciliation and privacy amplification steps before the original key can be securely reconstructed by Bob.

Here, we theoretically analyze a fundamental CV QKD protocol (see Fig. 1) based on Ref. [4] in the microwave range in order evaluate its experimental perspectives. The protocol relies on the application of two operations: squeezing and displacement. The latter encodes a secret key in the signal, while the former ensures the unconditional security of the protocol. The resulting displaced squeezed state corresponds to a so-called "cipher", which can be safely distributed between two communicating parties (Alice and Bob). This QKD protocol exploits the uncertainty relation between the conjugate pair of electromagnetic field quadrature components $\hat{p}$ and $\hat{q}$ by encoding a continuous Gaussian-distributed key into either p- or q-squeezed states. It can be shown that the information acquired by a potential eavesdropper Eve on the key

[1]We acknowledge support by the German Research Foundation under Germany's Excellence Strategy (EXC-2111 – 390814868), the Elite Network of Bavaria through the graduate program ExQM, and the EU Flagship project QMiCS (Grant No. 820505).

elements encoded in p or q is compensated by a respective reduction of the key information on the amplitude available at the Bob side.

In the context of propagating quantum microwaves, superconducting Josephson parametric amplifiers (JPA) play a central role. Flux-driven JPAs can routinely produce propagating squeezed states with squeezing levels up to 10 dB below the vacuum limit [5]. In combination with cryogenic directional couplers, one can reliably generate displaced squeezed microwave states [6] as required for the proposed CV-QKD protocol.

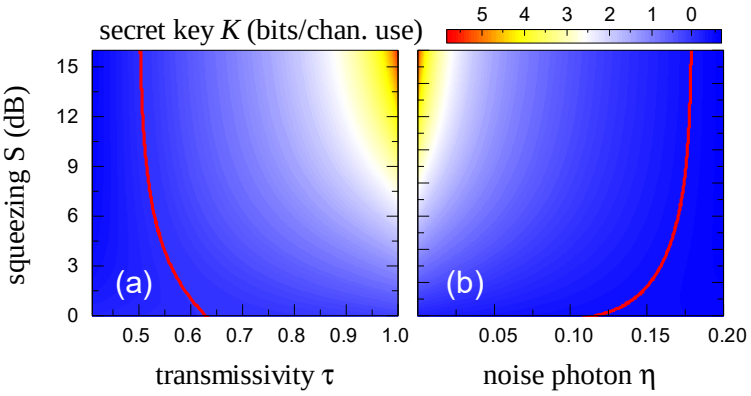

Figure 2: **(a)** Secret key values in the DR case versus squeezing level S below the vacuum limit and transmissivity τ assuming non-ideal squeezed states with noise $n = 0.1$ and $\eta = 0$. **(b)** Secret key values in the DR case versus squeezing level S and noise η with $n = 0.1$ and $\tau \to 1$. Red lines separate the regions of positive (secure) and negative (insecure) keys.

In order to quantify the amount of secure information communicated between Alice and Bob according to our QKD protocol with displaced squeezed microwave states, we numerically calculate the secret key in the direct reconciliation case (DR) for a wide range of transmission losses (characterized with τ) and typical (for cryogenic experiments) values for the noise photon number η. Additionally, we assume nonideal squeezing, as it is the case for our JPAs. This nonideality can be modeled by a finite number of noise photons $n > 0$ above the vacuum limit at the input of the squeezing operation [2]. The dependence of the secret key K on the squeezing level S of the displaced squeezed states, transmissivity τ, and noise photon number η is shown in Fig. 2. Here, we observe that the communication is secure up to transmissivity $\tau = 0.5$ and $\eta = 0.184$. The transmissivity threshold is expected, as the communication cannot be secure in the DR case if Eve receives more than 50 % of Alice's signals. The noise threshold is harder to interpret and must be studied further.

In conclusion, one can observe that positive secure key rates in the microwave QKD are definitely achievable for typical values of squeezing, transmissivity, and noise in the cryogenic environment. Furthermore, by considering realistic microwave losses and noise in the atmosphere [3], one can expect that microwave QKD protocols might be also viable in open-air environment for short-distance secure communication.

References

[1] C. J. Axline, L. D. Burkhart, W. Pfaff, M. Zhang, K. Chou, P. Campagne-Ibarcq, P. Reinhold, L. Frunzio, S. M. Girvin, L. Jiang, M. H. Devoret, and R. J. Schoelkopf, Nature Physics **14**, 705–710 (2018).
[2] S. Pogorzalek, K. G. Fedorov, M. Xu, A. Parra-Rodriguez, M. Sanz, M. Fischer, E. Xie, K. Inomata, Y. Nakamura, E. Solano, A. Marx, F. Deppe, and R. Gross, Nat. Comm. **10**, 2604 (2019).
[3] M. Sanz, K. G. Fedorov, F. Deppe, and E. Solano, 2018 IEEE Conference on Antenna Measurements Applications (CAMA) 1–4 (2018).
[4] N. J. Cerf, M. Lévy, and G. V. Assche, Phys. Rev. A **63**, 052311 (2001).
[5] L. Zhong, E. P. Menzel, R. D. Candia, P. Eder, M. Ihmig, A. Baust, M. Haeberlein, E. Hoffmann, K. Inomata, T. Yamamoto, Y. Nakamura, E. Solano, F. Deppe, A. Marx, and R. Gross, New Journal of Physics **15**, 125013 (2013).
[6] K. G. Fedorov, L. Zhong, S. Pogorzalek, P. Eder, M. Fischer, J. Goetz, E. Xie, F. Wulschner, K. Inomata, T. Yamamoto, Y. Nakamura, R. Di Candia, U. Las Heras, M. Sanz, E. Solano, E. P. Menzel, F. Deppe, A. Marx, and R. Gross, Physical Review Letters **117**, 1–5 (2016).

Probing the Electronic System of an Organic Conductor Near the Mott Transition by Magnetic Quantum Oscillations

S. Oberbauer, W. Biberacher, M. V. Kartsovnik
N. D. Kushch [1]

Despite the great amount of work devoted to the properties of a metal approaching the Mott-insulator transition (MIT), some key theoretical predictions are still awaiting experimental verification. For example, there is no clarity about the predicted [1–3] pseudogap formation or about the exact behavior of the quasiparticle effective mass m, a sensitive probe of the electronic correlation strength, in the direct neighborhood of the first-order bandwidth-controlled MIT. It is generally believed that the mass increases due to enhanced many-body renormalization near the transition. However, an explicit verification of the dependence of the mass renormalization factor on the correlation strength ratio U/t [3–8] is missing. To fill this gap of knowledge, we have chosen the layered organic charge transfer salt κ-(BEDT-TTF)$_2$Cu[N(CN)$_2$]Cl (hereafter κ-Cl) as a model systems for a bandwidth-controlled quasi-two-dimensional Mott insulator and traced the evolution of its conduction system near the MIT using the magnetic quantum oscillation technique. The antiferromagnetic Mott-insulating (AFI) state of κ-Cl turns into the metallic and superconducting state in a first-order phase transition under a pressure of $20 - 40$ MPa. In order to better pick out the role of the proximity of κ-Cl to the MIT, we included a reference material, κ-(BEDT-TTF)$_2$Cu(NCS)$_2$ (hereafter κ-NCS), in the experiment. The latter salt is very similar to κ-Cl, but metallic already at ambient pressure.

Figure 1(a) shows the low-temperature interlayer resistivity of κ-Cl as a function of magnetic field $B \perp$ layers, measured at different pressures p. The displayed pressure range, 20 to 100 MPa, includes both the purely metallic (M) region and the transitional region where the M and AFI states coexist. The latter is manifested by a dramatic enhancement of the resistivity at fields $B > 10$ T, at which the low-B superconducting state is suppressed.

Quantum oscillations of resistivity (the Shubnikov-de Haas (SdH) effect) with only a weakly p-dependent frequency are found at all pressures, see inset in Fig. 1(a). Sizeable oscillations exist even very close to the lower border of the coexistence region, $p_{c2} \simeq 20$ MPa. Moreover, the scattering rate evaluated from the oscillation analysis shows no increase upon entering the coexistence range. Thus, our experiment provides a firm evidence of a large coherent Fermi surface, without any sign of a pseudogap even in the direct proximity to the AFI state.

A further insight into the conduction system is gained from the analysis of the T-dependent SdH amplitude yielding the effective cyclotron mass of charge carriers m_c. We have found that for both salts, κ-Cl and κ-NCS, the mass rapidly increases at decreasing pressure, which is attributed to enhancement of the many-body renormalization effect upon approaching the MIT. The behavior of the renormalization factor $m_c/m_{c,\mathrm{b}}$, where $m_{c,\mathrm{b}} = 2.8m_0$ is the single-particle band cyclotron mass [10] and m_0 the free electron mass, is shown in Fig. 1(b). In the purely M region the data is remarkably well described by the simple relation $m_c \propto (p - p_c)^{-1}$ with $p_c \approx -400$ MPa. This functional dependence is perfectly consistent with the renowned Brinkman-Rice [4] and the dynamical mean-field [5] theories, predicting a linear relationship between the Fermi-liquid quasiparticle residue $Z = m_{c,\mathrm{b}}/m_c$ and the correlation strength ratio U/t, once we assume a linear pressure dependence of U/t.

There is, however, an important quantitative discrepancy: the experimentally observed pressure dependence is much steeper than predicted. The upper axis of the inset in Fig. 1(b) shows

[1] Institute of Problems of Chemical Physics, Chernogolovka 142432, Russia

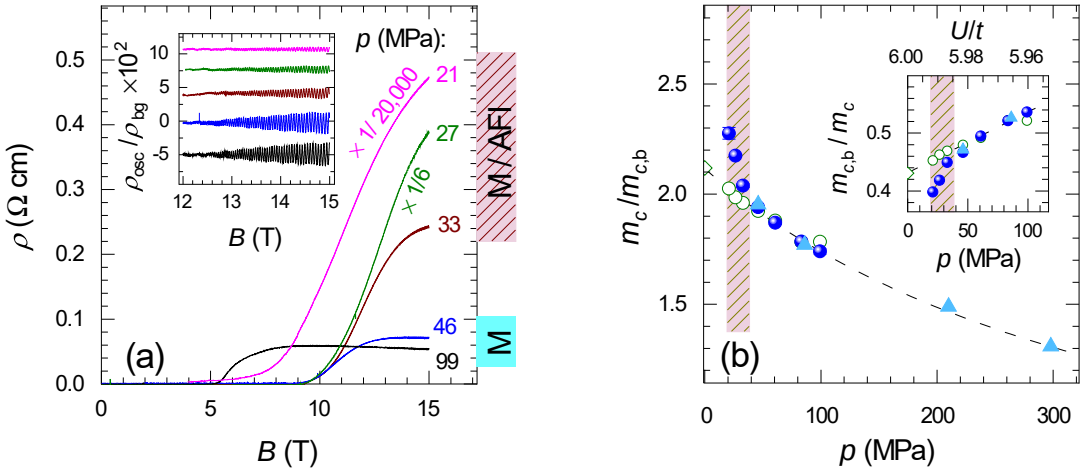

Figure 1: (a) Interlayer resistivity of κ-Cl as a function of the out-of-plane magnetic field recorded at different pressures, $T = 0.1K$. Inset: oscillating component of the resistivity, normalized to the monotonic B-dependent background. The curves are vertically shifted for clarity. (b) Pressure dependence of the effective cyclotron mass in units of the band mass. Filled circles and triangles represent samples #1 and #2 of κ-Cl, respectively. The data for the κ-NCS sample, measured simultaneously with κ-Cl sample #1, is shown by open symbols. The $P = 0$ point is taken from Ref. 9. Inset: The inverse renormalization factor $m_{c,b}/m_c = Z$ as a function of P (lower axis) and of U/t (upper axis). The dashed line is a linear fit to the $Z(P)$ dependence. The shaded area indicates the transitional pressure range where the M and AFI phases coexist.

the U/t scale based on the p-dependent band structure calculations [11]. The resulting slope of the linear $m_{c,b}/m_c(p)$ dependence is an order of magnitude higher than the theoretical values [4, 5]. While a number of more advanced recent theories [3, 6–8] show some deviations from the above-mentioned models, they are way too small to explain this discrepancy.

Another striking anomaly is found for κ-Cl in the M/AFI coexistence region. By contrast to the fully metallic κ-NCS salt following the inverse-linear $m_c(p)$ dependence down to ambient pressure, κ-Cl displays a clear acceleration in the interval $20\,\mathrm{MPa} < p < 40\,\mathrm{MPa}$, which exactly coincides with the M/AFI region. This finding urges further theoretical effort to elucidate the impact of the microscopic phase coexistence on the conduction system inside the M domains.

Finally, the remarkable similarity of the cyclotron masses in κ-Cl and κ-NCS in the homogeneous M region implies that the correlation strength ratio U/t be the same for both salts. In this case, the primary reason for the difference in the ambient-pressure ground states of the two materials appears to lie in different degrees of geometrical frustration. Thus, our experiment provides a strong support for the theoretical prediction of a crucial role of frustration effects in the κ salts [12].

References

[1] J. Kang, S.-L. Yu, T. Xiang, and J.-X. Li, Phys. Rev. B **84**, 064520 (2011).
[2] C.-D. Hébert, P. Sémon, and A.-M. S. Tremblay, Phys. Rev. B **92**, 195112 (2015).
[3] O. Parcollet, G. Biroli, and G. Kotliar, Phys. Rev. Lett. **92**, 226402 (2004).
[4] W. F. Brinkman, and T. M. Rice, Phys. Rev. B **2**, 4302–4304 (1970).
[5] A. Georges, G. Kotliar, W. Krauth, and M. J. Rozenberg, Rev. Mod. Phys. **68**, 13–125 (1996).
[6] B. J. Powell, and R. H. McKenzie, Phys. Rev. Lett. **94**, 047004 (2005).
[7] T. Watanabe, H. Yokoyama, Y. Tanaka, and J.-i. Inoue, J. Phys. Soc. Jpn. **75**, 074707 (2006).
[8] H. Park, K. Haule, and G. Kotliar, Phys. Rev. Lett. **101**, 186403 (2008).
[9] J. Caulfield, W. Lubczynski, F. L. Pratt, J. Singleton, D. Y. K. Ko, W. Hayes, M. Kurmoo, and P. Day, J. Phys.: Condens. Matter **6**, 2911 (1994).
[10] J. Merino, and R. H. McKenzie, Phys. Rev. B **62**, 2416–2423 (2000).
[11] H. C. Kandpal, I. Opahle, Y.-Z. Zhang, H. O. Jeschke, and R. Valentí, Phys. Rev. Lett. **103**, 067004 (2009).
[12] T. Koretsune, and C. Hotta, Phys. Rev. B **89**, 045102 (2014).

© Walther-Meißner-Institute

Raman Study of Cooper Pairing Instabilities in $(Li_{1-x}Fe_x)OHFeSe$

G. He, D. Jost, A. Baum, R. Hackl [1]
D. Li, P.P. Shen, Z.X. Zhao,X.L. Dong [2,3]

Since the discovery of the Fe-based superconductors (FeSCs) in 2008 the mechanism of Cooper pairing has attracted a lot of attention. Similar to the cuprates, superconductivity in FeSCs occurs close to magnetic order making spin-fluctuations a natural candidate for a pairing glue. In Fe pnictides, many experimental and theoretical results support $s_{\pm}$ pairing where a $(0, \pi)$ scattering vector approximately connects the hole pocket at Γ point and the electron pocket at X point (near-nesting condition), thereby inducing a π phase shift of the order parameter on the two Fermi pockets. However, the absence of a hole pocket in some heavily electron-doped Fe chalcogenides challenges the nesting picture. The following questions should be addressed: (i) What is the pairing interaction and symmetry in heavily electron-doped Fe chalcogenides and (ii) is there a generic pairing mechanism in Fe pnictides and chalcogenides?

Electronic Raman scattering may contribute useful information to understand unconventional superconductivity [1–4]. In addition to the gap formation and the pair-breaking peaks at approximately twice the gap energy, collective excitations, such as Bardasis-Schrieffer (BS) modes [5] and Leggett modes [6] from pairing channels orthogonal to the ground state and number-phase fluctuations between different Fermi surface sheets, respectively, appear in the Raman response, which are related to details of the pairing potential $V_{\mathbf{k}\mathbf{k}'}$. Thus, the careful study of putative collective modes offers an opportunity to clarify the competing superconducting instabilities and the related pairing glue.

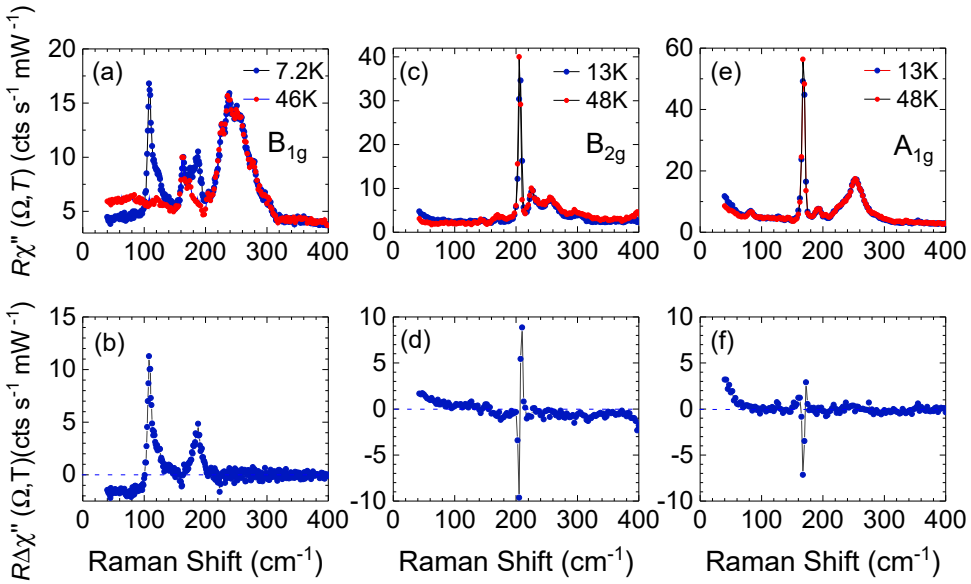

Figure 1: (a),(c),(e) Raman spectra of $(Li_{1-x}Fe_x)OHFeSe$ in B_{1g}, B_{2g}, and A_{1g} symmetry at temperatures as indicated. (b),(d),(f) Difference $R\Delta\chi''$ of the superconducting and normal spectra. From Ref. [7].

We studied the temperature and polarization dependence of the Raman response in $(Li_{1-x}Fe_x)OHFeSe$ having a T_c of 42 K. The main results are shown in Fig. 1. Two well-

[1]Financial support: German Research Foundation (DFG) through the coordinated programme TRR80 (Projekt-ID 107745057) and project HA 2071/12-1 (R.H.), the Alexander von Humboldt Foundation (G.H.)

[2]Institute of Physics, Chinese Academy of Sciences, Beijing 100190, China

[3]D.L., P.P.S., Z.X.Z., and X.L.D. were supported by National Natural Science Foundation of China (No. 11834016), and the National Key Research and Development Program of China (Grant No. 2017YFA0303003) and Key Research Program of Frontier Sciences of the Chinese Academy of Sciences (Grant No. QYZDY-SSW-SLH001).

defined features at 110 and 190 cm^{-1} in B_{1g} but not in A_{1g} and B_{2g} symmetry are found in the superconducting state. At least the resolution-limited line at 110 cm^{-1} is a candidate for a collective mode being either related to a sub-leading pairing interaction or a number-phase oscillation between the electron bands.

The collective modes appearing in B_{1g} symmetry suggest that there exists another orthogonal subdominant pairing channel which can be either a low-order d-wave interaction [see Fig. 2 (a)] or an s-wave interaction. The existence of two separate gaps, as evident from STS and ARPES, does not favor the former case. Thus, the possible pairing interactions include spin-fluctuation pairing between the electron bands and the incipient hole band and pairing between the hybridized electron bands (see Fig. 2(c)]. The absence of gap features in A_{1g} and B_{2g} symmetry favors the latter case since the incipient bands would leave an imprint in the Raman spectra. Thus, in spite of various differences between the pnictides and chalcogenides, we demonstrate the similarity of the respective pairing states and the importance of band structure effects in the Fe-based compounds.

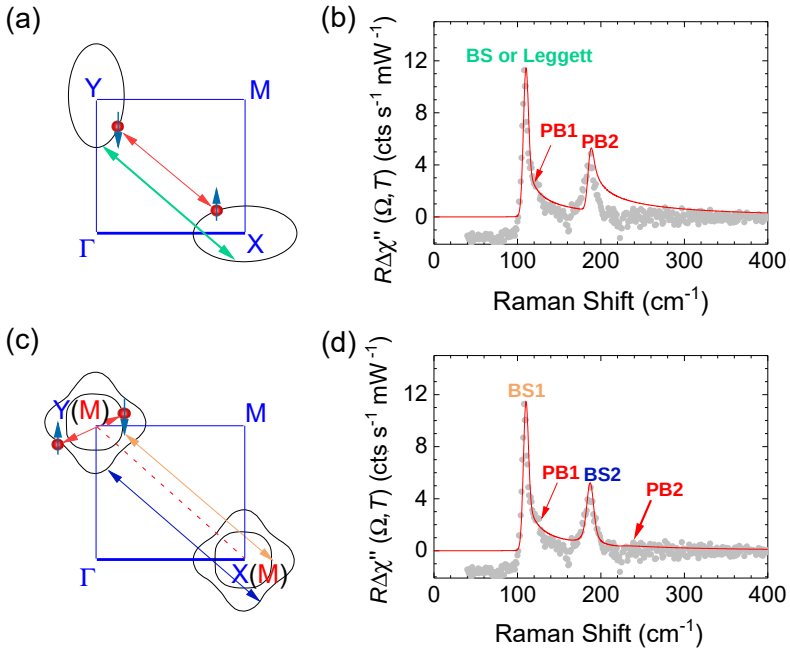

Figure 2: Interactions and related phenomenological spectra. (a),(c) Illustration of the superconducting ground state and possible subdominant interactions in the first BZ. The blue solid lines indicate the first quadrant of the 1 Fe BZ boundary. The 2 Fe BZ boundary in (c) is illustrated by the red dashed line. The Fermi pockets are shown by the black solid curves. The red double arrows indicate the pairing interaction in (a) and (c). The green double arrow in (a) and the orange and dark blue ones in (c) indicate the possible subdominant pairing interactions. (b), (d) Experimental results (grey dots) and phenomenology (red curves). The fitting results correspond to the situations in (a) and (c). The BS or Leggett modes and the pair-breaking (PB) peaks are indicated. From Ref. [7].

References

[1] T. P. Devereaux, and R. Hackl, Rev. Mod. Phys. **79**, 175–233 (2007).
[2] F. Kretzschmar, B. Muschler, T. Böhm, A. Baum, R. Hackl, H. H. Wen, V. Tsurkan, J. Deisenhofer, and A. Loidl, Phys. Rev. Lett. **110**, 187002 (2013).
[3] T. Böhm, A. F. Kemper, B. Moritz, F. Kretzschmar, B. Muschler, H. M. Eiter, R. Hackl, T. P. Devereaux, D. J. Scalapino, and H. H. Wen, Phys. Rev. X **4**, 041046 (2014).
[4] T. Böhm, F. Kretzschmar, A. Baum, M. Rehm, D. Jost, R. H. Ahangharnejhad, R. Thomale, C. Platt, T. A. Maier, W. Hanke, B. Moritz, T. P. Devereaux, D. J. Scalapino, S. Maiti, P. J. Hirschfeld, P. Adelmann, T. Wolf, H. H. Wen, and R. Hackl, Npj Quantum Mater. **3**, 48 (2018).
[5] A. Bardasis, and J. R. Schrieffer, Phys. Rev. **121**, 1050 (1961).
[6] A. J. Leggett, Prog.Theor. Phys. **36**, 901 (1966).
[7] G. He, D. Li, D. Jost, A. Baum, P. P. Shen, X. L. Dong, Z. X. Zhao, and R. Hackl, Phys. Rev. Lett. **125**, 217002 (2020).

Anomalous spin Hall Angle of a Metallic Ferromagnet Determined by a Multiterminal Spin Injection/Detection Device

T. Wimmer, B. Coester, S. Geprägs, H. Huebl, R. Gross and M. Althammer [1]
S. T. B. Goennenwein [2]

The spin Hall effect (SHE) is at the origin of a plethora of transport effects relevant for spintronics applications. Its capability to convert charge into spin current in non-magnetic metals is conveniently expressed in terms of the phenomenological spin Hall angle θ_{SH}, whereas its microscopic origin lies in the spin-orbit coupling (SOC). Ferromagnetic metals (FMs) with typically large SOC have only recently received broader attention regarding their pure spin current transport properties. Due to their finite magnetic order, however, the broken time reversal symmetry in these FMs results in richer spin current generation than in non-magnetic metals, as manifested for example in the anomalous spin Hall effect (ASHE).

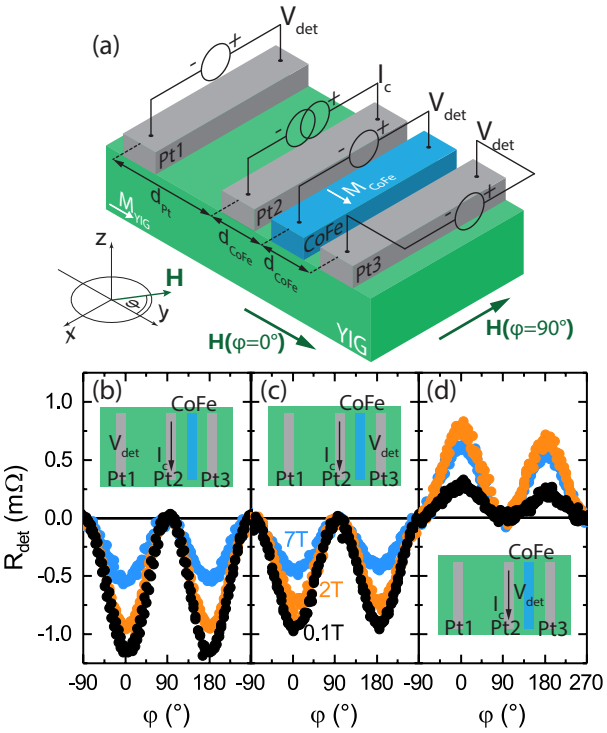

Figure 1: (a) Device scheme: A charge current I_q is fed through the Pt2 electrode, leading to a magnon injection into YIG and a lateral diffusion of these that is electrically detected at the Pt electrodes ('Pt1' and 'Pt3') and the FM electrode ('CoFe') as the detector voltage V_{det}. In (b)-(d) the magnon transport signal R_{det} measured using the Pt1 (b), Pt3 (c) and CoFe (d) detector is plotted versus the direction of the in-plane magnetic field.

The magnetism & spintronics related research at the WMI hinges on materials with large spin Hall angles since they are promising for low power consumption memory devices. In our work, we make use of a magnon transport device [1, 2] to determine the anomalous spin Hall (ASH) angle θ_{ASH} of the FM alloy $Co_{25}Fe_{75}$ (CoFe). The corresponding device is sketched in Fig. 1(a) and features four metallic electrodes – one made of CoFe and three made of Pt – deposited onto a ferrimagnetic insulator yttrium iron garnet (YIG) thin film. We will show that our device offers a suitable platform to quantify the spin Hall efficiency in magnetic materials, which is a challenging task with usual magnetotransport techniques [3].

In our experiments, a DC charge current I_c applied to the Pt2 electrode (the injector) generates a spin accumulation at the Pt/YIG interface via the SHE, which in turn induces a non-equilibrium magnon accumulation in the YIG. These magnons diffuse and are detected as a voltage V_{det} at the Pt1, Pt3 and CoFe electrodes (see Fig. 1(a)) via the inverse SHE/ASHE. In Fig. 1(b)-(d), $R_{det} \propto V_{det}/I_c$ is measured as a function of the magnetic field orientation φ defined in Fig. 1(a). Comparing the detector signals R_{det} recorded across Pt1 and Pt3 (panel (b) and (c), respectively), we find that the amplitude of the typical $\sin^2(\varphi)$-dependence is considerably smaller than for the Pt3 measurement. Although their separation to the injector Pt2 are equal ($d_{Pt} = 2d_{CoFe}$, cf. Fig. 1(a)), the magnon diffusion towards Pt3 is reduced due to a partial absorption of magnons in the CoFe electrode. The detector signal R_{det} measured at

[1]This work is funded by the German Research Foundation under Germany's Excellence Strategy (EXC-2111 – 390814868) and project AL 2110/2-1.
[2]Fachbereich Physik, Universität Konstanz, 78457 Konstanz, Germany

the CoFe electrode (Fig. 1(d)) exhibits a reversed polarity, indicating a negative ASH angle $\theta_{\mathrm{ASH}}^{\mathrm{CoFe}}$ in CoFe compared to the positive spin Hall angle $\theta_{\mathrm{SH}}^{\mathrm{Pt}}$ in Pt. Unlike the magnetic field suppression observed for the Pt detector strips in panel (b) and (c), we find a significant enhancement of R_{det} for increasing magnetic fields up to $\mu_0 H = 2\,\mathrm{T}$ for the CoFe detector due to the saturation of its magnetization. This increase is attributed to a field-induced increase of $\theta_{\mathrm{ASH}}^{\mathrm{CoFe}}$.

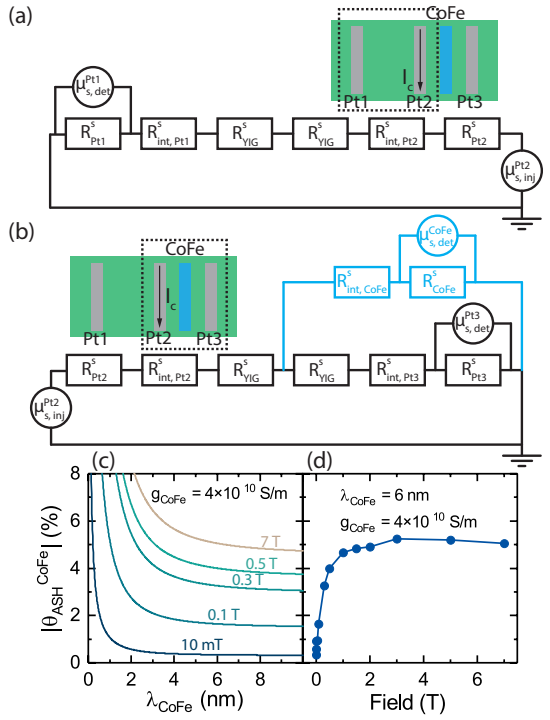

Figure 2: Equivalent spin-resistor network for (a) the Pt2-Pt1 contact pair and (b) the Pt2-CoFe-Pt3 contact configuration. (c) Experimentally determined absolute value of the anomalous spin Hall angle $\Theta_{\mathrm{ASH}}^{\mathrm{CoFe}}$ as a function of the spin diffusion length λ_{CoFe} for various external magnetic fields. (d) ASH angle of CoFe as a function of the applied magnetic field, assuming a spin diffusion length $\lambda_{\mathrm{CoFe}} = 6\,\mathrm{nm}$.

We have modeled the magnon spin transport in our device by employing an equivalent spin-resistor circuit model for the Pt2-Pt1 contact pair and the three-terminal Pt2-CoFe-Pt3 contacts shown in Fig. 2(a) and (b), respectively. Three different resistors are used in the model: R_i^{s} is the spin resistance of electrode i (with i = Pt1, CoFe, Pt3), $R_{\mathrm{int},i}^{\mathrm{s}}$ is the interface spin resistance of the corresponding electrodes and $R_{\mathrm{YIG}}^{\mathrm{s}}$ is the YIG spin resistance calculated for a distance of d_{CoFe}. For both circuits shown in Fig. 2(a) and (b), the "spin battery" of the network is characterized by the injected spin chemical potential $\mu_{\mathrm{s,inj}}^{\mathrm{Pt2}} \propto I_{\mathrm{c}}$ at the YIG/Pt2 interface. The spin chemical potential "drop" across each detector i is given by $\mu_{\mathrm{s,det}}^{i} \propto V_{\mathrm{det}}^{i}$ with V_{det}^{i} the detector voltage signal of electrode i. For each detector i, we can then calculate the general spin transfer efficiency as $\eta_{\mathrm{s}}^{i} = \frac{\mu_{\mathrm{s,det}}^{i}}{\mu_{\mathrm{s,inj}}^{\mathrm{Pt2}}} \propto \frac{V_{\mathrm{det}}^{i}}{I_{\mathrm{c}}}$. Applying Kirchhoff's laws to the spin-resistor network shown in Fig. 2 (a) and (b), we obtain the spin transfer efficiency of the Pt1, Pt3 and CoFe detectors respectively as $\eta_{\mathrm{s}}^{\mathrm{Pt1}} = \frac{R_{\mathrm{Pt1}}^{\mathrm{s}}}{R_{\mathrm{tot}}^{\mathrm{s,A}}}$, $\eta_{\mathrm{s}}^{\mathrm{Pt3}} = \frac{R_{\mathrm{Pt3}}^{\mathrm{s}}\zeta}{R_{\mathrm{tot}}^{\mathrm{s,B}}(1+\zeta)}$ and $\eta_{\mathrm{s}}^{\mathrm{CoFe}} = \frac{R_{\mathrm{CoFe}}^{\mathrm{s}}}{R_{\mathrm{tot}}^{\mathrm{s,B}}(1+\zeta)}$. Here, $\zeta = [R_{\mathrm{int,CoFe}}^{\mathrm{s}} + R_{\mathrm{CoFe}}^{\mathrm{s}}]/[R_{\mathrm{YIG}}^{\mathrm{s}} + R_{\mathrm{int,Pt3}}^{\mathrm{s}} + R_{\mathrm{Pt3}}^{\mathrm{s}}]$ and $R_{\mathrm{tot}}^{\mathrm{s,A}}$, $R_{\mathrm{tot}}^{\mathrm{s,B}}$ are the total resistances of the spin-resistor networks in Fig. 2(a) and (b), respectively.

On the basis of these equations, we can calculate the ASH angle $\theta_{\mathrm{ASH}}^{\mathrm{CoFe}}$ of CoFe as a function of its spin diffusion length λ_{CoFe}. The result is shown in Fig. 2(c) for different magnetic fields, where $\theta_{\mathrm{ASH}}^{\mathrm{CoFe}}$ saturates as a function of λ_{CoFe} at around $\sim 7\,\mathrm{nm}$. Finally, we estimate the field dependence of $\theta_{\mathrm{ASH}}^{\mathrm{CoFe}}$ by assuming $\lambda_{\mathrm{CoFe}} = 6\,\mathrm{nm}$. Plotting $\theta_{\mathrm{ASH}}^{\mathrm{CoFe}}$ as a function of magnetic field in Fig. 2(d), we find that $\theta_{\mathrm{ASH}}^{\mathrm{CoFe}}$ rapidly increases with increasing magnetic field (as M_{CoFe} saturates) and reaches its maximum value for about 2 T-3 T at $\sim 5\,\%$.

References

[1] L. J. Cornelissen, J. Liu, R. A. Duine, J. B. Youssef, and B. J. van Wees, Nature Physics **11**, 1022–1026 (2015).
[2] S. T. B. Goennenwein, R. Schlitz, M. Pernpeintner, K. Ganzhorn, M. Althammer, R. Gross, and H. Huebl, Applied Physics Letters **107**, 172405 (2015).
[3] T. Wimmer, B. Coester, S. Geprägs, R. Gross, S. T. B. Goennenwein, H. Huebl, and M. Althammer, Applied Physics Letters **115**, 092404 (2019).

Spin Hall Magnetoresistance in Antiferromagnetic Insulators

M. Opel, S. Geprägs, J. Fischer[1]*, P. Schwenke, M. Althammer, H. Huebl, R. Gross* [2]
O. Gomonay [3,4]

Compared to ferromagnets, antiferromagnetic (AFM) materials promise improved performance for spintronic devices: they are robust against external magnetic field perturbations and allow for faster magnetization dynamics. The correct determination of their AFM state, however, is challenging due to the absence of a macroscopic magnetization. Recently [1], we demonstrated that the AFM spin structure can be probed via simple electrical transport experiments, utilizing the spin Hall magnetoresistance (SMR). Representing a well-known manifestation of spin current physics, the SMR is based on an interfacial exchange of angular momentum from the sublattice magnetizations to the conduction electrons of a metallic top electrode with large spin-orbit coupling [2, 3].

We investigate the easy-plane antiferromagnetic insulators (AFI) α-Fe_2O_3 (hematite) [4] and NiO [5] in epitaxial thin film bilayer heterostructures with a heavy metal Pt top electrode. In angle-dependent magnetoresistance (ADMR) measurements, we rotate an external magnetic field in the film plane, record the longitudinal and the transverse resistivity of Pt, and observe characteristic resistivity modulations (blue and red in Fig. 1). The data follow a sinusoidal behavior, expected from SMR theory [3] and reported earlier for prototypical collinear ferrimagnetic insulating (FMI) $Y_3Fe_5O_{12}$/Pt bilayers (black in Fig. 1) [2]. Although the 180° periodicity of the oscillations is the same for AFI/Pt and FMI/Pt, we recognize striking differences in their amplitude and phase.

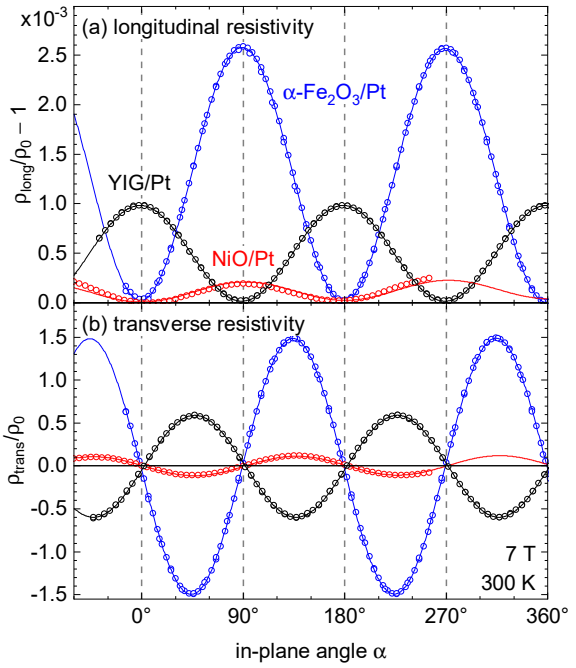

Figure 1: In-plane ADMR at 300 K in a magnetic field of 7 T of antiferromagnetic (0001)-oriented α-Fe_2O_3/Pt (blue) and (111)-oriented NiO/Pt (red) bilayers as well as a ferrimagnetic (001)-oriented $Y_3Fe_5O_{12}$ (YIG)/Pt bilayer (black). The symbols represent the normalized (a) longitudinal (ρ_{long}) and (b) transverse (ρ_{trans}) resistivities measured while rotating the magnetic field in the film plane. The data are plotted as a function of the magnetic field orientation α. The lines are fits to the data using $\cos 2\alpha$ and $\sin 2\alpha$ functions.

The ADMR of the antiferromagnetic α-Fe_2O_3/Pt (blue symbols in Fig. 1) and NiO/Pt (red symbols in Fig. 1) bilayers reveal the same angle dependence, which is, however, shifted by 90° relative to that of the ferrimagnetic insulator $Y_3Fe_5O_{12}$/Pt bilayer (black symbols in Fig. 1). To explain the data, we consider two antiferromagnetically coupled magnetic sublattices $\mathbf{M}^A$ and $\mathbf{M}^B$. In *ferrimagnets* with $|\mathbf{M}^A| > |\mathbf{M}^B|$ (e.g. $Y_3Fe_5O_{12}$), the net magnetization $\mathbf{M} = \mathbf{M}^A + \mathbf{M}^B$ will follow the external magnetic field $\mathbf{H}$, resulting in $\mathbf{M}||\mathbf{H}$. From SMR theory [3], the resistivites then write $\rho^{\mathrm{FMI}}_{\mathrm{long}}(\alpha) = \rho_0 + \frac{\rho_1}{2}(1 + \cos 2\alpha)$ and $\rho^{\mathrm{FMI}}_{\mathrm{trans}}(\alpha) = \frac{\rho_3}{2}\sin 2\alpha$. In *antiferromagnets* with $\mathbf{M}^A = -\mathbf{M}^B$

[1]Present address: Unité Mixte de Physique, CNRS, Thales, Université Paris-Sud, 91767 Palaiseau, France
[3]Institut für Physik, Johannes Gutenberg Universität Mainz, 55128 Mainz, Germany
[2]Supported by the German Research Foundation via Germany's Excellence Strategy (EXC-2111-390814868).
[4]supported by the Alexander von Humboldt Foundation, EU FET Open RIA Grant no. 766566, and the German Research Foundation (project SHARP 397322108)

(e.g. NiO), however, the situation is more complex. For magnetic field rotations in the easy plane, the magnetic sublattices rotate perpendicular to **H** within the film plane and we expect $\rho_{\text{long}}^{\text{AFI}}(\alpha) = \rho_0 + \frac{\rho_1}{2}(1 - \cos 2\alpha)$ and $\rho_{\text{trans}}^{\text{AFI}}(\alpha) = -\frac{\rho_3}{2}\sin 2\alpha$. Our data very nicely follow these expectations as demonstrated by fits according to the above equations (lines in Fig. 1).

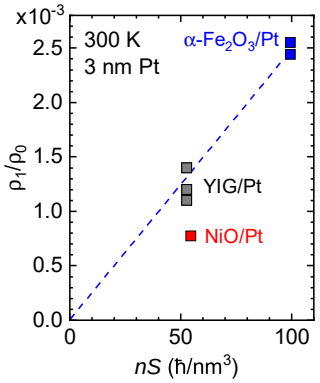

Figure 2: Scaling behavior of the maximum SMR amplitude ρ_1/ρ_0 at 300 K from different FMI/Pt [2] or AFI/Pt [4, 5] samples with a Pt thickness of 3 nm. The values are plotted versus the product of the spin S of the magnetic ions times their volume density n in the "bulk" of the FMI or AFI. The dashed blue line is a guide to the eye.

While the phase of ρ_{long} and ρ_{trans} is well understood, the amplitudes ρ_1/ρ_0 and ρ_3/ρ_0 are still a matter of debate. Our epitaxial, antiferromagnetic α-Fe_2O_3 thin films implemented in a heterostructure with a 3 nm thin Pt electrode show the highest SMR amplitudes reported in literature so far [4]. The exceptional value of $\rho_1/\rho_0 = 0.25\%$ even exceeds the established data from ferrimagnetic $Y_3Fe_5O_{12}$/Pt and points to a "more efficient" spin transfer between the spin polarization of the conduction electrons in the metallic Pt and the localized magnetic moments in the magnetically ordered insulator. Following indication that ρ_1/ρ_0 depends on the interface magnetization, we determine the volume density n of the magnetic ions in the magnetically ordered materials from the dimensions and compositions of the respective unit cells. We note that we consider *all* magnetic ions of *all* sublattices, independent of their spin orientation. We find clear evidence for a monotonous correlation between ρ_1/ρ_0 and the Fe^{3+} ion density n for $Y_3Fe_5O_{12}$/Pt ($n = 21.10\,Fe^{3+}/nm^3$) and α-Fe_2O_3/Pt ($n = 39.81\,Fe^{3+}/nm^3$). For NiO/Pt with its densely packed fcc structure, however, $n = 54.69\,Ni^{2+}/nm^3$ is highest while ρ_1/ρ_0 reaches only 0.77×10^{-3}.[5] This discrepancy is resolved by taking into account the lower spin state of $S = 1$ in Ni^{2+} as compared to $S = 5/2$ in Fe^{3+}. Remarkably, ρ_1/ρ_0 follows the same universal trend when plotted versus n times S (Fig. 2). We note that nS is equivalent to the magnetization $|\mathbf{M}|$ for *ferro*magnetic materials. In *ferri*magnets like $Y_3Fe_5O_{12}$, however, nS does not represent $|\mathbf{M}|$, but the sum of the absolute values of the sublattice magnetizations $|\mathbf{M}^A| + |\mathbf{M}^B|$. The same is true for antiferromagnets with their vanishing net magnetization.

In summary, we present a comprehensive picture of the spin Hall magnetoresistance (SMR) in ferrimagnetic and AFI/heavy metal thin film bilayer heterostructures. We show that the SMR provides information about the orientation of the Néel vector in AFIs. Since the SMR is a comparably simple method and also applicable at high magnetic fields, it could become a valuable tool for reading out magnetization states in the emerging field of AFM spintronics.

References

[1] S. Geprägs, M. Opel, J. Fischer, O. Gomonay, P. Schwenke, M. Althammer, H. Huebl, and R. Gross, Journal of Applied Physics **127**, 243902 (2020).
[2] H. Nakayama, M. Althammer, Y.-T. Chen, K. Uchida, Y. Kajiwara, D. Kikuchi, T. Ohtani, S. Geprägs, M. Opel, S. Takahashi, R. Gross, G. E. W. Bauer, S. T. B. Goennenwein, and E. Saitoh, Phys. Rev. Lett. **110**, 206601 (2013).
[3] Y.-T. Chen, S. Takahashi, H. Nakayama, M. Althammer, S. T. B. Goennenwein, E. Saitoh, and G. E. W. Bauer, Phys. Rev. B **87**, 144411 (2013).
[4] J. Fischer, M. Althammer, N. Vlietstra, H. Huebl, S. T. Goennenwein, R. Gross, S. Geprägs, and M. Opel, Phys. Rev. Applied **13**, 014019 (2020).
[5] J. Fischer, O. Gomonay, R. Schlitz, K. Ganzhorn, N. Vlietstra, M. Althammer, H. Huebl, M. Opel, R. Gross, S. T. B. Goennenwein, and S. Geprägs, Phys. Rev. B **97**, 014417 (2018).

[5] We note that in Ref. [5] ρ_1/ρ_0 for NiO/Pt did not saturate at the maximum available magnetic field of 17 T and is therefore underestimated.

Magnon Transport Experiments in Three-Terminal Yig/Pt Nanostructures Acquired via dc and ac Detection Techniques

J. Gückelhorn, T. Wimmer, S. Geprägs, H. Huebl, R. Gross, M. Althammer [1]

The search for novel routes to efficiently store and process information in electronic devices is of key relevance. In the field of spintronics, pure spin currents are discussed for information transport at low dissipation levels. In magnetically ordered insulators (MOIs), spin currents are carried by magnons, the elementary excitations of the spin system. Heterostructures consisting of spin-orbit coupled heavy metals (HM) and MOIs allow us to study pure spin current transport by all-electrical means on a fundamental level. In our experiments, we utilize the fact that in such bilayer systems incoherent magnons in the MOI can be excited electrically as well as thermally, which then can be detected electrically in the HM utilizing the inverse spin Hall effect (SHE). Recently, the manipulation of magnon currents has been shown in a three-terminal arrangement in yttrium iron garnet (YIG)/Pt bilayers [1, 2].

The design of such a device is shown in Fig. 1(a). A charge current I^{inj} is applied to a Pt strip (injector), injecting magnons into YIG via both the SHE and Joule heating. There, magnons diffuse away from the injection region and then are electrically detected via the inverse SHE as a voltage signal at a second Pt strip (detector). A dc charge current $I_{\mathrm{dc}}^{\mathrm{mod}}$ applied to a third Pt strip (modulator) placed between these two Pt strips allows us to manipulate the magnon transport from injector to detector via a SHE induced spin accumulation and Joule heating effects [1]. In our experiments, the YIG thin film with a thickness of 11 nm was grown via pulsed laser deposition on a (100)-oriented $Gd_3Ga_5O_{12}$ substrate. The three Pt strips were deposited by dc sputtering and patterned via e-beam lithography.

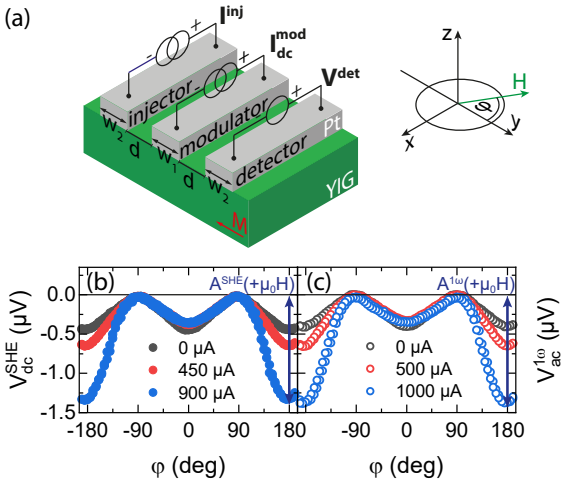

Figure 1: (a) Sample configuration and the magnetic field geometry used in the experiments. Detector signals (b) $V_{\mathrm{dc}}^{\mathrm{SHE}}$ and (c) $V_{\mathrm{ac}}^{1\omega}$ plotted as a function of the magnetic field orientation with constant magnitude $\mu_0 H = 50\,\mathrm{mT}$ for positive modulator currents $I_{\mathrm{dc}}^{\mathrm{mod}}$ at 280 K. The dc and ac detector signals induced by SHE magnon transport are in perfect agreement.

Here, we compare two measurement schemes, both allowing to investigate the magnon transport in three-terminal devices: (i) a dc-technique utilizing the current reversal method and (ii) an ac-technique based on lock-in detection [3]. For the dc-technique, we vary the dc charge current at the injector $(+I^{\mathrm{inj}}, 0, -I^{\mathrm{inj}})$, while a constant charge current $I_{\mathrm{dc}}^{\mathrm{mod}}$ is applied to the modulator. At the same time, we measure for each configuration the voltage $V_{\mathrm{dc}}^{\mathrm{det}}$ at the detector. Utilizing an advanced current reversal scheme allows us to differentiate the voltage contributions $V_{\mathrm{dc}}^{\mathrm{SHE}}$ due to the SHE-induced magnons and the contributions due to the thermally injected magnons. In contrast, for the ac-technique, we simultaneously apply an ac charge current $(I^{\mathrm{inj}} \sin(\omega t))$ to the injector and a dc charge current $I_{\mathrm{dc}}^{\mathrm{mod}}$ to the modulator and measure the detector voltage $V_{\mathrm{ac}}^{\mathrm{det}}$ via lock-in detection. While the first harmonic signal $V_{\mathrm{ac}}^{1\omega}$ corresponds to the SHE-induced magnons, the second harmonic signal is correlated to the thermally injected magnons. Both schemes allow to disentangle the detector voltages generated by I^{mod} and I^{inj}, ensuring that we only account for the magnon transport between injector and detector.

[1] We gratefully acknowledge financial support from the German Research Foundation under Germany's Excellence Strategy (EXC-2111 – 390814868) and project AL 2110/2-1.

Our theoretical detector voltage model predicts that $V_{\mathrm{dc}}^{\mathrm{SHE}}$ and $V_{\mathrm{ac}}^{1\omega}$ should be identical if only contributions linear in I^{inj} contribute. To verify this model, we conducted angle-dependent measurements for the dc and ac case as shown in Fig. 1(b) and 1(c), respectively. While we observe in both cases the distinctive $\cos^2\varphi$ modulation for magnon transport between the injector and detector for $I_{\mathrm{dc}}^{\mathrm{mod}} = 0$, the signal for $I_{\mathrm{dc}}^{\mathrm{mod}} > 0$ is significantly increased at $\varphi = \pm 180°$ and decreased at $\varphi = 0°$. Comparing the signals $V_{\mathrm{dc}}^{\mathrm{SHE}}$ and $V_{\mathrm{ac}}^{1\omega}$ we observe good agreement both regarding the angle dependence and the absolute magnitude.

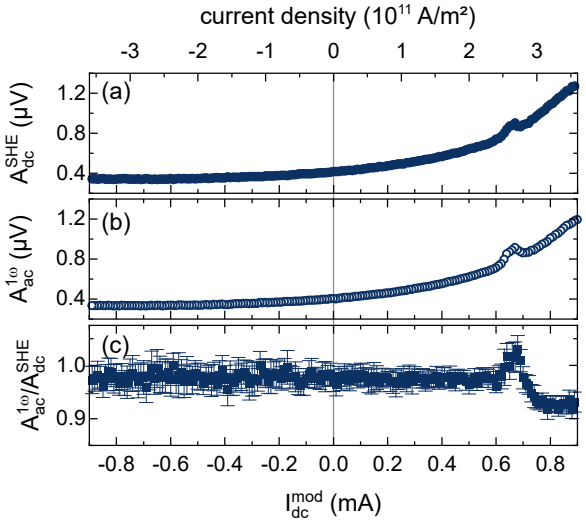

Figure 2: Extracted amplitudes (a) $A_{\mathrm{dc}}^{\mathrm{SHE}}$ and (b) $A_{\mathrm{ac}}^{1\omega}$ for $\mu_0 H = 60\,\mathrm{mT}$ of the SHE injected magnon transport signal versus the dc charge current $I_{\mathrm{dc}}^{\mathrm{mod}}$. (c) Ratio of the extracted amplitudes $A_{\mathrm{dc}}^{\mathrm{SHE}}$ and $A_{\mathrm{ac}}^{1\omega}$. For large modulator current values, the ratio clearly deviates from 1.

For a better quantitative comparison of the detected voltages, we extract the signal amplitudes $A_{\mathrm{dc}}^{\mathrm{SHE}}(+\mu_0 H)$ and $A_{\mathrm{ac}}^{1\omega}(+\mu_0 H)$ as a function of $I_{\mathrm{dc}}^{\mathrm{mod}}$, shown in Fig. 2(a) and 2(b), respectively. At first sight, both curves and signal amplitudes seem to exhibit a similar behavior. In the low bias regime ($|I_{\mathrm{dc}}^{\mathrm{mod}}| \leq 0.55\,\mathrm{mA}$) we can model the signal amplitudes by a superposition of a linear (SHE) and quadratic (Joule heating) dependence. For larger currents ($I_{\mathrm{dc}}^{\mathrm{mod}} > 0.55\,\mathrm{mA}$) the amplitudes $A_{\mathrm{dc}}^{\mathrm{SHE}}$ and $A_{\mathrm{ac}}^{1\omega}$ exhibit a pronounced deviation from this behavior. The enhanced magnon conductance is in agreement with our previous work, which we attribute to a zero effective damping state via SHE induced damping-like spin-orbit torque underneath the modulator [2]. To check whether or not the amplitudes agree for the dc and ac configuration, the ratio $A_{\mathrm{ac}}^{1\omega}/A_{\mathrm{dc}}^{\mathrm{SHE}}$ is plotted in Fig. 2(c) versus $I_{\mathrm{dc}}^{\mathrm{mod}}$. In the low and negative bias regime the ratio is nearly constant with $A_{\mathrm{ac}}^{1\omega}/A_{\mathrm{dc}}^{\mathrm{SHE}} \simeq 1$, while the ratio for $I_{\mathrm{dc}}^{\mathrm{mod}} > 0.55\,\mathrm{mA}$ exhibits a clear deviation from 1. This indicates higher order contributions to the detector voltage originating from I^{inj} and not only from I^{mod} in this regime. Furthermore, we find good agreement between our model and the thermally injected magnons, however their signals are not suitable to detect higher order contributions. For details, we refer the reader to Ref. [3].

Our experimental results demonstrate that the dc and ac techniques are both well suited to investigate incoherent magnon transport. However, while we observe a full quantitative agreement between the schemes in the low bias regime, we find clear deviations above a certain threshold. This indicates a contribution of higher order in I^{inj}, shedding new light onto nonlinear effects on the magnon conductance. Our findings contribute to the understanding of the manipulation of magnon currents using a three-terminal device, which is crucial for implementing a logic based on incoherent magnons.

References

[1] L. J. Cornelissen, J. Liu, B. J. van Wees, and R. A. Duine, Physical Review Letters **120**, 097702 (2018).
[2] T. Wimmer, M. Althammer, L. Liensberger, N. Vlietstra, S. Geprägs, M. Weiler, R. Gross, and H. Huebl, Phys. Rev. Lett. **123**, 257201 (2019).
[3] J. Gückelhorn, T. Wimmer, S. Geprägs, H. Huebl, R. Gross, and M. Althammer, Applied Physics Letters **117**, 182401 (2020).

Dark States in Phononic Networks

T. Luschmann, D. Schwienbacher, R. Gross, H. Huebl [1]

Mechanical resonator networks are currently discussed in the context of model systems giving insight into problems of condensed matter physics including effects in topological phases. Here, we discuss networks based on three high-quality factor nanomechanical string resonators (nanostrings) made from highly tensile-stressed Si_3N_4. The strings are strongly coupled via a shared support and thus can form a fully mechanical, classical multi-level system. Moreover, the individual strings are tunable in frequency, which allows us to explore their coupling behaviour using continuous wave spectroscopy and time domain techniques. Here, we extend the previous work performed on two coupled strings [1] to three coupled resonators and discuss the additional features of the inter-string dynamics, such as the formation of dark states.

We experimentally realize the three-level system in the form of three nano-mechanical string resonators sharing a disk-shaped support structure (see Fig. 1). These high-Q harmonic oscillators are freely suspended silicon nitride nano-strings labeled (A,B,C) with Q-factors in the 1.5×10^5 range. The strings are defined onto a $t_{SiN} = 90\,\text{nm}$ thick, highly tensile-strained, Si_3N_4(SiN) film using electron beam lithography and released using reactive ion etching. The central clamping pad has a diameter of 2 µm and is partially suspended (cf. Fig. 1 inset)), enabling a mechanical coupling between the individual strings' modes with a coupling rate in the kHz range. To investigate the mechanical resonators within the nano-string network, we use a free space optical interferometer, where we spatially select each of the nano-strings and optically probe their oscillation state. To avoid air-damping and maintain the high-Q factors of the strings, the whole sample is operated in vacuum ($p < 0.01\,\text{Pa}$). A previously developed frequency tuning scheme based on the geometric non-linearity [1] allows the control of the resonance frequency of the individual modes of the network.

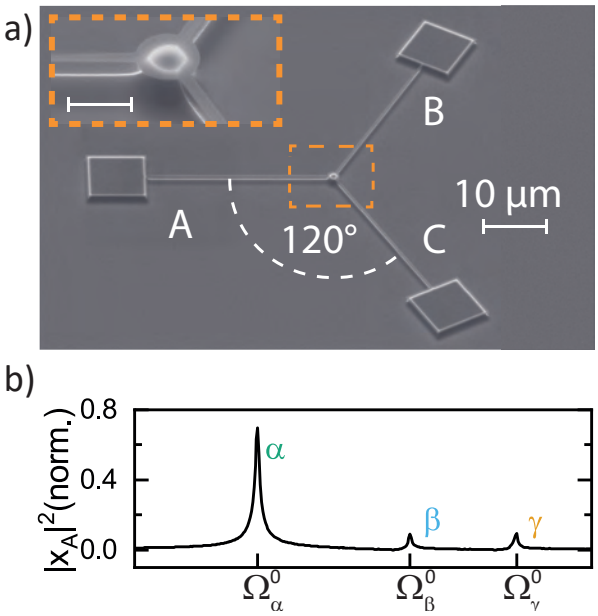

Figure 1: (a) Tilted scanning electron micrograph image of the nano-string network. Three mechanical string resonators are mechanically coupled via a disk-shaped shared support in the center of the equi-angular network. The inset shows a detailed view of the coupling region. The circular coupler (scale bar = 2 µm) is partly suspended realizing the interaction between the nano-strings. (b) Mode distribution of the string network, read out via resonator A. The modes α, β and γ are distinguishable.

Figure 1(b) shows the excitation state in terms of the squared displacement amplitude $|x_A|^2$ of nano-string A using a controlled stimulus and vector network analysis. We observe the dominant response of the mode α at Ω^0_α, which is the natural mode of the optically probed nano-string A. In addition, we detect signatures of the β and γ modes at Ω^0_β and Ω^0_γ (which can be associated with the natural modes of nano-string B and C), due to the intermodal coupling.

[1] We acknowledge funding by the EU Horizon 2020 research and innovation program under grant agreement No. 736943 and the German Research Foundation) under Germany's Excellence Strategy (EXC-2111-390814868).

For this experiment, we configure the frequencies of all three modes to become degenerate. Figure 2(a), focussing on the interaction region, shows the measured thermal displacement spectrum as function of the resonance frequency of the α mode. Initially, at $\Delta\Omega_\alpha/2\pi = \Omega_\alpha - \Omega_\alpha^0 <= 11\,\mathrm{kHz}$, the resonance frequencies are set to prepare the modes β and γ in a hybridized state with the normal mode frequencies $\Omega_+^{\beta,\gamma}$ and $\Omega_-^{\beta,\gamma}$ located at $\Delta\Omega/2\pi$. We then increase the frequency of mode α towards $\Omega_+^{\beta,\gamma}$ and $\Omega_-^{\beta,\gamma}$ until we reach the region of interest, where all modes are resonant with each other and investigate the characteristic spectrum by optically probing the displacement of nano-string B. At $\Delta\Omega_\alpha/2\pi = 11\,\mathrm{kHz}$, the crossing of the β and γ mode can be treated independently of the third mode and an analytic description of the spectrum is possible. However, this changes as soon as the α mode starts to interact with the hybridized modes ($12\,\mathrm{kHz} <= \Omega_\alpha/2\pi <= 16\,\mathrm{kHz}$). This becomes apparent from the formation of an avoided crossing between mode α and the lower branch of the initially hybridized β and γ modes and the shift of the $\Omega_+^{\beta,\gamma}$ branch to higher frequencies. At around $\Delta\Omega_\alpha/2\pi = 14\,\mathrm{kHz}$, we find a suppression of the thermal displacement of one of the modes, i.e. a dark state. Here, the uncoupled frequencies of mode α, β, and γ become degenerate and the central of the three hybridized modes quenches. While analytic models cannot grasp the full richness of the spectrum, numerical simulations can be used to predict the frequency and amplitude evolution as shown in Fig. 2 b). Here, we have encoded the simulated displacement noise amplitude in the size of the symbols. Given the independently determined coupling strengths, we find an excellent agreement between our observations and modelling.

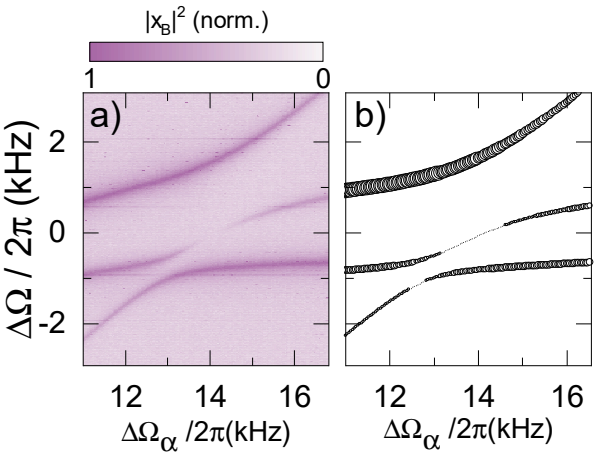

Figure 2: a) Thermal displacement spectrum of nano-string B showing the normalized mechanical response $|x_B|^2$ during a tuning sequence which tunes all three modes to a degenerate frequency. At $\Delta\Omega_\alpha/2\pi \approx 14\,\mathrm{kHz}$ we observe the quenching of one of the modes, i.e. the appearance of a dark mode. (b) Numerical simulation of the resonance frequencies from the measurement shown in (a). The area of the data-points shows the amplitude of the mode at a given point in the spectrum. A bias was added to make small amplitudes, especially in the range of the dark-mode, visible.

In summary, we experimentally investigated a nano-string network comprised of three nano-mechanical resonators with independently tunable resonance frequencies. This configuration allows us to test the complex problem of a fully coupled three-level system and examine configurations with and without the existence of an analytic description, a situation which is closely related to the classical analog of the generalized Landau-Zener problem. We explored the formation of dark states, which are of relevance in the context of information storage, as they are considered to offer an improved robustness against noise. For more details we refer the reader to Ref. [2], where we have also investigated the temporal evolution in the fully coupled regime.

References

[1] M. Pernpeintner, P. Schmidt, D. Schwienbacher, R. Gross, and H. Huebl, Phys. Rev. Applied **10**, 34007 (2018).
[2] D. Schwienbacher, T. Luschmann, R. Gross, and H. Huebl, arXiv:2011.08080 [cond-mat] (2020). arXiv:2011.08080 [cond-mat].

Application–Oriented Research

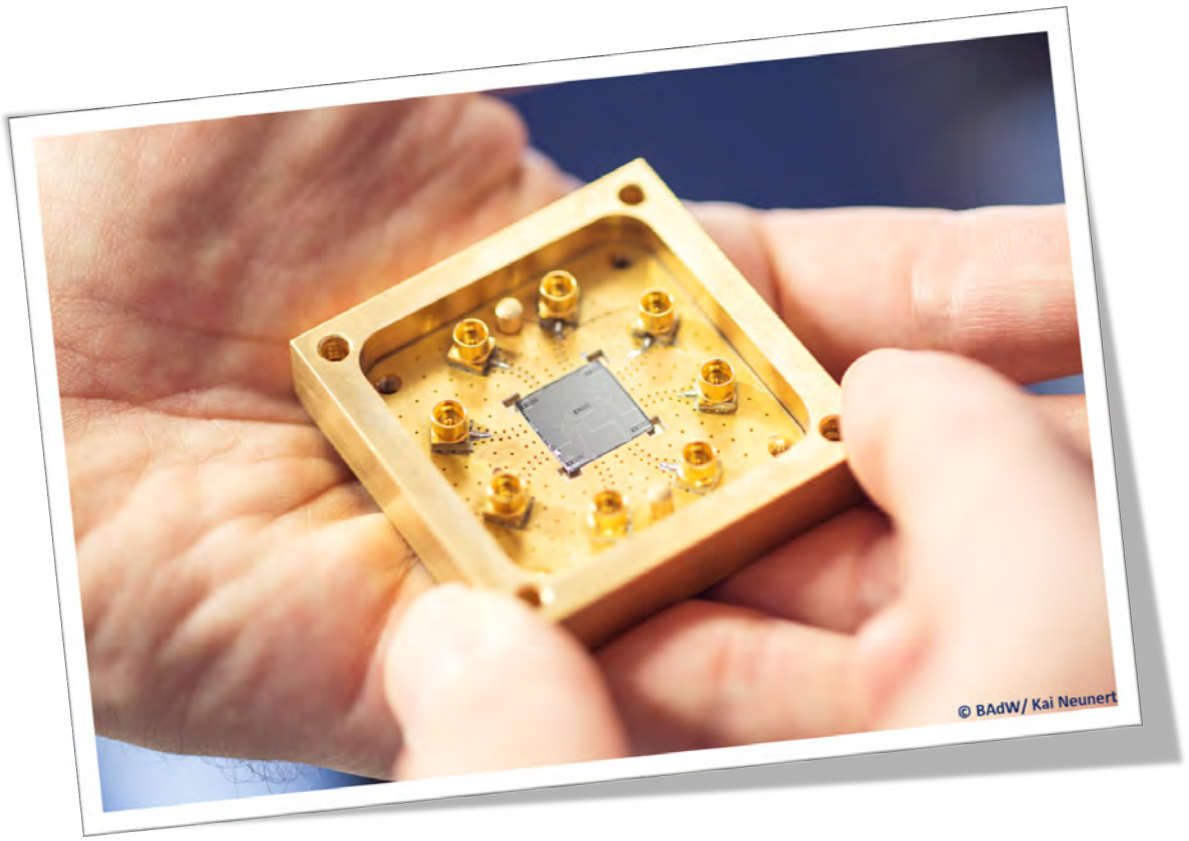

Towards a Salable Millikelvin Cryolink Between Two Dilution Refrigerators

F. Deppe, M. Renger, M. Partanen, S. Pogorzalek, Q.-M. Chen, Y. Nojiri, A. Marx, K. G. Fedorov, R. Gross, [1]

Traditionally, quantum communication is dominated by optical frequencies because of their small susceptibility to room temperature thermal fluctuations and their potential compatibility with existing glass fiber networks appear favorable for the signal transmission process itself. This mindset makes sense when one wants to encode classical information in a intrinsically secure way. However, a true quantum internet should transmit quantum information between multiple quantum computing nodes. Hence, the properties of the nodes become even more important than those of the signal transmission. As it turns out, the to date most promising platform for quantum computing are superconducting circuits, which operate at microwave frequencies and millikelvin temperatures inside dilution refrigerators. Here, established IT companies (Google, IBM, Intel) and eager start-ups (Rigetti, IQM, etc.) have already developed chips with up to 50 qubits without jeopardizing gate fidelities above 99 %.

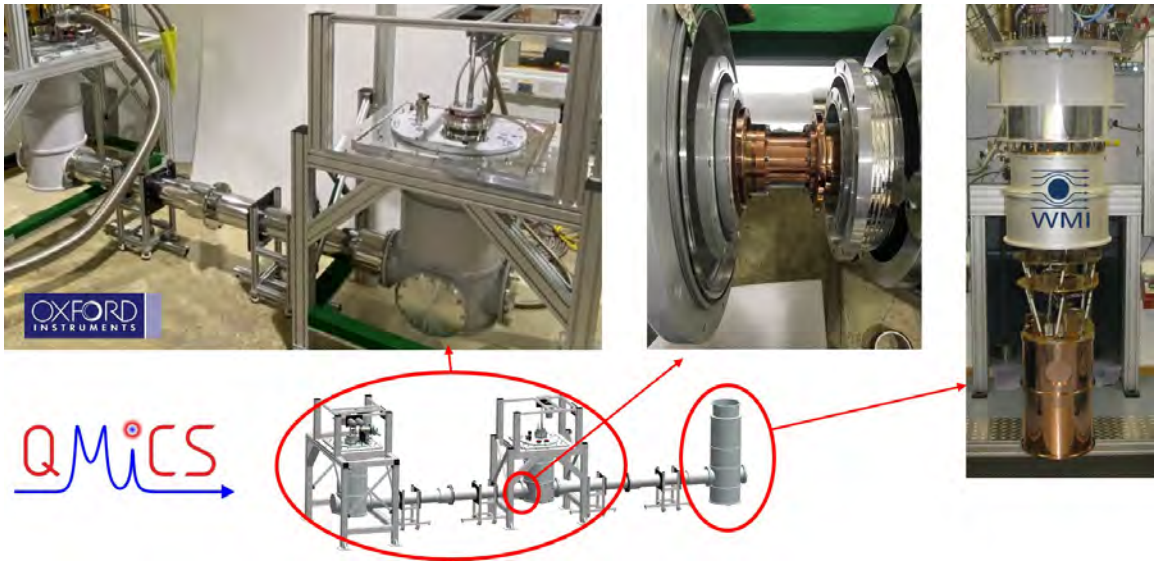

Figure 1: Cryolink between two dilution refrigerators. Bottom: CAD drawing of final layout. Top left: Installation during factory acceptance test at OINT. Top center: opened connection between link element and port of the CNN tailset. Top right: Alice fridge at WMI with partially mounted tailset.

The obvious next step is to think how to interconnect such chips to local area quantum networks (QLAN) or even quantum supercomputers. The key problem is here that, despite years of research efforts, optics-to-microwave man microwave-to-optics conversion has not even reached the percent level for actual quantum states. Furthermore, the compatibility of the fabrication process for such converters with that of high-performance superconducting qubits is unclear. Therefore, WMI as an institute with considerable cryogenics knowhow focuses on quantum microwave communication for QLAN applications. Our approach has two important advantages. First, microwaves are the natural frequency scale of superconducting quantum circuits and, therefore, frequency conversion losses trivially vanish. Second, since superconducting quantum processors require cooling in dilution fridges anyways, the cryogenic challenge reduces to the development of a suitable millikelvin cryolink be-

[1] We acknowledge support by the German Research Foundation under Germany's Excellence Strategy (EXC-2111 – 390814868), the Elite Network of Bavaria through the graduate program ExQM, and the EU Flagship project QMiCS (Grant No. 820505).

Figure 2: Cryolink between two dilution refrigerators. Left: CNN with all four link segments connected. Right: Bob fridge.

tween two fridges. We perform this task within the EU quantum Flagship project QMiCS (https://qmics.wmi.badw.de) together with our partner Oxford Instruments Nanotechnology Ltd. (OINT).

Photographic impressions of the installation are shown in Fig. 1. Specifically, the cryolink should connect a WMI homemade fridge ("Alice fridge") over a distance of 6.6 m to a commercial dilution refrigerator from OINT ("Bob fridge") via an intermediate cryogenic networking node (CNN). The CNN ensures straightforward scalability to larger distances and allows signals to be routed between fridges in multiple directions to create a truly interconnected quantum network. For Alice fridge, WMI and OINT have designed a suitable customized tailset with ports for the cryolink. Alice fridge, the CNN, and Bob fridge are located in different, neighboring labs at WMI. In a first step, Bob fridge and the CNN have been connected by the half cryogenic link over a distance of 3.3 m. Temperatures achieved at the center of the link are found to be as low as 35 mK (factory acceptance test at OINT, nuclear orientation thermometry) and 35 mK (site acceptance test at WMI, resistance thermometry).

After the successful site acceptance test of the half link, all four link segments have been connected to the CNN as shown in Fig. 2. Bob fridge has been wired with four microwave lines, 72 additional twisted-pair dc lines, two 4–8 GHz cryogenic high-electron-mobility transistor amplifiers, and cryogenic circulators. Furthermore, the pumps of Bob fridge have been moved out of the original pump rack to account for the limited space in the labs. Notably, a recent cool-down of Bob fridge has shown no noticeable performance changes. In collaboration with the external company KEYCOM, we have found a scalable way to produce impedance-matched superconducting NbTi coaxial cables [1]. We have measured the loss at 6 GHz to be as low as 2 dB/km, a value comparable to commercial optical fibers.

In summary, WMI has almost finished installing and testing the cryolink developed by QMiCS partner OINT. So far, performance is well within specifications. Currently, WMI is about to insert three low-loss coaxial NbTi microwave cables into the full link, followed by final mechanical, thermal, and transmission tests.

References

[1] M. Pfeiffer. *Superconducting cables for quantum microwave communication*. Bachelor's thesis, Technische Universitä München (2020).

Interferometric Josephson Mixer for Quantum Microwave Circuits

M. Partanen, S. Gandorfer, K. G. Fedorov, S. Pogorzalek, M. Renger, J. Lamprich, Q.-M. Chen, Y. Nojiri, A. Marx, R. Gross, F. Deppe [1]

A Josephson mixer (JM) is a versatile tool for signal processing and transformation in circuit quantum electrodynamics. An especially relevant application of JMs is the quantum radar protocol [1], which utilizes entanglement in continuous-variable propagating microwaves emitted by Josephson parametric amplifiers (JPAs) [2, 3]. Earlier implementations of the JM were typically based on a Josephson ring modulator [4, 5]. However, these devices operate in a frequency-nondegenerate mode, while the frequency degenerate JM was missing so far. Importantly, the frequency-degenerate scheme promises straightforward bandwidth multiplexing, while frequency-nondegenerate approaches are expected to suffer from frequency crowding issues. Here, we report on a frequency-degenerate JM built from separate, well-characterized components. Notably, building the JM from separate components enables one to optimize and control each component separately. Thus, it is more straightforward to utilize the JM in a specific application.

Our JM circuit is structured as an interferometer, which enables the desired input-output relations, as discussed below. Interferometers are of fundamental importance in high-precision measurements in modern physics. They take the advantage of the wave nature of the electromagnetic radiation in terms of constructive and destructive interference. Our circuit resembles the well-known Mach-Zehnder interferometer and is schematically presented in Fig. 1. The interferometer consists of two commercial 180° hybrid ring beam splitters (splitting ratio 50:50), and two custom-made flux-driven JPAs. Furthermore, we separate the incoming and reflected signal with a circulator before each JPA. The hybrid rings, JPAs, and circulators are connected using superconducting (NbTi) coaxial cables.

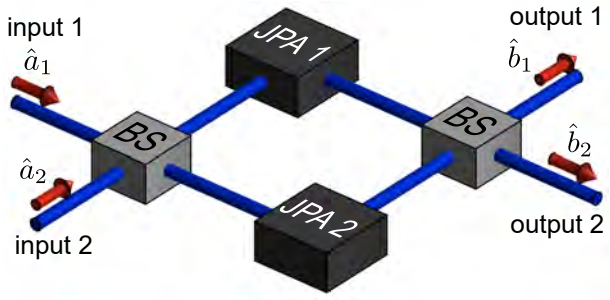

Figure 1: Schematic presentation of the circuit. Two microwave input lines are connected to a hybrid ring beam splitter (BS). Subsequently, the signal in each branch enters a Josephson parametric amplifier (JPA 1 and JPA 2). Input and output signals from both JPAs are separated by a circulator (not explicitly shown). Both signal paths are then recombined by a second BS. The components are connected with low-loss superconducting coaxial cables (blue). The annihilation operators at the input and output ports are denoted by $\hat{a}_i$ and $\hat{b}_i$, $i \in \{1, 2\}$.

We operate the JPAs in the phase-sensitive amplification mode. We can adjust the amplification gain and angle individually for both JPAs by changing the amplitude or phase of the respective pump tone. Thus, we can adjust the JPA parameters to obtain the typical input-output relation for the JM,

$$\begin{pmatrix} \hat{b}_1 \\ \hat{b}_2 \end{pmatrix} = \begin{pmatrix} \sqrt{G}\hat{a}_1 + \sqrt{G-1}\hat{a}_2^\dagger \\ \sqrt{G}\hat{a}_2 + \sqrt{G-1}\hat{a}_1^\dagger \end{pmatrix}, \tag{1}$$

where the gain G is assumed to be equal for both JPAs.

[1] We thank K. Inomata and Y. Nakamura for providing the Josephson parameteric amplifiers used in these experiments. We acknowledge support by the German Research Foundation under Germany's Excellence Strategy (EXC-2111 – 390814868), the Elite Network of Bavaria through the graduate program ExQM, and the EU Flagship project QMiCS (Grant No. 820505).

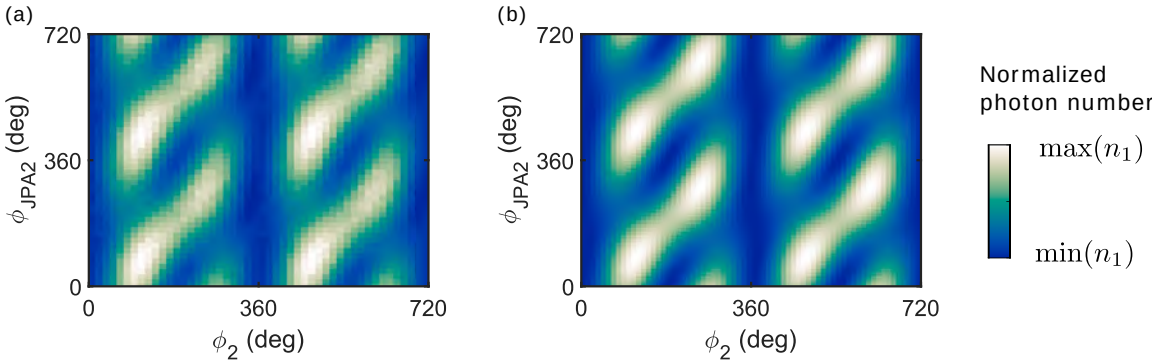

Figure 2: (a) Experimental and (b) theoretical photon number n_1 at output 1 as a function of phase ϕ_2 of the coherent signal incident at input 2 and the amplification phase ϕ_{JPA2} of at JPA 2. Here, the phases of input 1 and JPA 1 are kept constant, $\phi_1 = \phi_{JPA1} = 0$. In order to better visualize the periodic response, we plot the data with a measurement span of 360° in both directions over a range of 720°. The periodic structure of the measurement results allows for an accurate *in-situ* calibration of phase offsets. The circuit is operated at a frequency of 5.4 GHz.

We investigate the JM circuit at a temperature of approximately 50 mK generated by a home-made dilution refrigerator. The operation frequency of the JPAs is adjusted by applying dc bias currents to external superconducting coils, which introduce a magnetic flux through a superconducting quantum interference device of the JPA. We demonstrate the operation of the JM circuit over a broad range of control parameters. To this end, we apply coherent input signals to the two input ports with phases ϕ_1 and ϕ_2. Furthermore, we control the amplification angles ϕ_{JPA1} and ϕ_{JPA2}. We compare the experimental results to theoretical predictions obtained using a quantum mechanical model similar to the one used in Ref. [3]. For simplicity, we omit losses in the theory model and assume a unidirectional photon transfer. The experimental and theoretical results exhibit excellent agreement as shown in Fig. 2. Hence, the circuit can be operated as a JM by carefully selecting the control parameters.

In the future, our JM with an interferometric structure may find applications in quantum sensing applications. In particular, the frequency degenerate scheme [1] with a JM appears a promising candidate for a quantum radar with a sensitivity beyond the limits achievable by classical methods.

References

[1] U. Las Heras, R. Di Candia, K. G. Fedorov, F. Deppe, M. Sanz, and E. Solano, Sci. Rep. **7**, 9333 (2017).
[2] K. G. Fedorov, S. Pogorzalek, U. Las Heras, M. Sanz, P. Yard, P. Eder, M. Fischer, J. Goetz, E. Xie, K. Inomata, Y. Nakamura, R. Di Candia, E. Solano, A. Marx, F. Deppe, and R. Gross, Sci. Rep. **8**, 6416 (2018).
[3] S. Pogorzalek, K. G. Fedorov, M. Xu, A. Parra-Rodriguez, M. Sanz, M. Fischer, E. Xie, K. Inomata, Y. Nakamura, E. Solano, A. Marx, F. Deppe, and R. Gross, Nat. Commun. **10**, 2604 (2019).
[4] N. Bergeal, F. Schackert, M. Metcalfe, R. Vijay, V. E. Manucharyan, L. Frunzio, D. E. Prober, R. J. Schoelkopf, S. M. Girvin, and M. H. Devoret, Nature **465**, 64–68 (2010).
[5] E. Flurin, N. Roch, J. D. Pillet, F. Mallet, and B. Huard, Phys. Rev. Lett. **114**, 090503 (2015).

Automated Calibration and Control of Superconducting Resonators with Tunable Nonlinearity

Q.-M. Chen, M. Fischer, Y. Nojiri, S. Pogorzalek, M. Renger, M. Partanen, K. G. Fedorov, A. Marx, F. Deppe, R. Gross [1]

Superconducting nonlinear resonators are useful devices for quantum simulation because of the good control and long coherence time. Here, we investigate a system of two coupled superconducting nonlinear resonators with a nonlinearity tunable over two orders of magnitude [1]. As the first step towards quantum simulation, we develop an automated procedure allowing us to characterize both system Hamiltonian and dissipation rates, and to realize *in-situ* tuning of the resonance frequencies and nonlinearities of the two resonators.

Using standard circuit quantization [2, 3], we write the full system description as

$$H = \sum_{j=1,2} \omega_j a_j^\dagger a_j + U_j a_j^\dagger a_j^\dagger a_j a_j + g_{12}\left(a_1^\dagger a_2 + a_1 a_2^\dagger\right) + \xi_j\left(a_j e^{i\omega_{\mathrm{d}_j} t} - a_j^\dagger e^{-i\omega_{\mathrm{d}_j} t}\right), \tag{1}$$

$$\dot{\rho} = -i\left[H, \rho\right] + \sum_{j=1,2} \frac{\gamma_{\mathrm{in}_j} + \gamma_{\mathrm{ex}_j}}{2}\left(2a_j \rho a_j^\dagger - a_j^\dagger a_j \rho - \rho a_j^\dagger a_j\right). \tag{2}$$

Here, ω_j, U_j, γ_{in_j}, and γ_{ex_j} are the resonance frequency, Kerr-nonlinearity, internal and external dissipation rates of the resonator mode a_j, respectively. The quantity ξ_j is the strength of the driving field with frequency ω_{d_j} that is applied to the jth resonator, and g_{12} is the coupling strength between the two resonators. Besides controlling frequency and strength of the microwave driving fields, we also apply the currents I_1 and I_2 to the two on-chip antennas to tune the frequencies and nonlinearities of the two resonators. A sample photograph is shown in Fig. 1(a).

The challenge of a full calibration of the described driven-dissipative system includes, but is not limited to, the large parameter space and the dependence among different parameters. These effects make manual fitting of the model to the acquired data difficult. In addition, the calibration should be repeated several times in future experiments. Hence, we develop an automated and standardized procedure that allows us to characterize the full system with little human intervention and thus enables *in-situ* tuning of the resonance frequencies and nonlinearities of the two resonators. The automated calibration procedure consists of four major steps:

1. **Closed system calibration:** Sweep the two antenna currents and measure the reflection coefficient for both resonators. By fitting 15 parameters, one obtains a calibration of the closed-system parameters from Eq. (1), such as ω_j, U_j, and g. In this way, one achieves individual control of the frequency and nonlinearity of the two resonators [4].
2. **Open system calibration:** Tune one resonator to the desired frequency while detuning the other one, and measure the reflection coefficient of the former. By applying a circle fitting procedure [5], one obtains the decay rates, γ_{in_j} and γ_{ex_j}, in Eq. (2).
3. **Output line calibration:** Actively heat a thermally weakly coupled 30 dB attenuator in either of the sample inputs, and measure power of the reflected signal at a frequency 200 MHz off-resonant to the resonator. By following the method introduced in Ref. [6], one obtains the power gain G_j and noise temperature, T_j, of the two output channels. These parameters will be used to calculate the photon numbers $\langle a_j^\dagger a_j \rangle$ inside the resonators.

[1] We acknowledge support by the German Research Foundation under Germany's Excellence Strategy (EXC-2111 – 390814868), the Elite Network of Bavaria through the graduate program ExQM, and the EU Flagship project QMiCS (Grant No. 820505).

(a)

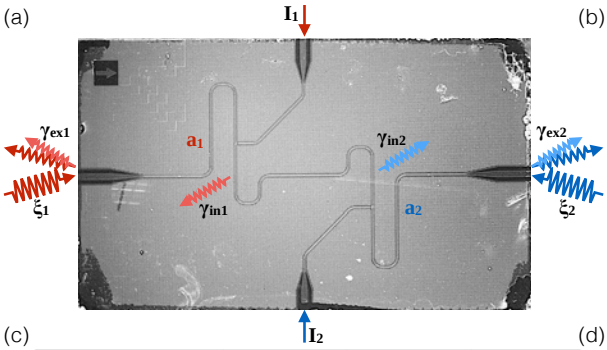

(b)

CPW resonator	
length L	7.395×10^{-3} m
inductance per meter l	4.598×10^{-7} H
capacitance per meter c	1.697×10^{-10} F
SQUID #1, #2	
critical current I_{J_1}, I_{J_2}	1.566×10^{-6} A, 1.416×10^{-6} A
shunting capacitance C_{J_1}, C_{J_2}	9.394×10^{-16} F, 1.168×10^{-15} F
asymmetry d_{J_1}, d_{J_2}	2.136×10^{-1}, 1.937×10^{-1}
Antenna #1, #2	
flux offset $\Phi_{1,\mathrm{off}}$, $\Phi_{2,\mathrm{off}}$	$-3.902 \times 10^{-1}\,\Phi_0$, $-1.149 \times 10^{-1}\,\Phi_0$
flux change per current $d\Phi_1/dI_1$, $d\Phi_2/dI_1$	$6.088 \times 10^{-4}\,\Phi_0$/A, $9.927 \times 10^{-4}\,\Phi_0$/A
flux change per current $d\Phi_1/dI_2$, $d\Phi_2/dI_2$	$-3.715 \times 10^{-5}\,\Phi_0$/A, $-5.054 \times 10^{-4}\,\Phi_0$/A

(c)

resonant frequency ω_2	6.9362 GHz	7.0831 GHz	7.1225 GHz
loaded quality factor Q_{l_2}	3524.8	6977.6	9348.1
internal quality factor Q_{i_2}	3932.6	9658.5	13613.3
external quality factor Q_{c_2}	$32700.3 - 6505.5i$	$24201.4 - 4763.2i$	$29836.7 - 56.7i$
internal decay rate γ_{i_2}	$2\pi \times 1763.8$ kHz	$2\pi \times 733.4$ kHz	$2\pi \times 523.2$ kHz
external decay rate γ_{c_2}	$2\pi \times 204.0$ kHz	$2\pi \times 281.8$ kHz	$2\pi \times 238.7$ kHz

(d)

CH #1	7.0 GHz	CH #2	7.0 GHz
Power gain G_1	116.63 dB	Power gain G_2	109.94 dB
Noise temperature T_1	3.34 K	Noise temperature T_2	4.32 K
Input Attenuation A_1	111.33 dB	Input Attenuation A_2	108.61 dB

Figure 1: (a) Optical photograph of the two-resonator sample. (b)-(d) Results of the automated calibration procedure (closed-system, open-system, output line, input line) described in the main text for one example working point.

4. **Input line calibration:** Apply an off-resonant driving field to either of the sample inputs and measure the power of the reflected signal. In combination with the above results, one can calibrate the driving strength, ξ_j from Eq. (1) [7].

In each step, an optimal calibration of the relevant parameters are obtained by numerical optimization algorithms. It results in a calibration precision not accessible in a manual fashion. Among different steps, the intermediate results are exchenged automatically without possible conflicts regarding parameter interdependence. Figures 1(b)-(d) summarizes the central calibration results of the described automated procedure for a particular working point. The values agree well with the expectations from the design and previous manual simulation results. For example, the calibrated characteristic impedance of the transmission line resonator is found to be 52 Ω, which is very close to the design value of 50 Ω.

In summary, we have developed an automated procedure that realizes a full calibration of a driven-dissipative system consisting of two flux-tunable tunable nonlinear resonators. The automation and standardization of the processes greatly reduces the effort required for calibration, which allows us to precisely and reliably tune the system parameters *in situ*. Our work paves the way to the next, more complex experiments towards quantum simulation with this device.

References

[1] M. Fischer, Q.-M. Chen, C. Besson, P. Eder, J. Goetz, S. Pogorzalek, M. Renger, E. Xie, M. J. Hartmann, K. G. Fedorov, A. Marx, F. Deppe, and R. Gross. In-situ tunable nonlinearity and competing signal paths in coupled superconducting resonators. Submitted for publication, arXiv:2009.13492 (2020).
[2] M. Leib, F. Deppe, A. Marx, R. Gross, and M. J. Hartmann, New Journal of Physics **14**, 075024 (2012).
[3] J. Bourassa, F. Beaudoin, J. M. Gambetta, and A. Blais, Phys. Rev. A **86**, 013814 (2012).
[4] Q.-M. Chen, Y. Nojiri, S. Pogorzalek, M. Renger, K. G. Fedorov, A. Marx, F. Deppe, and R. Gross. Automated calibration and tuning of an array of superconducting nonlinear resonators. Unpublished (2020).
[5] Q.-M. Chen, Y. Nojiri, S. Pogorzalek, M. Renger, K. G. Fedorov, A. Marx, F. Deppe, and R. Gross. Determination of internal and external quality factors for coplanar waveguide resonators. Unpublished (2020).
[6] M. Mariantoni, E. P. Menzel, F. Deppe, M. A. Araque Caballero, A. Baust, T. Niemczyk, E. Hoffmann, E. Solano, A. Marx, and R. Gross, Phys. Rev. Lett. **105**, 133601 (2010).
[7] F. R. Ong, M. Boissonneault, F. Mallet, A. Palacios-Laloy, A. Dewes, A. C. Doherty, A. Blais, P. Bertet, D. Vion, and D. Esteve, Phys. Rev. Lett. **106**, 167002 (2011).

Leakage Reduction in Superconducting Qubit Gates via Optimal Control

S. Filipp [1]
M. Werninghaus, F. Roy, D. Egger[2]*, S. Machnes, F. Wilhelm*[3]

Superconducting qubits are a promising candidate to realize large scale quantum computing systems. Reaching high speed, high fidelity qubit operations requires precise control over the shape of the underlying pulses. For weakly anharmonic systems, such as superconducting transmon qubits, short gates lead to leakage to states outside of the computational subspace. Control pulses designed with open-loop optimal control may reduce such leakage. However, model inaccuracies can severely limit the usability of such pulses.

In our recent publication [1], we implemented a closed-loop optimization that simultaneously adapts all control parameters based on measurements of a cost function built from Clifford gates. We directly optimize the amplitude and phase of each sample point of the digitized control pulse. We thereby fully exploit the capabilities of the pulse generation electronics and create a 4.16 ns single-qubit pulse with 99.76 % fidelity and 0.044 % leakage. This is a seven-fold reduction of the leakage rate and a three-fold reduction in standard errors of the best DRAG pulse we have calibrated at such short durations on the same system.

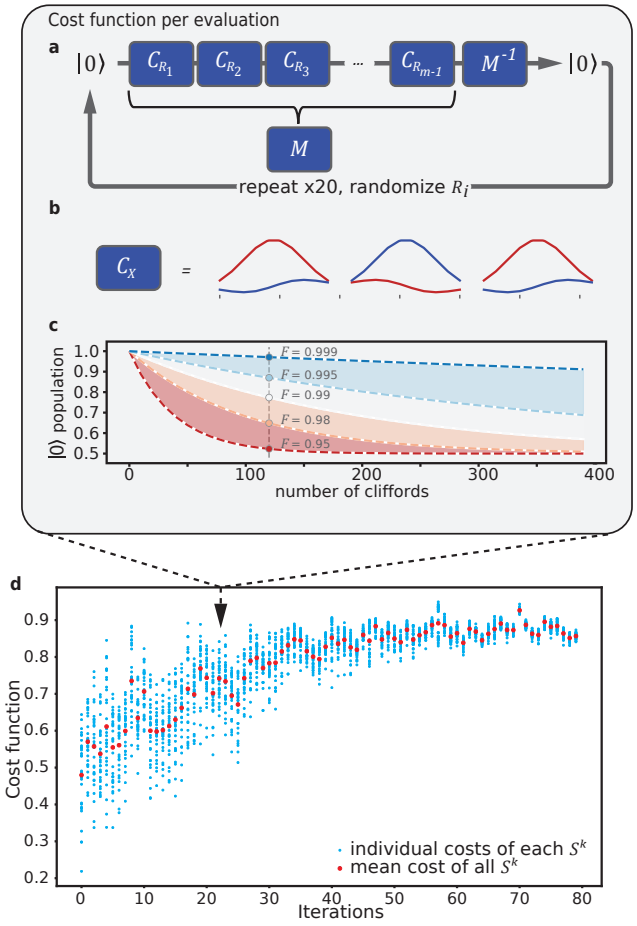

Figure 1: Schematic visualization of the composition of a Clifford gate from pulses based on a specific pulse shape. The Inphase- and Quadrature- components of the pulse envelopes are displayed in red and blue, respectively. (c) Simulated datasets showing the cost function for m=120 Clifford gates as a point on the full randomized benchmarking curves for several fidelities. (d) Experimental data of a full optimization run for a 23-dimensional parameter space. The blue points represent the cost function of each candidate pulse shape based on a unique parameter set evaluated using 20 Clifford sequences. The red points represent the average cost function at each iteration of the optimizer.

We have focused on improving the efficiency of the data extraction to tune-up qubit gates implemented by complex pulses. We have implemented restless measurements [2] as well as the multi-variable optimization algorithm CMA-ES, replacing conventional one-dimensional methods such as Nelder-Mead. We have implemented ORBIT, an indicator of gate fidelity based on Randomized Benchmarking, as a cost function to optimize. It relies on fixed-length sequences of Clifford gates which are designed to perform a net-identity

[1]This work was supported by the European Commission Marie Curie ETN QuSCo (Grant Nr. 765267), the IARPA LogiQ program under contract W911NF-16-1-0114-FE and the ARO under contract W911NF-14-1-0124.
[2]IBM Quantum, IBM Research Zurich
[3]Saarland University

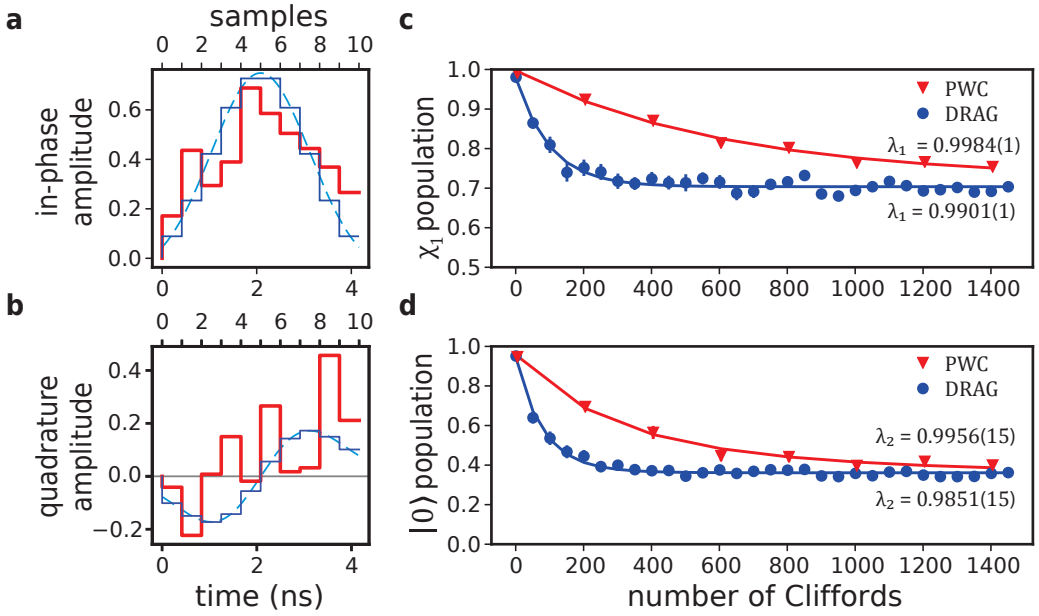

Figure 2: Black box optimized pulses; (a) in-phase and (b) quadrature component of the initial (blue) and updated pulses (red). (c) population in the computational subspace versus length of randomized benchmarking sequences. (d) remaining population in the ground state of the qubit versus length of randomized benchmarking sequences.

operation, see Fig. 1(a). Each Clifford gate is composed from up to three pulses based on the same pulse shape applied with different phase offsets. Figure 1(c) shows the behavior of full Randomized benchmarking curves as well as the ORBIT sequence at $m = 120$ Clifford gates for different average gate fidelities of the Clifford gateset. As a result, the optimization simultaneously optimizes the pulse shape and the Clifford gateset derived from it. We have recently demonstrated that we are able to reliably optimize pulse shapes with up to 55 parameters using this method, see Fig. 1(d).

Our findings show that the methods above enable the design of complex pulses which outperform commonly used pulse shapes by a large margin when using fast controls. We perform a black-box optimization to iterate on state-of-the-art pulse shapes using piecewise-constant amplitude corrections resulting in vastly different pulse shapes, see Fig. 2. We characterize the leakage of the optimized pulses by measuring the amount of qubit population outside of the computational subspace χ_1 with leakage randomized benchmarking measurements. The pulses optimized with our methods achieve a significant reduction of leakage and standard errors alike.

References

[1] M. Werninghaus, D. J. Egger, F. Roy, S. Machnes, F. K. Wilhelm, and S. Filipp. Leakage reduction in fast superconducting qubit gates via optimal control. arXiv:2003.05952 [quant-ph] (2020).
[2] M. Rol, C. Bultink, T. O'Brien, S. de Jong, L. Theis, X. Fu, F. Luthi, R. Vermeulen, J. de Sterke, A. Bruno, and et al., Phys. Rev. Appl. 7 (2017).

Materials, Thin Film and Nanotechnology, Experimental Techniques

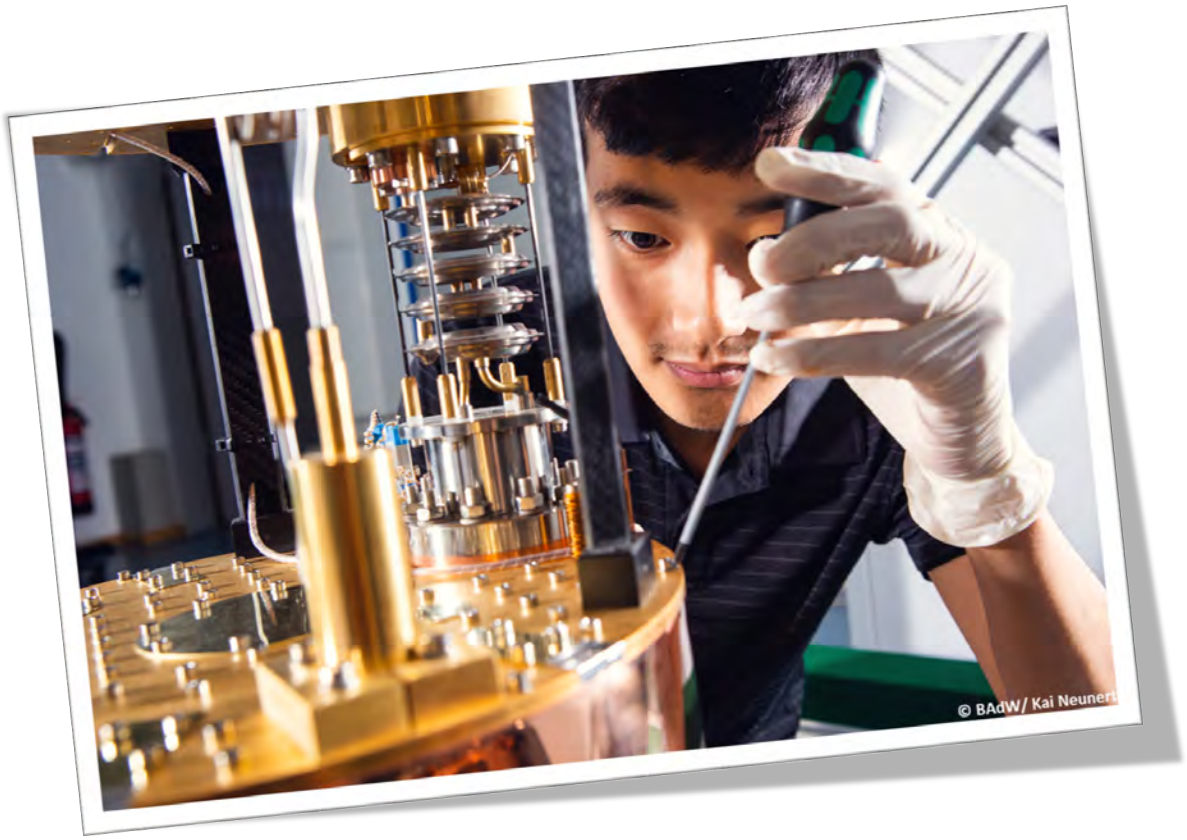

Dielectric Loss Analysis of Evaporated Superconducting Aluminum Resonators

Y. Nojiri, C. Scheuer, Q.-M. Chen, M. Renger, K. G. Fedorov, A. Marx, F. Deppe, R. Gross [1]

Quantum computers based on superconducting circuits have received much attention in the are of quantum information, quantum simulation, and quantum engineering. Meanwhile, several companies are working in this field (e.g., Google, IBM, Rigetti, IQOM), and some of them are offering first devices with several 10s of physical qubits for commercial use. Nevertheless, also research laboratories must keep optimizing their fabrication process to an extent allowing them to investigate novel paths and aspects. In this context, one important aspect is a long coherence time to preserve quantum information. One of the main hurdles for realizing a good superconducting qubit is the internal loss related to the substrate surface. This can originate from two-level-systems formed by defects in the substrate and oxides between the metal/surface interfaces [1, 2] or from the resist, which contaminates the insulator part of Josephson junctions and results in an "aging" effect [3, 4]. Indeed, the current WMI fabrication process yields coherence times of 1–5 µs, while other groups already achieve coherence times on the order of 100 µs. Due to its small area, the junction itself does not limit the qubit coherence in the current WMI process. Here, we therefore investigate the internal quality factor of coplanar waveguide aluminum resonators at millikelvin temperatures to optimize our fabrication process. Sweeping both probe power and sample temperature, we are able to separate the two-level-systems from the quasi-particle contribution [2, 5]. The inverse internal quality factor δ_i (loss tangent) can be decomposed into a power- and temperature-dependent part δ_TLS (two-level-systems), an only temperature-dependent part (thermal quasi-particles) δ_qp, and other losses δ_0 (including eddy currents, non-thermal quasi-particles, etc.) [2, 5].

$$\delta_\mathrm{i}(P,T) = \delta_\mathrm{TLS,0}\frac{\tanh(\hbar\omega_\mathrm{r}/2k_\mathrm{B}T)}{\sqrt{1+(P/P_\mathrm{c})^{\beta/2}}} + \delta_\mathrm{qp}(T) + \delta_0\,. \tag{1}$$

Here, $\delta_\mathrm{TLS,0}$ is the zero-temperature loss tangent due to two-level-systems, ω_r the resonance frequency, P_c the characteristic power for two-level system saturation, β an empirical exponent, P the probe power, T the temperature, $\hbar$ the reduced Planck constant, and k_B the Boltzmann constant.

Our standard fabrication process consists of the following steps: cleaning of the high-resistivity silicon substrate from protective resist, spin coating of the actual resist, electron beam lithography, resist development, evaporation of aluminum and oxidation , and lift-off. The oxidation is not strictly necessary for resonators, but is kept since it will be required for the Josephson junctions later. In a first step, we focus on the surface cleaning at the beginning of the process and before depositing the Al film. From literature, various improvements are known: ashing, Ar ion milling, hydrofluoric acid treatment, and annealing [1, 3, 6]. In this report, we focus on the first two list items, adapting them to the WMI machines and conditions. The ashing process used between cleaning and spin coating, as well as between development and evaporation, aims at removing organic substances such as resit residues with oxygen. In order to get rid of the natural surface oxide, which contains especially many two-level-systems, Ar ion milling or HF treatment are in common. In case of Ar ion milling, one physically attacks the silicon oxide surface. This step has to be conducted *in situ* in the evaporation system to avoid reoxidizing [6].

[1] We acknowledge support by the German Research Foundation under Germany's Excellence Strategy (EXC-2111 – 390814868), the Elite Network of Bavaria through the graduate program ExQM, and the EU Flagship project QMiCS (Grant No. 820505).

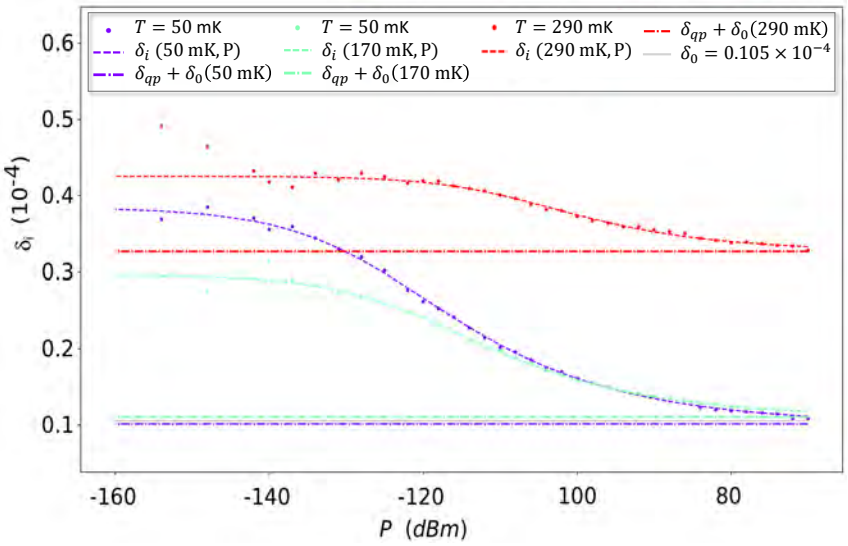

Figure 1: Loss tangent δ_i of a resonator with ω_r =5.7 GHz on a chip with "3 min O_2 ashing plus Ar ion milling" treatment as a function of the probe power for T =50 mK, 170 mK, and 290 mK. Dots represent data, dashed lines fits to Eq. (1), dash-dotted lines show $\delta_{qp}(T) + \delta_0$ and the Grey line δ_0

.

Here, we show preliminary results for resonators with different fabrication processes: no additional treatment (current standard process), 3 min O_2 ashing plus Ar ion milling, and 3 min O_2+Ar ashing plus Ar ion milling. An typical measurement is shown in Fig. 1. A summary of the present status is shown in Tab. 1. So far, we do not recognize significant improvement by an ashing and ion milling treatment. In case of ashing, this is expected since the organic residues do not contribute to two-level-systems, but only to the aging of (currently not present) Josephson junctions. For Ar ion milling, the energy of the Ar ions appears not to be suitable yet and needs further optimization. As an outlook, we plan to hydrofluoric acid treatment and annealing of the Si substrate before depositing the metal.

cleaning process	ω_r (GHz)	$\delta_{TLS,0}/10^{-5}$	$\delta_0/10^{-5}$
no ashing + no milling	5.82	1.52	1.38
	6.21	1.59	15.8
3 min O_2 ashing + milling	5.77	1.92	1.09
	6.14	1.89	10.8
	7.02	2.77	1.84
3 min O_2+Ar ashing + no milling	5.75	1.80	18.4
	7.00	1.89	3.62

Table 1: Two-level-system losses $\delta_{TLS,0}$ and other losses δ_0 of Al resonators fabricated with different methods.

References

[1] S. Fritz, L. Radtke, R. Schneider, M. Weides, and D. Gerthsen, Journal of Applied Physics **125** (2019).
[2] C. Müller, J. H. Cole, and J. Lisenfeld, Reports on progress in physics. Physical Society (Great Britain) **82**, 124501 (2019).
[3] D. Diesing, A. W. Hassel, and M. M. Lohrengel, Thin Solid Films **342**, 282–290 (1999).
[4] J. K. Julin, P. J. Koppinen, and I. J. Maasilta, Applied Physics Letters **97**, 22–25 (2010).
[5] J. Goetz, F. Deppe, M. Haeberlein, F. Wulschner, C. W. Zollitsch, S. Meier, M. Fischer, P. Eder, E. Xie, K. G. Fedorov, E. P. Menzel, A. Marx, and R. Gross, Journal of Applied Physics **119** (2016).
[6] A. Dunsworth, A. Megrant, C. Quintana, Z. Chen, R. Barends, B. Burkett, B. Foxen, Y. Chen, B. Chiaro, A. Fowler, R. Graff, E. Jeffrey, J. Kelly, E. Lucero, J. Y. Mutus, M. Neeley, C. Neill, P. Roushan, D. Sank, A. Vainsencher, J. Wenner, T. C. White, and J. M. Martinis, Applied Physics Letters **111** (2017).

© Walther-Meißner-Institute

Rare Earth Garnets: Crystal Growth by the Traveling Solvent Floating Zone (TSFZ) Method

Andreas Erb

Yttrium iron garnet ($Y_3Fe_5O_{12}$, YIG) is a ferrimagnetic insulator with a Curie temperature of about 550 K. It shows a strong Faraday effect, high Q-factors at microwave frequencies and a very small linewidth in electron spin resonance. YIG is used in microwave, optical and in magneto-optical applications, solid-state lasers, in data storage and in nonlinear optics. Therefore this compound has been widely studied and has triggered the growth of YIG using various crystal growth techniques like growth from high temperature solutions, vapor phase growth or hydrothermal solutions. Despite these widespread applications the supply with single crystals of YIG is difficult and expensive. In an earlier article we already reported about the crystal growth of the YIG compound [1]. Ever since the crystals have been used in a large variety of experiments at the Walther Meißner Institute by the magnetism group, where YIG is used as a substrate for various experiments. Crystal growth of various oxides using the TSFZ zone method is one of the specialities of the Walther-Meißner Institute. Since the magnetism group was also interested in compensated rare earth ion garnets $RE_3Fe_5O_{12}$ for spin current experiments using RE=Gd or Er as the rare earth ion, we also fabricated $Gd_3Fe_5O_{12}$ (GdIG) as well as $Y_3Fe_5O_{12}$ (ErIG) bulk single crystals.

Since the phase diagrams of both GdIG and ErIG are unknown the phase diagram of YIG was used as a starting point. Yttrium Iron Garnet is a non-congruently melting compound which makes it impossible to grow the crystals from a stoichiometric melt. The phase diagram of YIG has been reported by Van Hook [2] in the early sixties.

According to the phase diagram shown in Fig. 1, we selected a composition around 20 mol percent Y_2O_3 in $YFeO_3$ as a solvent for the crystals growth of YIG. The solvent pellet of about 0.5 gr. was placed in between feed and seed rod in our image furnace (Crystal Systems Inc., Japan). Melting was obtained at around 1500 °C in pure oxygen and the molten zone was moved through the feed rod by moving the mirror system of the furnace. Due to the relatively high solubility of $Y_3Fe_5O_{12}$ in its solvent a remarkable high growth velocity of up 4 mm per hour can be reached in this diffusion controlled process.

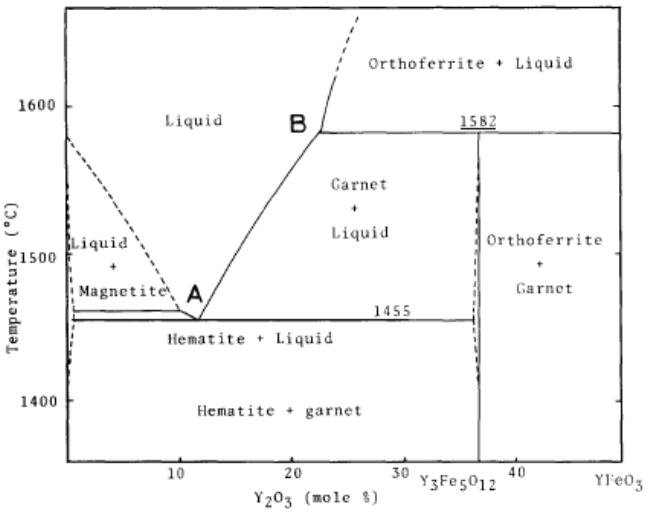

Figure 1: Phase relations in the system Fe_2O_3 - $YFeO_3$. Along the liquidus line between A and B, the $Y_3Fe_5O_{12}$ is in a thermodynamic equilibrium with a iron rich melt, which therefore can be used as a solvent for the TSFZ growth of YIG.

Lacking a phase diagram for the growth of GdIG and ErIG the parameters used for the growth of YIG were initially used in the growth of GdIG and ErIG. We observed a marked contrast both in the melting point and also in the solubility of the garnet in the flux. Melting point and solubility was found to be lower for GdIG and even lower for ErIG. Adjusting temperatures and flux composition accordingly this problem can be principally solved, however, both temperature and solubility have consequences for the growth velocity under which a stable growth can be obtained. While YIG has a near 50% solubility

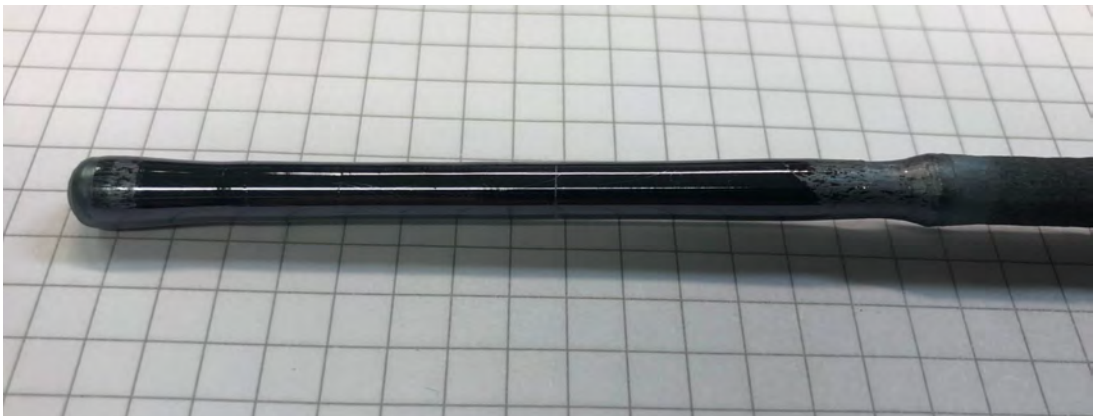

Figure 2: $Gd_3Fe_5O_{12}$ single crystal grown by the TSFZ method. The single crystalline part is 7 cm long and 6 mm in diameter and can be already envisioned by the smooth and shine surface. That particular specimen was grown at a rate of only 0.5 mm/h.

in its flux, the solubility of Gd is perhaps only 35% and even lower for Er. Together with the also lower growth temperatures this leads to a reduced growth velocity of maximum 1 mm per hour for GdIG and 0.5 mm per hour for ErIG.

Fig. 2 shows one of the grown single crystals of $Gd_3Fe_5O_{12}$. In lack of an oriented seed on the first growth experiments, grain selection of the predominant grain took place due to the different growth velocities in the different crystal orientations. We found that the crystals grew within a few degrees around the crystallographic [111]-direction. Subsequent growth experiments were then in most cases performed with [111]-oriented seed crystals cut from the ingot of the first crystal growth experiments. But also [100]-oriented growth can be performed using seed crystals of this orientation. Monocrystallinity and orientation could be easily checked using the Real Time Laue Backreflection camera (Multiwire Lab. Ltd. and Laue-Camera GmbH) at the crystal laboratory of the faculty of physics TUM. From the ingots we of the different growth experiments, many substrates were produced with different crystallographic orientations and with fine polished finish. The quite unique single crystals of GdIG paved the way for interesting findings obtained by the magnetism group of the Walther Meißner Institute [3].

If one is able to find the appropriate growth regime, e.g. the temperature and concentration interval on the liquidus line, the growth of the other rare earth iron garnets as well as many other congruently and non-congruently melting compounds can be performed using the elegant and efficient TSFZ method. However, there are limits for the growth by TSFZ as well: If the solubility of the compound in the solvent or flux is below about 20 %, both the growth rate and achievable stability drop dramatically and the growth of the compound becomes increasingly difficult or impossible. Good examples are the 123 high-T_c-superconductors, where the solubility in their flux is only about 10% and no successful TSFZ growth experiments are reported to this date, while in the case of the 214-compounds the solubility reaches 20% and crystals of this family have been grown at the WMI very successfully.

References

[1] A. Erb, WMI Ann. Rep. **2012**, 87 (2012).
[2] H. V. Hook, J. Am. Ceram. Soc. **45**, 162 (1962).
[3] L. Liensberger, A. Kamra, H. Maier-Flaig, S. Geprägs, A. Erb, S. Goennenwein, R. Gross, W. Belzig, H. Huebl, and M. Weiler, Phys. Rev. Lett. **123**, 117204 (2019).

New UHV System for Qubit Fabrication Goes into Operation

Stephan Geprägs, Thomas Brenninger, Achim Marx, Matthias Althammer, Rudolf Gross [1]

With increasing complexity of superconducting quantum circuits, a well-controlled fabrication process is mandatory in order to obtain a reasonable fabrication yield. Therefore, in the proposal for the new Cluster of Excellence **Munich Center for Quantum Science and Technology (MCQST)**, a request for an automated UHV fabrication system for superconducting quantum circuits was included. Fortunately, the funding for such a system has been granted by the German Research Foundation via MCQST. After a Europe-wide tender the flexible UHV system MEB 550 S4-I of the company PLASSYS Bestek could be ordered in 2019. We are very grateful to DFG and MCQST for making the purchase of this fabrication tool possible. It will be of key relevance for improving the coherence time of superconducting qubits and their reproducible fabrication with small parameter spread.

Figure 1: The Plassys UHV deposition system installed at WMI. Left part: loadlock with the sample transfer rod, middle part: sputter deposition chamber, right part: deposition/oxidation and electron beam evaporation chambers. The deposition/oxidation chamber is positioned atop the evaporation chamber separated by a horizontal gate valve. Not shown is the computer system for process control.

Due to Covid-19 related delays the new PLASSYS MEB 550 S4-I UHV system was delivered and installed only in November 2020. The system is fully automated and consists of a load-lock and two further UHV chambers for sputter deposition of niobium and titanium and for electron beam deposition of aluminium and titanium. The load-lock is equipped with a Kaufman type ion gun for cleaning and etching wafers by neutralized argon or oxygen ions. It also contains an ozone source for removing organic contaminants. In the UHV sputter deposition chamber there are two 3-inch magnetrons which are compatible with RF and DC power. The magnetrons are oriented in a confocal sputter-up configuration over a spinning 4-inch substrate. The water-cooled substrate holder is suspended from the top plate and receives the carrier from the load-lock. Its planetary rotation is compatible with the confocal configuration

[1]Supported by the German Research Foundation under Germany's Excellence Strategy (EXC-2111 – 390814868).

of the magnetrons. The substrate can be RF polarized for cleaning before deposition or for ion assistance during deposition.

The electron beam evaporator and the motorized substrate holder are placed in two separate UHV chambers. These deposition/oxidation and evaporation chambers are positioned on top of each other and can be separated by a horizontal gate valve. In this way, the oxidation of the metals in the crucibles is avoided during the oxidation of the thin film surface between two subsequent evaporation steps in a shadow evaporation process. To provide flexibility in material choice, the evaporation chamber is equipped with a linear 8×15 ccm electron beam evaporator from Thermionics. In the deposition/oxidation chamber, a high-density atomic oxygen plasma can be generated by a 2.45 GHz ECR microwave source in the vicinity of the substrate. Furthermore, the deposition/oxidation chamber is equipped with a residual gas analyser based on a mass spectrometer up to 100 amu with a thoriated iridium filament. An ozone treatment can be applied to the wafers both in the load-lock and deposition/oxidization chamber. A key part of the deposition/evaporation chamber is the fully automated motorized substrate holder, allowing for tilting and spinning substrates with a size up to 4 inch. This substrate holder provides full flexibility for the two-angle shadow evaporation process. A software controlled oxidation process ensures high reproducibility of oxygen partial pressure and duration of exposure. A rear heating system allows for substrate temperatures up to 750°C.

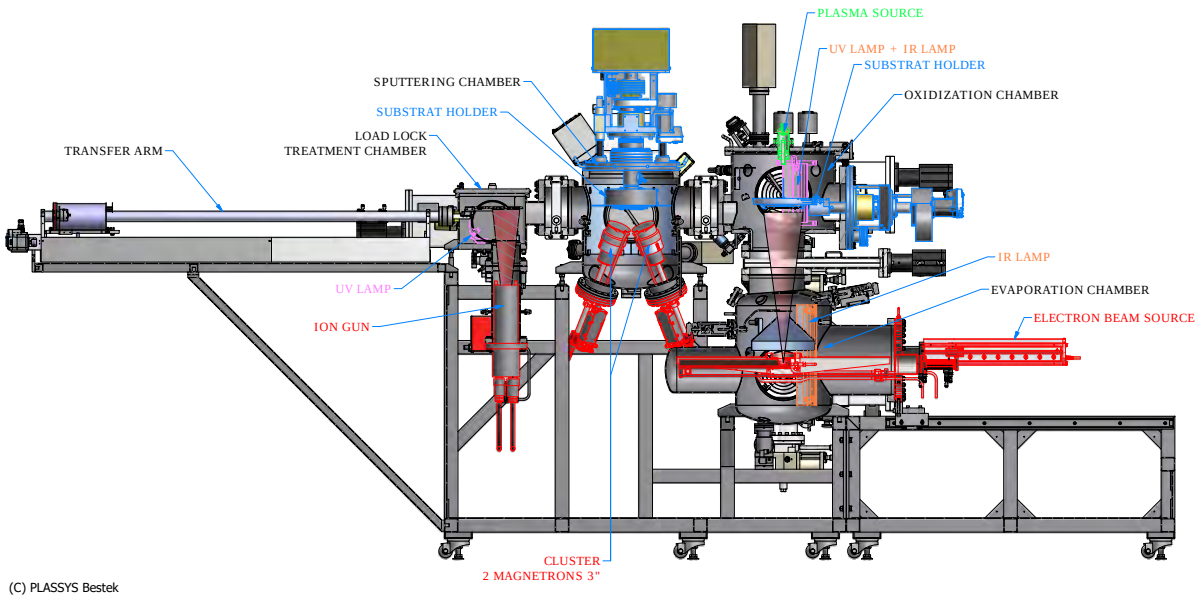

Figure 2: Functional drawing of the PLASSYS MEB 550 S4-I UHV system.

There are full access hinged doors on all chambers for easy loading/unloading and maintenance. The doors are sealed with differentially pumped double Viton seals (except for the load-lock). Using two cryopumps, a base pressure below 5×10^{-10} mbar and below 5×10^{-9} mbar is reached for the evaporation and sputter chamber, respectively. Heat sources inside the chambers allow for easy chamber baking. All processes including transfer of the wafers from the load-lock to the deposition chambers are fully computer controlled. There are closed loop regulations for deposition and oxidation processes. All steps of the individual processes can be easily automated using a simple scripting language.

The successful installation of large-scale equipment requires significant pre-planning and careful preparation of the required technical infrastructure. Therefore, we would like to thank all engineers, technicians and members of the mechanical workshop for there professional support, making the installation of the PLASSYS system possible in a very short time.

New Bluefors XLD 1000 Dry Dilution Refrigerator

Achim Marx, Leon Koch, Rudolf Gross [1]

Already during the preparation of the proposal for the new Cluster of Excellence **Munich Center for Quantum Science and Technology (MCQST)** in 2017, it became evident that there is a strong need for cryogen-free dilution refrigerators with large cooling power and sample space for the research activities on superconducting quantum circuits. This is in particular relevant for the installation and test of circuits and components for superconducting quantum computers which are rapidly growing in size and complexity. Fortunately, the funding for such a dilution refrigerator has been granted by the German Research Foundation via MCQST and a powerful XLD 1000 system of the company Bluefors Oy could be ordered in 2019. We are very grateful to DFG and MCQST for supporting the purchase of this important new instrumentation.

Despite the Covid-19 pandemic the new XLD 1000 system has been delivered in time in the middle of 2020 and meanwhile is in operation. The XLD Series of Bluefors has been chosen since it is particularly suited for demanding experiments that require large experimental space and superior performance of the cryogen-free dilution refrigerator measurement system. For example, the XLD 1000 system can accommodate more than 300 coaxial microwave lines and nevertheless provides a base temperature of about 10 mK. A single push of a button initiates a fully automated cool-down sequence from room to base temperature.

Figure 1: New Bluefors XLD 1000 Dry Dilution Refrigerator after installation at WMI. All the compressors and the gas handling systems are located in a technical room underneath the laboratory (photo: MCQST/Jan Greune).

A big advantage of the Bluefors XLD 1000 dry dilution refrigerator is the fact that it features very large experimental space at all temperature stages and an experimental volume with a diameter of 50 cm and a height of 55 cm below the mixing chamber plate. In the initial stage (limited by the available budget), there have been 40 microwave input and 8 microwave output lines installed. However, the elegant side loading mechanism allows the straightforward installation of additional lines. In its final development stage this refrigerator can host several experiments at the same time, even if many input and output lines are required for each single experiment. The system reaches a base temperature below 10 mK. The dilution unit is designed for high

[1]Supported by the German Research Foundation under Germany's Excellence Strategy (EXC-2111 – 390814868).

throughput and provides for a cooling power of more than 1 mW at 100 mK (30 µW at 20 mK). Therefore, this refrigerator is well suited to host several experiments at the same time.

The XLD 1000 dilution refrigerator is equipped with two pulse tube refrigerators (Cryomech PTR 420 with 2 W cooling power at 4 K each). The cool-down and warm-up of the refrigerator can be handled fully automatic. Oil-free pumps and compressors in the gas handling unit guarantee minimal maintenance requirements with service interval up to 3 years. Moreover, the system is equipped with a unique long-life cold trap that allows for continuous operation of the system for up to three years. The trap is integrated with the system and does not need any cryogenic liquids to operate.

Figure 2: Left: WMI students working on the new Bluefors XLD 1000 cryogen-free dilution refrigerator. Left: Microwave lines connecting to equi-temperature plates (photos: BAdW/ Kai Neunert).

Figure 3: The technical director of WMI, Achim Marx, smiling after the successful installation of the XLD 1000 system even in Corona times (photo: BAdW/ Kai Neunert).

It is important to note that due to the Covid-19 pandemic the installation of the system could not be done by the company due to travelling restrictions for the technicians. Therefore, the installation was done by the WMI scientists and technicians themselves. Due to the longstanding experience present at WMI the installation could be completed in record time without any major problems. We would like thank the technical director of WMI, Achim Marx, and his team for making this possible.

Cryogen-Free Dilution Refrigerator with Pulse Tube Shutoff Option

K. Uhlig

Introduction After our first presentation of a cryogen-free ("dry") dilution refrigerator (DR) in 2002 [1], DRs have become standard millikelvin coolers over the years. It is not so much their refrigeration power or their base temperature that stand out with the present commercial models, but rather their geometrical dimensions. Mounting platforms of the mixing chamber with a diameter of up to 1 m have become available, an increase of about a factor of 5 compared to "wet" DRs with He_{liq} precooling. To precool the dilution unit in a dry DR from room temperature to about 3 K, a pulse tube cryocooler (PTC) is used.

The big advantage of PTCs compared to other types of closed cycle coolers is that they have no moving piston in their setup. Mechanical vibrations are therefore almost entirely avoided. However, very small vibrational disturbances still exist. E.g., the helium gas which is run back and forth to the pulse tubes has a non-negligible mass; for our small PTC it is about 20 g and for a big PTC it is closer to 100 g. Thus, the total weight of the cryostat oscillates. With the varying pressure in the pulse tubes their length and diameter vary slightly - a problem that has to be taken care of in practically all dry DRs. Another source of vibration is the soft connection line between the rotary valve of the PTC and the cryostat. This line expands and contracts during operation and therefore applies a varying force on the DR. The helium gas in the pressure lines is exposed to the vibrations of the compressor; when the rotary valve is open, these vibrations are transmitted to the cryostat.

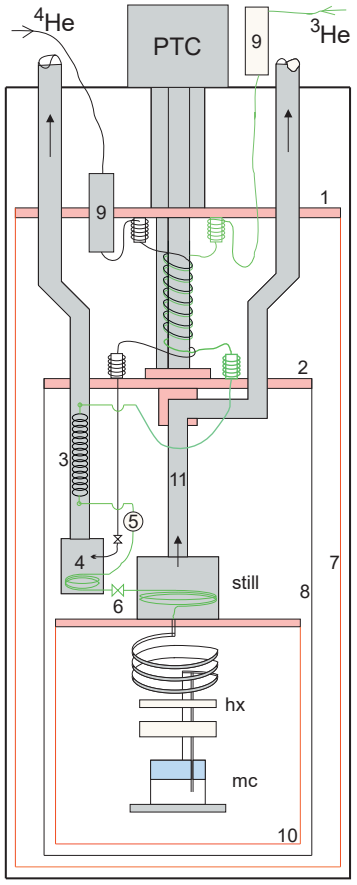

Figure 1: Section of the cryostat: 1 - 1st stage of PTC; 2 - 2nd stage of PTC; 3 - counterflow heat exchanger in the 1 K-stage; 4 - pot of 1 K-stage; 5 - thermometer; 6 - flow impedance; 7 - rad. shield; 8 - inner vacuum can; 9 - charcoal traps; 10 - still rad. shield; 11 - still pumping line

Experimental and results The purpose of this work is to eliminate even the small vibrational disturbances by temporarily shutting off the PTC while the dilution circuit remains in operation. A section of this DR is given in Fig. 1. The cryostat not only contains the usual PTC and dilution circuit, but also a separate ^{4}He 1 K-circuit [2]. Its pot is large (100 cm^3). Before the PTC is turned off the pot is filled with He_{liq} and then the 1 K-stage is operated in single-cycle mode. It serves as a cold reservoir for cooling the dilution circuit during the off-period of the PTC. In contrast to standard dry DRs, the inlet line of the DR is run through a counterflow heat exchanger (cfhx) in the pumping line of the 1 K-stage for precooling ("3" in Fig. 1) and then through a heat exchanger in the pot ("4" in Fig. 1) where the ^{3}He flow is condensed. Precooling the ^{3}He flow is most important to keep the rate of evaporation in the pot as low as possible. Then the liquefied ^{3}He is expanded in a flow restriction ("6" in Fig. 1) and run to the cold stage of the dilution unit.

After the PTC is turned off, the heat conduction of the 1st stage produces a sizeable heat leak into the cryostat of about 6 W; the heat leak of the 2nd stage amounts to 0.3 W [3]. These heat

leaks cause a gradual warming of the PTC and its radiation shields ("1, 2, 7, 8" in Fig. 1). In a standard dry DR, the dilution process would end after about 30 minutes when the 2nd stage of the PTR reaches 10 K. In our DR, the pot of the 1 K-stage remains near its base temperature as long as there is liquid helium in it and the dilution circuit remains in operation during the shutoff of the PTC.

In Fig. 2 a three hour shutoff experiment is depicted (time span between the two red lines). After 3 hours the PTC is turned on; and after another 1.5 hours the 1 K-circuit is reactivated (blue line in Fig. 2). The most important temperature patterns are shown: The temperatures of the two stages of the PTC rose from 53 K to 103 K (1st stage) and from 2.5 K to 40 K (2nd stage; "a" and "b" in Fig. 2) during the shutoff. Curve "c" is the temperature of the ^{3}He flow after cooling in the cfhx in the 1 K-stage ("5" in Fig. 1). We note that the cfhx is very efficient as curve "c" remains below 3 K even at the highest temperature of the second pulse tube (40 K).

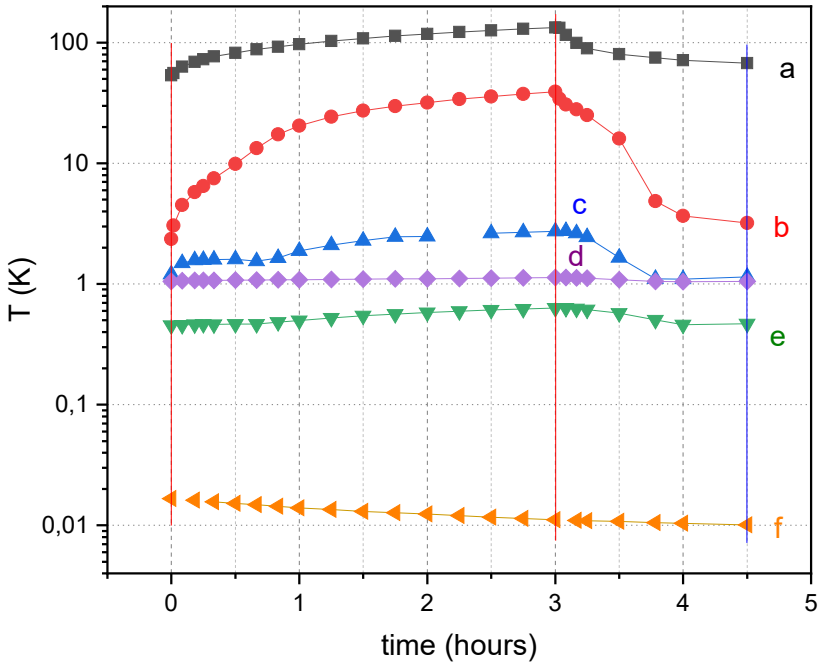

Figure 2: Temperature profiles of the dry DR as a function of time: a - PTC 1st stage; b - 2nd stage of PTC; c - temperature after cfhx ("5" in Fig. 1); d - pot temperature; e - still temperature; f - mixing chamber temperature

Curve "d" in Fig. 2 is the temperature of the 1 K-pot; it changed only little during the PTC shutoff from 1.05 K to 1.13 K. Curve "e" is the temperature of the still. It did rise from 0.45 K to 0.65 K, presumably by heat input through the pumping line of the still ("11" in Fig. 1). This heat input, calculated from the thermal conductivity of the tube, would be much higher than the refrigeration power of the still. However, the cold ^{3}He gas pumped from the still cooled the pumping line. Only a fraction of the enthalpy of the cold ^{3}He gas was used, though. Finally, curve "f" is the temperature of the mixing chamber. It was still on its way to the base temperature from the original cooldown. The base temperature of the DR is 4.3 mK, but in this experiment with a small ^{3}He-flow rate the base temperature would have been somewhat higher. Importantly, the mixing chamber temperature was not affected by the PTC shutoff. From here, the DR can be run with the 1 K-stage in operation or, equally well, without it. In case the 1 K-stage is on, the condensation pressure of the DR is low (0.1 to 0.2 bar). If it is off, the inlet pressure is higher (0.5 bar).

References

[1] K. Uhlig, Cryogenics **42**, 73–77 (2002).
[2] K. Uhlig, Cryogenics **66**, 6–12 (2015).
[3] Cryomech Inc.; private communication.

© Walther-Meißner-Institute

Experimental Facilities

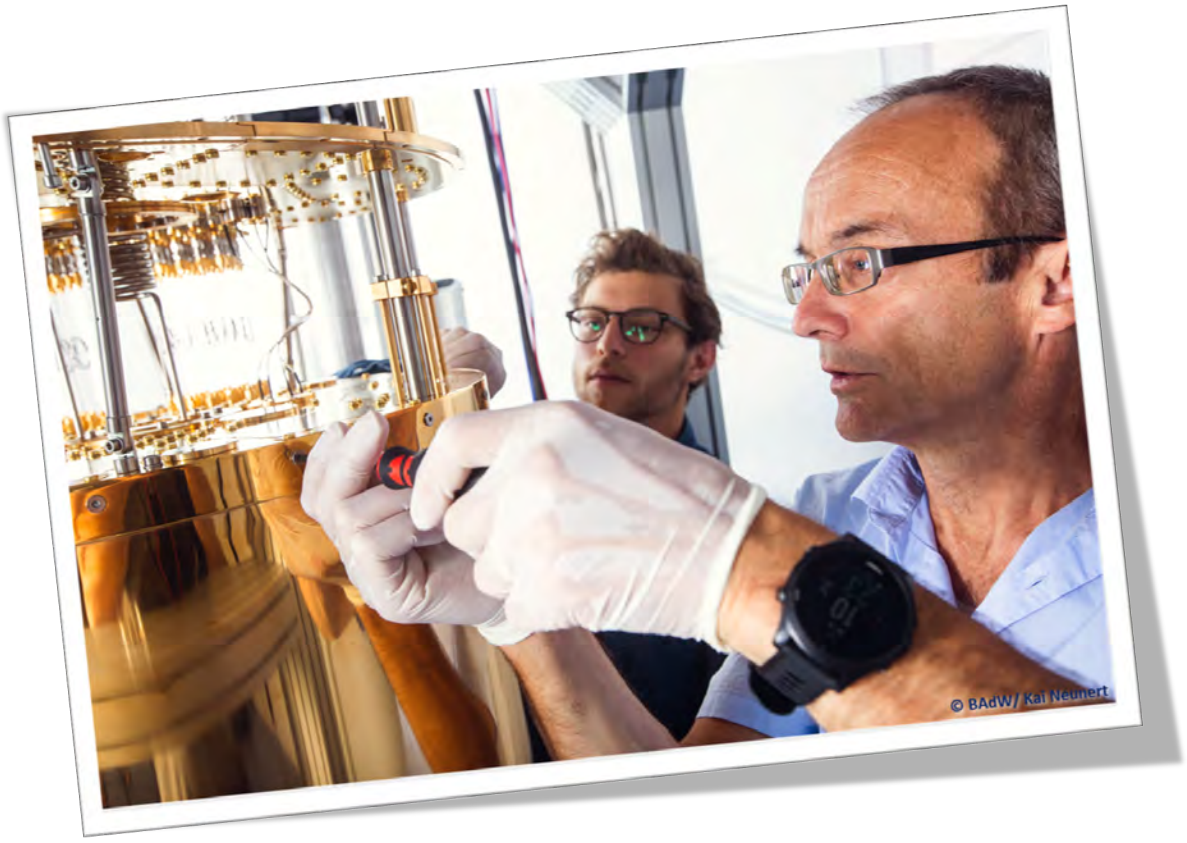

Overview of Key Experimental Facilities and Infrastructure

In the following basic information on the key experimental facilities and components of the technical infrastructure installed at the Walther-Meißner-Institute (WMI) is given.

UHV Laser-MBE

The WMI operates an UHV Laser-Molecular Beam Epitaxy (L-MBE) system for the growth of complex oxide heterostructures. The system has been designed to meet the special requirements of oxide epitaxy. The UHV cluster tool consists of the following main components:

- central transfer chamber;
- load-lock chamber with a heater system for substrate annealing;
- laser deposition chamber with a KrF excimer laser, *in-situ* reflection high energy electron diffraction (RHEED) system, laser substrate heating system, and atomic oxygen/nitrogen source; the RHEED system has been modified to allow for the operation at high oxygen partial pressure up to 0.5 mbar;
- surface characterization chamber with UHV scanning atomic force microscope (Omicron);
- metallization chamber with a four heart electron gun system and a liquid nitrogen cooled sample stage. The sample holder can be tilted for shadow evaporation.

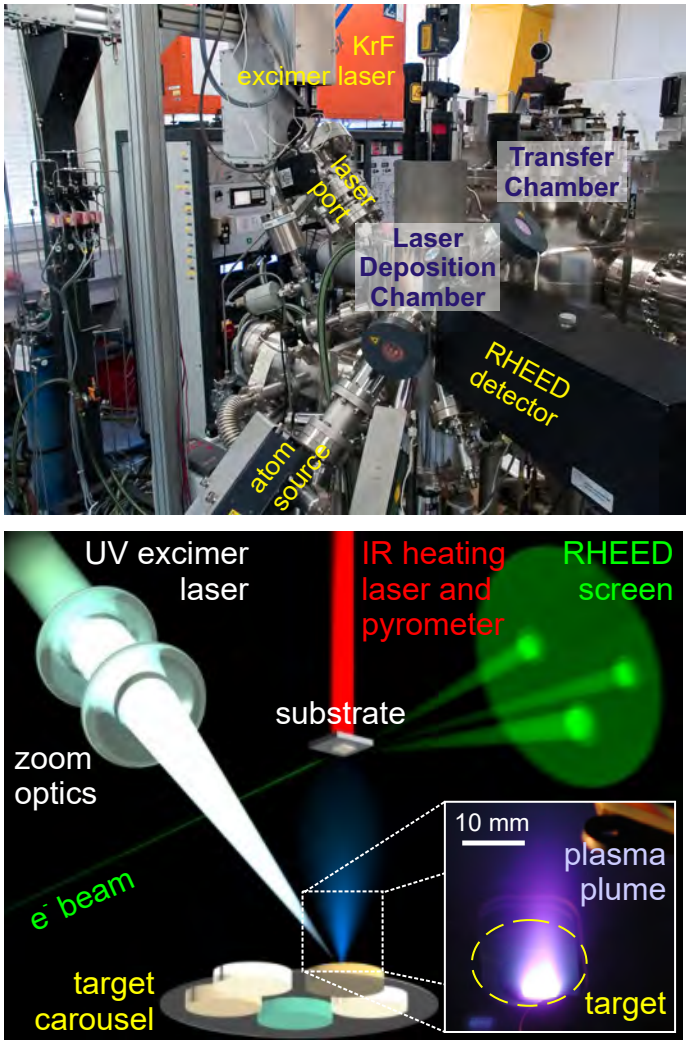

Figure 1: Top: UHV laser-molecular beam epitaxy system. Bottom: principle of the deposition process.

The system is used for the growth of complex oxide heterostructures consisting of superconducting, ferromagnetic, ferroelectric, and semiconducting materials such as high-temperature superconductors, doped manganites, (double) perovskites, magnetite, zinc oxide, rare earth iron garnets, pyrochlore iridates, etc.

The original laser molecular beam epitaxy system (laser-MBE) designed already in 1995/96 has been continuously upgraded and modified until today. In particular, the substrate heating system and the temperature control unit were changed from a resistive radiation heater to an infrared laser heating system (see Fig. 3, left) including a pyrometer for determining the sample temperature. In addition, a source for atomic oxygen and nitrogen has been installed. The main advantage of the new heating system is that only the substrate is heated while the surrounding parts are hardly affected (Fig. 3, right). In this way one can achieve a substantially better vacuum at temperatures well above 1000 °C. The achievable substrate temperature is limited by the melting point and the size of the substrate material (approx. 1410 °C for a 5 mm × 5 mm silicon substrate). The laser heating system has already been successfully used for removing the amorphous silicon oxide layer from the surface of silicon substrates at 1150 °C.

Figure 2: Pulsed Laser Deposition (PLD): When the pulse of the UV laser (KrF excimer laser, 248 nm) hits the target, the target material is ablated and the so-called laser "plume" containing highly excited atoms and molecules is formed.

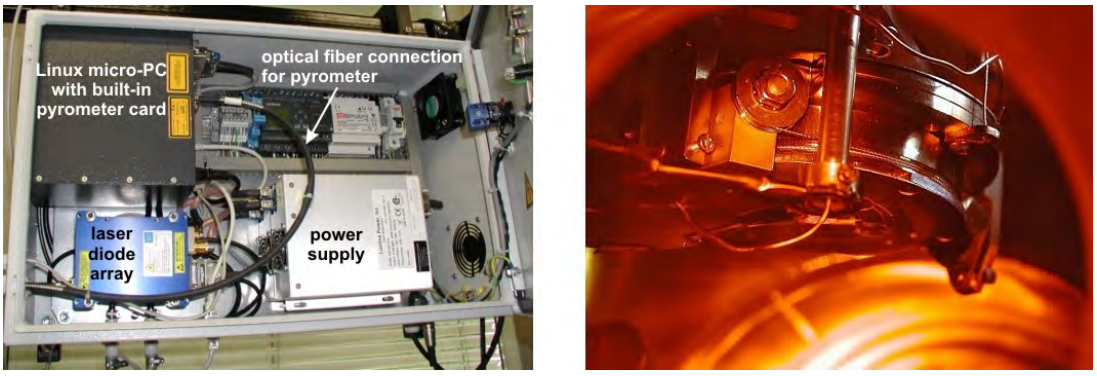

Figure 3: Components of the laser heating system: The substrate is heated using an IR diode laser head that is located in a separate box far away from the deposition chamber (left). The laser light is brought to the substrate (right) via an optical fiber.

We have further developed and installed a home-made telescope zoom optics for the pulsed UV laser light, consisting of in total five lenses on sliding lens holders allowing for a movement over a total distance of 1200 mm. The lens holders are attached to independent stepper motors, each connected to a controller providing an accurate positioning precision. The controllers are driven via a PC, thus allowing for a full automation of the lens system itself. With this telescope zoom optics we are able to change the area of the UV laser spot on the target, resulting in an accessible range of laser fluences from $\rho_L = 0.5\,J/cm^2$ to $5\,J/cm^2$. To maintain a stable laser fluence at the target, we have installed a so-called *intelligent* window (PVD Products) at the laser entrance port combining two unique features. First, it keeps the inner side of the entrance window free of coatings by blocking the ablated plasma plume via a rotatable disc consisting of UV grade fused silica. Second, an insertable mirror positioned in the light path after the disc allows to guide the incoming UV laser pulse through a side window, where its energy is determined by a pyroelectric detector. These measures help to improve the deposition processes by accurately monitoring ρ_L as one of the most critical process parameters.

UHV Sputter Deposition System – SUPERBOWLS

The UHV sputter deposition system was set up in 2017 and allows for the fully-automated fabrication of complex multilayers consisting of superconducting and magnetic materials. To avoid cross-contamination of the superconducting and magnetic materials the system consists of two separate deposition chambers (see Fig. 4). One deposition chamber is dedicated for superconducting materials (Non-Ferromagnet Chamber: NFC) and the other for the growth of magnetic materials (All Ferromagnet Chamber: AFC). The loadlock chamber is positioned between the two deposition chambers. It serves for inserting substrates and masks into the deposition chambers and enables the in-situ transfer of samples between the two deposition chambers. The system is designed for a face-down substrate orientation with the sputter source residing at the bottom of the deposition chambers. Both deposition chambers achieve a base pressure well below 8×10^{-10} mbar, paving the way for the deposition of high purity materials.

Figure 4: UHV sputter deposition system named «**SUPERBOWLS**». Left chamber is the NFC dedicated to the deposition of superconducting materials, right chamber is the AFC equipped with magnetic materials. Between the two deposition chambers resides the loadlock (LL).

The loadlock chamber is equipped with a substrate and mask storage cassette for up to six substrates. Halogen lamp heaters are installed in the loadlock for thermal precleaning of the substrates. The NFC is currently equipped with two 3 inch magnetrons and one 2 inch magnetron. In the AFC, eight 2 inch tiltable magnetrons are installed. In this chamber the sources can be either oriented into two confocal deposition clusters from 4 sources or 4 sources for face-to-face deposition, providing a large flexibility in the deposition conditions and enabling the fabrication of quaternary alloys from single element targets. All deposition sources are equipped with pneumatically actuated shutters, tilts, and linear translations. This allows for both face-to-face and confocal deposition from all three sources.

Both chambers are equipped with versatile substrate manipulators. They can accommodat substrates with a diameter of up to 2 inch and feature a resistive heater for substrate temperatures up to 800 °C, a motorized substrate shutter for wedge and step-profile deposition, a motorized linear translation for changing the source to substrate position, a main rotation to move the substrate in the chamber to the different deposition positions, a motorized substrate rotation at up to 40 rpm for homogenous deposition, and a quartz crystal microbalance (QCM) for growth rate monitoring. In addition, a Kaufmann source for reactive ion etching is installed in the system for in-situ surface cleaning procedures or even etching processes. Several 1 kW DC power and 600 W RF power supplies are used for the operation of the magnetrons. Mass flow controllers allow to change the composition of the process gas for reactive sputtering processes. More details can be found in the Annual Report 2017.

UHV Sputter Deposition System – ULTRADISC

In 2018, a new UHV sputter deposition system (1600 l/s turbo molecular pump, base pressure: $< 1 \times 10^{-9}$ mbar, automatic up- or down-stream pressure regulation: 8×10^{-4} mbar to 1×10^{-1} mbar) for the fabrication of superconducting thin films on large substrate areas has been installed.[1] The system consists of a main deposition chamber and a load lock, which is equipped with a motorized storage cassette for up to six substrates, a stab-in heater and a linear transfer arm for moving samples into and out of the main deposition chamber.

Figure 5: UHV sputter deposition system named **«ULTRADISC»**. The main chamber contains the deposition sources in the bottom flange and the substrate manipulator on the top flange.

The main deposition chamber has been designed for flexible and homogeneous deposition on substrates with a diameter of up to 100 mm. The substrate holder is electrically isolated to allow for a plasma directly underneath the substrate via applying a DC or RF bias to the substrate holder. A radiative carbide heater is used to homogeneously heat the substrate up to 950 °C. The substrate manipulator has 3 degrees of freedom to move the substrate in the deposition chamber. The main substrate rotation allows to move the substrate over the different deposition clusters. In addition, the distance between substrate and sources can be tuned by 100 mm via a motorized z-shift of the manipulator. For homogeneous deposition, the substrate itself can rotate with up to 30 rpm. An automated substrate shutter allows to protect the substrate from unintentional deposition. Moreover, a motorized wedge shutter enables the fabrication of controlled thickness variations over the area of the substrate.

Flexibility in materials choice is ensured by a total of 11 magnetron sources installed in the chamber. A total of 7 sources can be used for face-to-face deposition on the substrate for high growth rate deposition (several 10 nm/min). In addition, 8 sources can be manually tilted into three separate confocal deposition clusters, which enables simultaneous deposition from up to 3 sources. Automated control of the deposition times is achieved by the motorized shutters attached to each magnetron. The high-purity gas supply is realized via 4 independent mass flow controllers, allowing for flexible gas compositions for reactive sputter deposition of oxide and nitride materials. For more flexibility in reactive sputtering processes and for substrate cleaning purposes the confocal cluster is equipped with a RF discharge ion source (up to 1.0 kV). Two different grids suitable for nitrogen and oxygen or argon are currently available for the system. Two separate mass flow controllers are used to supply the high purity gases to the ion source. The system is fully automated by the supplied computer and software. More details can be found in the Annual Report 2018.

[1] The system is running under the acronym «ULTRADISC »: **U**nlimited **L**egendary **T**ool for **R**eliable **A**chievements in the **D**eposition of **I**ntegrated **S**uperconducting **C**omponents.

UHV Electron Beam Evaporation System

The UHV metal MBE system allows for the growth of high quality metallic thin films by electron beam evaporation and molecular beam epitaxy. The system is optimized for the fabrication of superconducting persistent current qubits by aluminum shadow evaporation. It is equipped with an improved substrate holder allowing for multi-angle shadow evaporation. The main components of the system are:

- UHV system with a process chamber with a base pressure below $\sim 1 \times 10^{-8}$ mbar pumped by a 1000 l/s turbo molecular pump with magnetic suspension of the rotor adequate for corrosive gases.
- Load-lock chamber equipped with a magnetic transfer system (push-pull positioner) for sample transfer without breaking the vacuum in the process chamber.
- Downstream pressure control by an adaptive pressure controlled gate valve.
- Electron beam evaporator with six 8 cm^3 crucibles embedded in a linearly movable water cooled rail providing six different materials.
- Film thickness measurement and closed loop evaporation rate control by a quartz crystal microbalance in combination with the evaporation controller.
- Effusion cell for molecular beam epitaxy processes.
- Ion sputtering gun for in-situ sample cleaning
- Manipulator with UHV stepping motors for automated and precise sample tilt and options for rotating and cooling the sample.

A precise and reproducible tilt of the sample is realized by a sample manipulator with process specific degrees of freedom. The downstream pressure control allows for a fast adjustment and precise control of the oxygen partial pressure. This is crucial for a well-defined oxidation process of the Josephson junctions barriers. The entire process can be performed fully automated via a touch screen and is controlled by a LabView program. Up to six effusion cells can be optionally added to the system allowing for further materials. The manipulator allows for further degrees of freedom that can be used to align the sample to the effusion cells, the ion sputtering gun and to measuring equipment such as ellipsometry or RHEED.

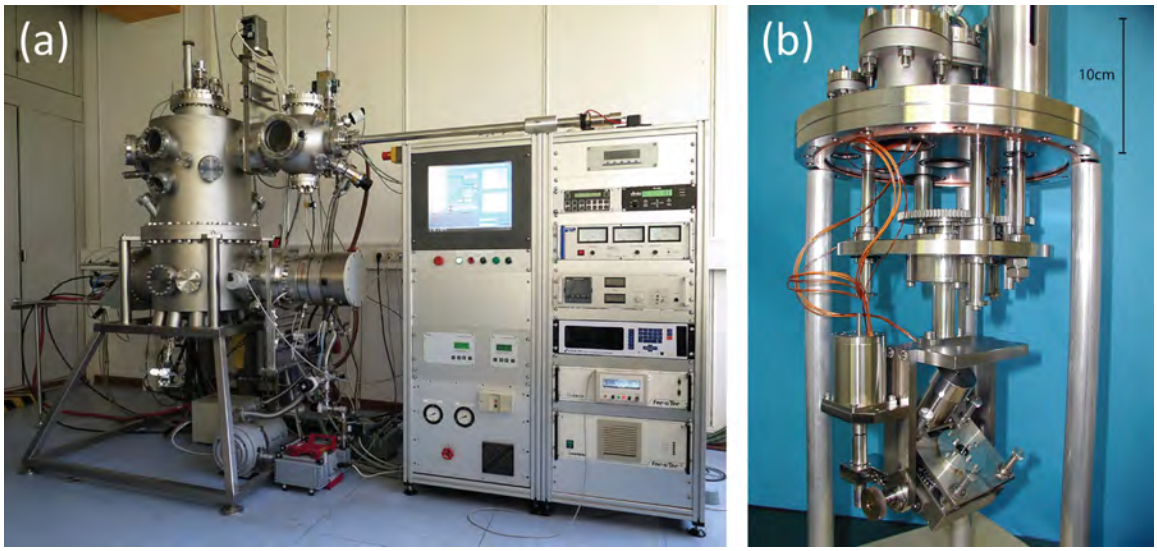

Figure 6: (a) Photograph of the UHV electron beam evaporation system. (b) Manipulator with UHV stepping motors for automated and precise sample tilt and options for rotation.

Single Crystal Growth and Synthesis of Bulk Materials

Transition metal oxides are of great interest due to their various interesting physical properties (e.g. high temperature superconductivity, colossal magnetoresistance, ferroelectricity, nonlinear optical properties etc.) and their high potential for applications. Therefore, the WMI operates a laboratory for the synthesis of bulk materials and single crystals of transition metal oxides. Besides various chamber- and tube furnaces a four-mirror image furnace is used for the crystal growth of various oxide systems. With this furnace crystals of many different compounds of the high temperature superconductors and various other transition metal oxides have been grown as single crystals using the traveling solvent floating zone technique. The furnace consists basically of 4 elliptical mirrors with a common focus on the sample rod and with halogen lamps in their other focus. By irradiation of the focused light the sample rod is locally heated and eventually molten. The molten zone can be moved up and down along the entire sample rod under simultaneous rotation. Due to the anisotropic growth velocity a preferential growth of those grains with the fastest growth velocity along the pulling direction is obtained and the formerly polycrystalline rod is transformed into a single crystal. Single crystal growth can be performed with this furnace at maximum temperatures up to 2200 °C in the pressure range from 10^{-5} mbar up to 10 bar and in oxidizing, reducing as well as inert atmosphere.

Figure 7: The four-mirror image furnace installed at the crystal laboratory of the WMI. Crystals can be grown by the floating zone and traveling solvent floating zone techniques at temperatures up to 2200 °C and pressures up to 10 bar.

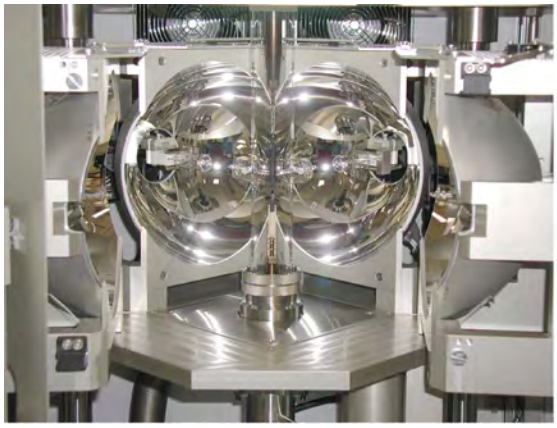

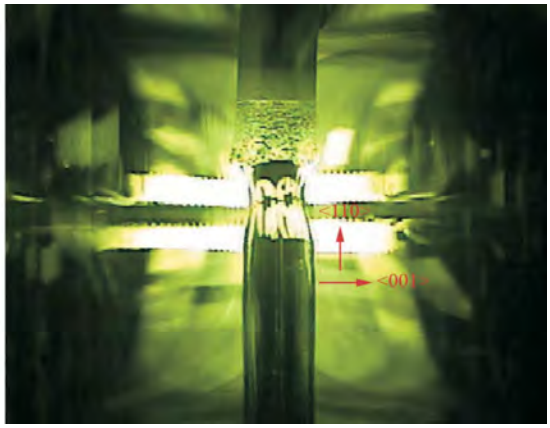

Figure 8: Left: Central part of the image furnace with four elliptical mirrors. In the center one can see the quartz tube with a polycrystalline rod. Right: View on the molten zone of $Pr_{2-x}Ce_xCuO_4$ (melting point: 1280 °C) obtained by a CCD camera.

© Walther-Meißner-Institute

The X-ray diffraction systems

For X-ray analysis the WMI operates two X-ray diffractometers (Bruker D8 Advance and D8 Discover). The two-circle system is used for powder diffraction. In this system the samples can be heated in oxygen atmosphere up to 1600 °C. It is equipped with a Göbel mirror and an area detector to save measuring time. The second system is a high resolution four-circle diffractometer that can be used for reciprocal space mappings. It is equipped with a Göbel mirror and an asymmetric two-fold Ge monochromator and allows for the texture analysis of thin film heterostructures, superlattices and single crystalline materials. In both systems measurements can be carried out fully computer controlled.

Beside these two Bruker X-ray systems a Laue camera for single crystal analysis and a Debye-Scherrer camera are available.

Figure 9: The two-circle X-ray diffractometer Bruker D8 Advance.

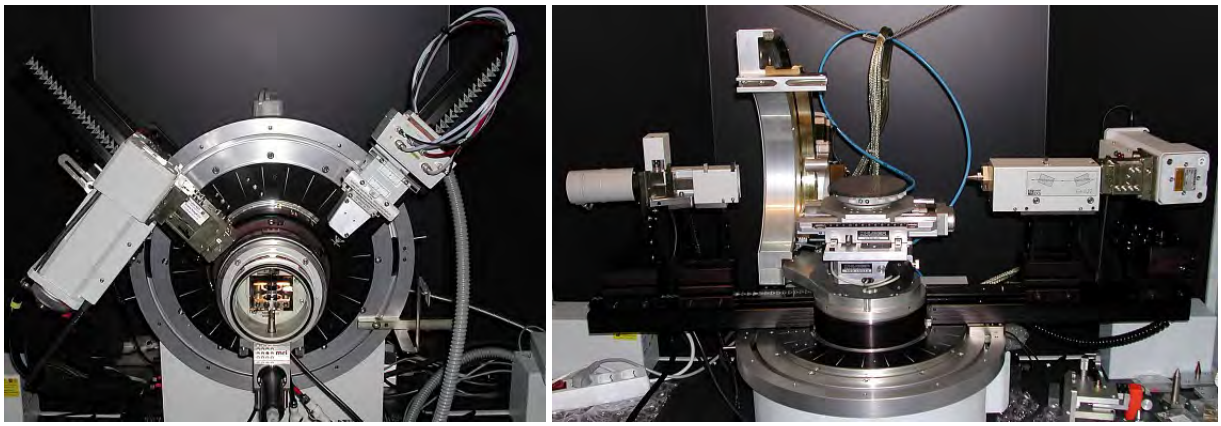

Figure 10: Left: High temperature sample holder of the D8 Advance system. Right: Four-circle high resolution X-ray diffractometer Bruker D8 Discover.

Figure 11: Quantum Design SQUID magnetometer.

The SQUID magnetometer

For the analysis of the magnetic properties of materials, a Quantum Design SQUID magnetometer system (Fig. 11) is operated at the WMI. The SQUID magnetometer allows for measurements in the temperature regime from 1.8 to 400 K and provides excellent sensitivity particularly in the low field regime. Due to the excellent sensitivity of the system, thin film samples with a very small sample volume can be analyzed. The SQUID magnetometer is equipped with a superconducting solenoid allowing for a maximum field of 7 T. At present, the magnetometer is used for the characterization of magnetic and superconducting materials (both in bulk and thin film form). Examples are the cuprate high temperature superconductors, the doped manganites, magnetite, the double perovskites, magnetic semiconductors, or multiferroics.

The High Field Laboratory

Transport and thermodynamic properties of samples are often studied as a function of the applied magnetic field. For such measurements several superconducting magnets are available at the WMI. Two of them (8/10 and 15/17 Tesla magnet system) are located in the high magnetic field laboratory in the basement of the WMI. The magnet systems are installed below the floor level to facilitate the access to the top flange and the change of the sample sticks. The magnet systems are decoupled from the building to avoid noise due to mechanical vibrations. A variety of sample holders can be mounted allowing for e.g. sample rotation during the measurement. For standard sample holders the accessible temperature regime is $1.5\,\mathrm{K} < T < 300\,\mathrm{K}$. However, also ^{3}He/^{4}He dilution refrigerator inserts ($T > 20\,\mathrm{mK}$) or high temperature units ($T < 700\,\mathrm{K}$) can be mounted. All measurements are fully computer controlled (by the use of the LabView software tool) allowing for remote control and almost continuous measurements.

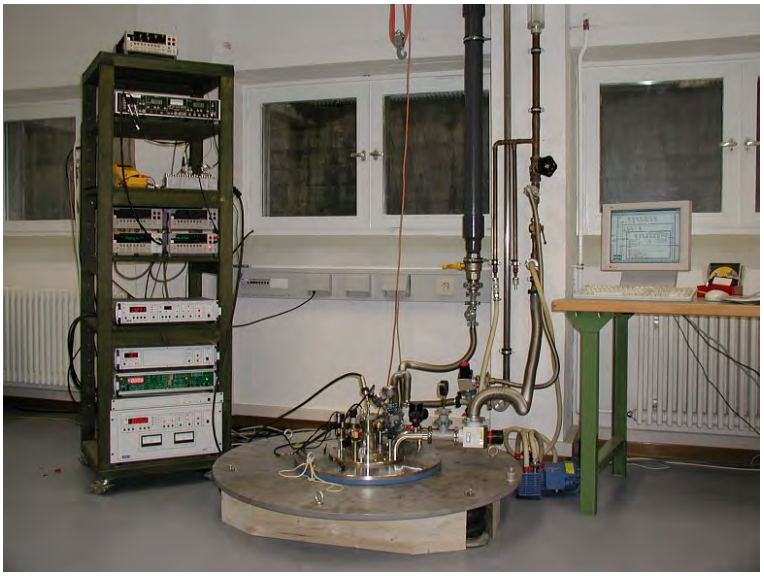

Figure 12: High field laboratory with Oxford 17 T magnet system.

Since 2012, a 3D vector magnet with variable temperature insert, allowing for 2.5 T in-plane and 6 T out-of-plane magnetic fields is available for thermal and electrical transport experiments. This system has been named "Chaos" cryostat (acronym for "Cold, Hot And Other Secret experiments"). It consists of a ^{4}He flow cryostat with a liquid nitrogen shield and in-

© Walther-Meißner-Institute

cludes a vertically oriented 6 T solenoid combined with two horizontally oriented split coil pairs. The magnet system can be operated in two ways:

- in a single axis mode: up to 6(2.5) T are provided in the vertical (horizontal) direction.
- in a arbitrary axis mode: the flux density vector can be oriented in arbitrary directions and the magnitude of the flux density is limited to 2.5 T.

The magnetic field is controlled by a Mercury IPS superconducting magnet power supply master/slave system. It provides output currents of up to 120 A in bipolar operation for each magnet axis. The control of the system is feasible either directly via touch-screen or remote using a LabView based software.

Figure 13: The 3D vector magnet with control electronics in the "CHAOS" Laboratory.

The Chaos cryostat has a IN100 variable temperature insert (VTI), enabling an operation for temperature setpoints between 1.5 K and 300 K. The temperature control of the sample space inside the VTI can be achieved via an automatic needle valve drive for helium flow control and/or an automatic heater system. The temperature of the VTI is read via a Cernox sensor fitted to the heat exchanger. A remote control of the system is realized by a LabView based software. It provides control of the VTI (heater, needle valve, temperature setpoint) and the IPS (control of the magnetic field setpoints and energizing rates for the three vector components of the field) as well as the display of the actual He and liquid nitrogen levels.

A further 3D vector magnet allowing for 1 T in-plane and 6 T out-of-plane magnetic fields is installed in the WMI Quantum Laboratories as part of a cryogen-free dilution system.

The Clean Room Facility

For the fabrication of nanostructures and quantum circuits including superconducting, spintronic and nanomechanical devices, the WMI operates a class 1000 clean room facility with an area of about 50 m^2. The clean room is subdivided into two parts for optical lithography and electron beam lithography, respectively. The clean room is equipped with the standard tools for optical lithography such as resist coaters, hot plates, wet benches, a Karl Süss MJB3 mask aligner, a direct laser writing system *PicoMaster 200* from 4 PICO, and an optical projection lithography system. The technical infrastructure for the clean room is located in the basement of the WMI directly below the clean room area.

Figure 14: Top: Part of the clean room facility with optical lithography equipment and clean room benches. Bottom: Resist coater and hot plates.

The clean room also is equipped with a reactive ion etching system, Plasmalab 80 Plus with ICP plasma source (Oxford Instruments Plasma Technology).

Electron Beam Lithography

A 100 kV Electron Beam Lithography System nB5 fabricated by NanoBeam Ltd., UK, is installed in the second part of the clean room facility. The nB5 is a round-beam step-and-repeat system oriented towards high-end R&D applications at universities and research institutes. It is designed for nanopatterning and mix-and-match lithography. The innovative design of the electron optics and automation system enhances its throughput and reliability. It is an ideal tool for nano-device research and production. The electron beam lithography is used for the fabrication of nanostructures in metallic and oxide systems required for the study of quantum effects in mesoscopic samples.

Figure 15: 100 kV Electron Beam Lithography System nB5 of NanoBeam Ltd., UK, inside the WMI cleanroom facility.

© Walther-Meißner-Institute

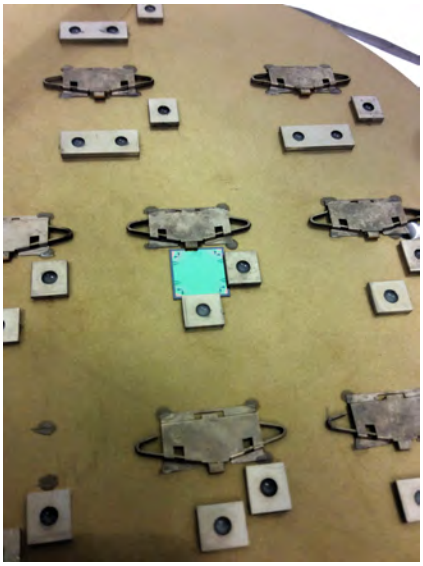

Figure 16: Chuck of the nB5 e-beam lithography system with a mounted $12 \times 12\,\mathrm{mm}^2$ silicon wafer.

The nB5 Electron Beam Lithography System employs low Coulomb-effect electron optics and sophisticated column designs to reduce beam size. The shorter optical column eliminates column bending and reduces system vibration. The modern electronics has low noise and low thermal effects. The perfectly integrated machine structure greatly improves system settling time and total stage move time. The advanced vibration tracking design enables the nB5 system to write on the fly. All these features combined with the fast deflection speed and high data processing rate make the nB5 the highest throughput system available today. Moreover, the nB5 requires undemanding cleanroom conditions, in particular regarding temperature stability, stray field magnitude, and floor vibration level.

The nB5 system is equipped with a thermal field emitter (TFE), an electrostatic lens and magnetic condenser lens, a conjugate beam blanking at $< 5\,\mathrm{ns}$ slew rate and a dual beam deflection. The latter is used to achieve ultra-high deflection speed for beam writing (clock rate: 55 MHz). The total deflection coverage is combined with the mainfield and the subfield and controlled by two independent deflection sub-systems (field size: $1000\,\mu\mathrm{m}$, address resolution: 1 nm). The characteristic performance parameters of the electron optics of the nB5 system are: (i) beam voltage range: 20 kV to 100 kV, (ii) minimum beam current: 0.1 nA, (iii) maximum beam current: 100 nA, (iv) theoretical beam size: 2.3 nm at 100 kV, (v) guaranteed writing beam size: $< 5\,\mathrm{nm}$ at 2 nA, (vi) beam current drift: $< 0.5\%$/hour at 5 nA, (vii) beam position drift: $< 50\,\mathrm{nm}$/hour for 3 nA beam current, including blanking, deflection and stage move.

The XY-stage allows for a traversal distance of 200 mm with a total stage move time of only 150 ms for 1 mm stage movement and a position measurement resolution of 0.3 nm using laser interferometry. The maximum substrate sizes are $2 - 8$ in for round substrates, $2 - 5$ for square glass masks up to 3 mm thickness. Finally, the nB5 system has airlock operation with automatic loading robotics with a loading cassette for 6 chucks with a maximum diameter of 8 inch.

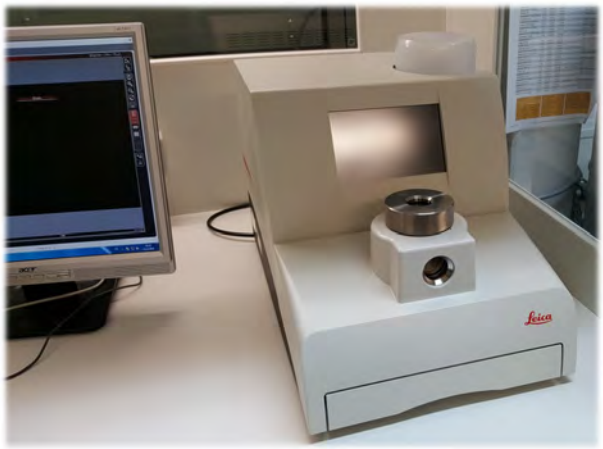

Figure 17: The fully automated Critical Point Dryer Leica EM CPD 300.

Automated Critical Point Dryer Leica EM CPD 300

The fabrication of nanomechanical systems requires the removal of solvent used for wet chemical processing by a critical point dryer. At WMI, we use the Critical Point Dryer Leica EM CPD 300, which allows the fully automated drying of biological specimens such as pollen, tissue, plants, insects etc., as well as NEMS (Nano Electro Mechanical Systems).

To ensure a low CO_2 consumption and a very short process time a new filler concept is used in the Leica EM CPD 300. Special attention has been put on safety issues by implementing software controlled cut-off functions and integrating a waste separator.

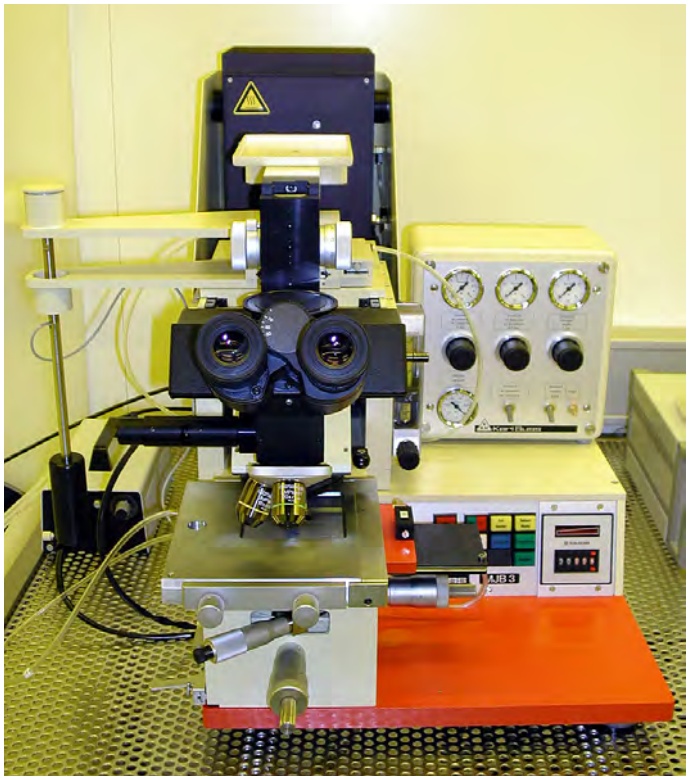

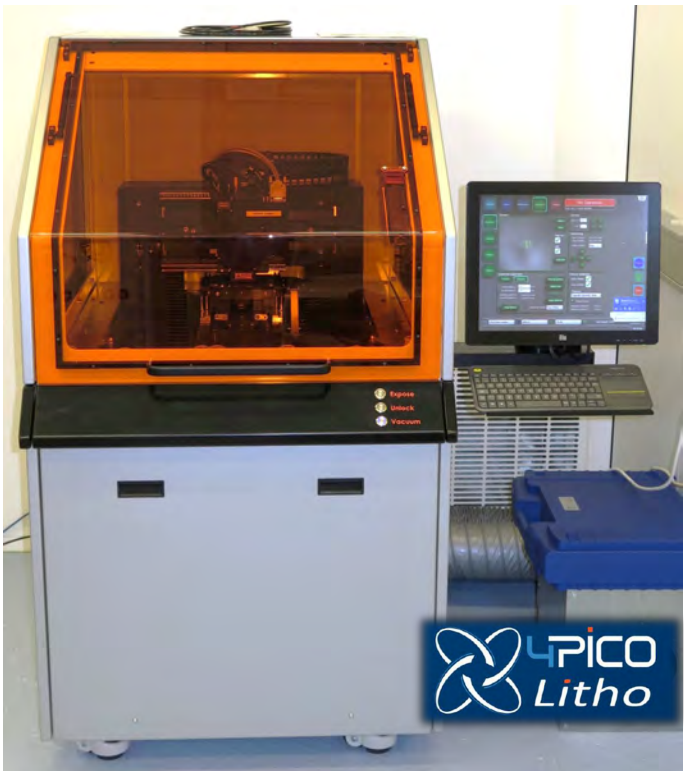

Figure 18: Top: Süss MJB 3 maskaligner for optical lithography. Bottom: Direct laser writing systems *PicoMaster 200*.

Optical Lithography

For optical lithography, a Karl Süss MJB 3 maskaligner or a direct laser writing system are used. The maskaligner operates in the 1 : 1 soft or hard contact mode and uses chromium metal masks.

The direct laser writing system *PicoMaster 200* (PM 200) of the company 4PICO accepts substrate sizes between $5\,\text{mm} \times 5\,\text{mm}$ and $200\,\text{mm} \times 200\,\text{mm}$ via a turnable chuck. For writing the pattern, it allows for three different spot sizes (300 nm/600 nm/900 nm) and a write speed of up to $7.7\,\text{mm}^2/\text{min}$. One can choose between two compact writing modules equipped with a 405 nm and a 375 nm laser diode, respectively. The user can easily switch between the two modules within minutes since the full optical path is contained in the modules. Both modules feature automatic focus correction for not too heavily varying resist thickness.

Low and Ultra-Low Temperature Facilities

Figure 19: The "dry" dilution refrigerator of the WMI.

Figure 20: Low-temperature unit of a WMI dilution refrigerator ready to go into a cryostat.

At the WMI, we have constructed the first dilution refrigerator with pulse tube pre-cooling for ultra-low temperature experiments. This type of refrigerator works without cryo-liquids, and thus is a lot more practical, more economical and more reliable than cryostats with liquid helium pre-cooling. These days, all major cryo-engineering companies are offering commercial versions of this Millikelvin cooler, and these so-called "dry" refrigerators outsell conventional refrigerators by a wide margin. The general construction concept of most manufacturers is unchanged from our original prototype, where the refrigerator consists of three basic components. The first cooling stage is a commercial pulse tube cryocooler which reaches a base temperature of 2.5 K. The second stage is a Joule-Thomson stage, and the last stage is a dilution refrigeration stage, where the lowest temperature of the cryostat is about 0.01 K (Fig. 19).

Figure 21: Two mixing chamber mounting plates with silver sponges. Those are needed to overcome the thermal resistance (Kapitza resistance) between the liquid ^{3,4}He and the mounting plate of the mixing chamber. To fabricate the mounting of the sponge (square pins embedded in the sponge) a spark erosion technique has been employed.

In many low temperature applications high refrigeration capacities are required. Our design allows for a high circulation rate of ^{3}He which in the end determines the cooling power of a dilution refrigerator. Presently our "dry" fridge reaches a refrigeration capacity of 700 µW at a temperature of the mixing chamber of 0.1 K, seven times the cooling power of the WMI nuclear demagnetization cryostat. Goals of our present work are a further increase of cooling power and a lower base temperature of the dry dilution refrigerator. A smaller version of our cryogen-free fridge has become commercially available later on by *VeriCold Technologies, Ismaning*) which was taken over by *Oxford Instruments* in 2007. It had a refrigeration capacity of 250 µW at a mixing chamber temperature of 0.1 K (Fig. 20).

The WMI also develops and fabricates dilution refrigerator inserts for temperatures down to

about 20 mK. The inserts fit into all cryogenic systems (e.g. superconducting magnets) having a two inch bore. They allow fast sample change and rapid cool down cycles of less than five hours. The dilution refrigerator inserts are engineered and fabricated in-house and are also provided to other low temperature laboratories for ultra-low temperature experiments.

Millikelvin Temperatures in Combination with 3D Vector Magnetic-Fields

Figure 22: The dilution refrigerator with the 3D vector magnet located in the Quantum Laboratories.

In one room of the WMI Quantum Laboratories a cryogen-free dilution refrigerator is installed. This system is equipped with a 3D vector magnet allowing for 1 T in-plane and 6 T out-of-plane magnetic fields. Additional microwave coaxial lines allow for the microwave spectroscopy up to 18 GHz under these experimental conditions.

Scientifically, several directions in the field of fundamental light-matter interaction are envisaged:

(i) Circuit quantum electrodynamics (circuit QED), where superconducting qubits form hybrids with microwave resonators. These experiments are time consuming, because quantum effects arise in the limit of low excitation numbers. Hereby, challenging requirements are imposed on the detection systems allowing to detect microwave signals in the attowatt regime.

(ii) Storage of quantum states. One possibility is the transfer of the quantum information contained in photons to long-lived spin states. Additionally, exchange coupled systems or ferromagetic systems come into focus, because the effective coupling strength scales with the square-root of the number of spins contributing. In general, we study the light-matter interaction with long-lived spin systems and integrate them into superconducting quantum circuits.

(iii) Spin systems. Here, our studies are not limited to paramagnetic spin systems, but also involve exchange coupled (ferro- or ferri-) magnetic systems. Hereby, magnetization damping can be investigated as a function of temperature, frequency and magnetic field direction.

(iv) Circuit electro-mechanical hybrid systems consisting of a nano-mechanical element coupled to a superconducting microwave resonator. In this context, sideband cooling of the mechanical system into its ground state and pulsed spectroscopy of hybrid system are performed and will be extended.

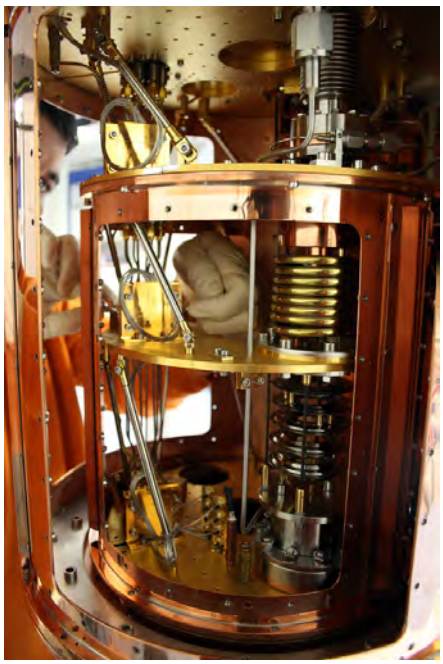

Figure 23: Inside of the dilution system. The windows of the 4 K and the still shield are removed providing access to the low temperature stages.

WMI Millikelvin Facilities for Experiments with Superconducting Quantum Circuits

The research on superconducting quantum circuits at WMI focuses mainly on systems sensitive to externally applied flux (flux qubits), circuit QED systems where flux qubits are coupled to transmission line resonators, squeezing physics in flux driven Josephson parametric amplifiers, and propagating quantum microwaves (e.g., quantum state reconstruction methods). In order to further develop our activities on quantum effects in the microwave regime, additional cryogenic capacities at millikelvin temperatures have been established. In addition to sufficient cooling power, the specifications for these cryostats are mainly dictated by the dimensions (typically a few centimeters in each direction) of bulky microwave components such as circulators or microwave switches.

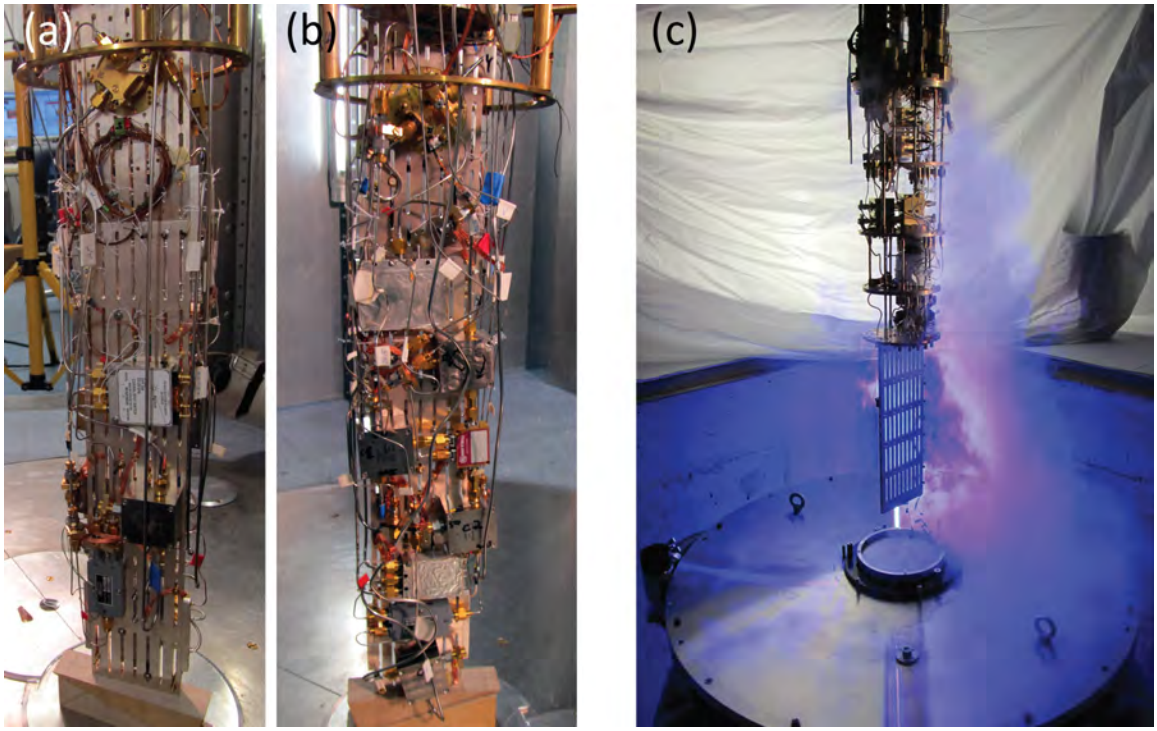

Figure 24: Liquid-helium precooled dilution refrigerators for experiments with superconducting quantum circuits. (a), (b) Back and front sides of the sample stage of the K12-refrigerator equipped with four circuit QED experiments. The height of the silver rod is 50 cm. (c) Sample stage and dewar of the dilution refrigerator in the quantum laboratory K04.

Two liquid-helium precooled dilution refrigerators are available for experiments with superconducting quantum circuits. The dilution refrigerator in laboratory K12 provides a sample space with a cylindrical volume with 11 cm diameter 55 cm height. The refrigerator is equipped with four microwave amplifiers at the 4 K-stage, seven broadband input lines and 80 twisted pair DC lines. This allows for mounting four experiments simultaneously to avoid idle times by interleaved measurements (see Fig. 24(a) and (b)). The base temperature of this refrigerator is 20 mK.

A new liquid-helium precooled dilution refrigerator for experiments with superconducting quantum circuits has been set up in the quantum laboratory K04. To provide enough space at the sample stage we have installed a Cryogenic Ltd. stainless steel dewar with a ^{4}He volume of 89 l. The time between two refills exceeds nine days. The cryostat is equipped with 16 coaxial measurement lines suitable for microwave frequencies down to the mixing chamber stage and low-noise cryogenic high electron mobility transistor (HEMT) amplifiers. Presently up to four samples can be mounted simultaneously to the sample stage. By expanding the number of input lines in the near future a more complex experiment can be set up. The cooling power of

the mixing chamber at 100 mK was determined to about 140 µW.

A new cryogen-free dilution refrigerator with a pulse tube refrigerator (PTR) for precooling and with a large sample stage has been set up in room K21 of the WMI Quantum Laboratories using the longstanding experience in dry dilution refrigerators at WMI. This refrigerator features large diameters (tens of centimeters) of all temperature stages providing sufficient space for advanced quantum experiments. The main components of the refrigerator are the PTR, a 1 K-stage and a dilution unit. The two stages of the PTR cool the incoming ^{4}He and the ^{3}He/^{4}He mixture as well as one radiation shield at each stage. To provide sufficiently high cooling power near 1 K to cool microwave components and cables, this refrigerator has been equipped with a 1 K-stage operating in a closed cycle. A refrigeration capacity of the 1 K-stage of up to 100 mW could be reached. The dilution refrigerator is precooled by a dedicated ^{4}He circuit. The minimum base temperature of the refrigerator is below 11 mK. The cooling power at 100 mK was determined to about 300 µW at the maximum ^{3}He flow rate.

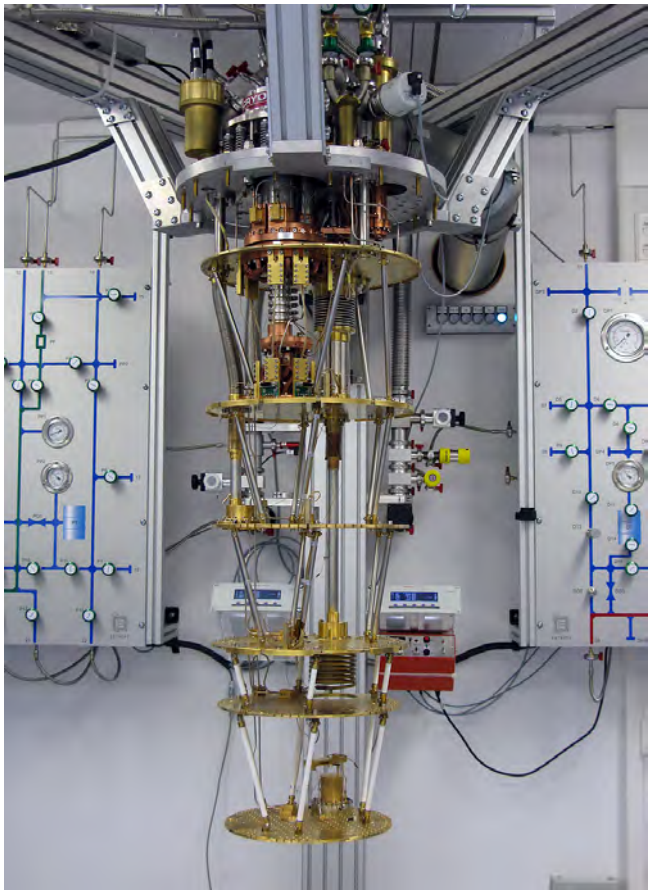

Figure 25: Dry dilution refrigerator with a large sample space.

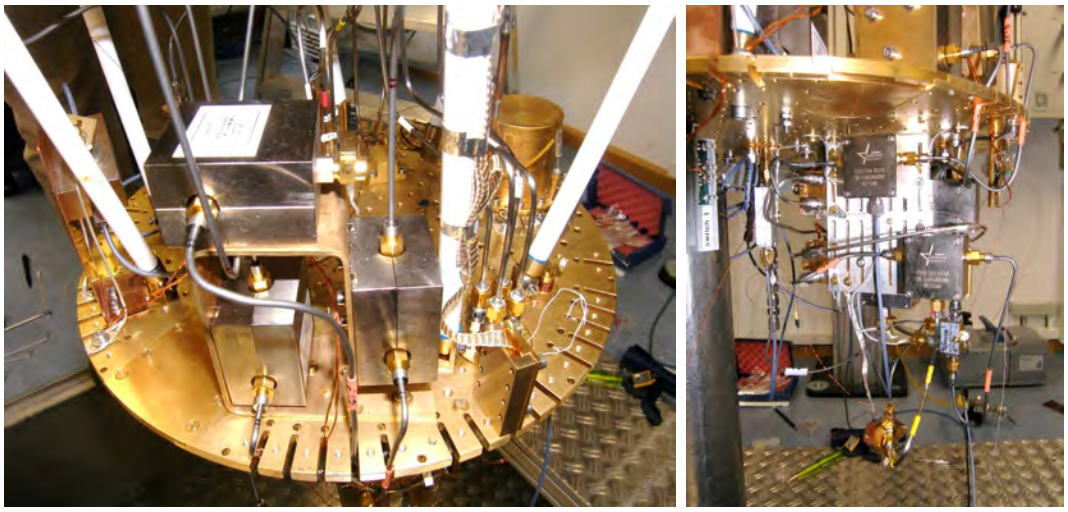

Figure 26: Low temperature platform of K21 dilution refrigerator with experimental setup for circuit QED experiments.

Statistics

Publications

1. **Observation of Antiferromagnetic Magnon Pseudospin Dynamics and the Hanle Effect**
Tobias Wimmer, Akashdeep Kamra, Janine Gückelhorn, Matthias Opel, Stephan Geprägs, Rudolf Gross, Hans Huebl, Matthias Althammer
Physical Review Letters **125**, 247204 (2020).

2. **Raman Study of Cooper Pairing Instabilities in ($Li_{1-x}Fe_x$)OHFeSe**
G. He, D. Li, D. Jost, A. Baum, P. P. Shen, X. L. Dong, Z. X. Zhao, and R. Hackl
Physical Review Letters **125**, 217002 (2020).

3. **Echo Trains in Pulsed Electron Spin Resonance of a Strongly Coupled Spin Ensemble**
Stefan Weichselbaumer, Christoph W. Zollitsch, Martin S. Brandt, Rudolf Gross, Hans Huebl
Physical Review Letters **125**, 137701 (2020).

4. **Nonreciprocal Dzyaloshinskii-Moriya magnetoacoustic waves**
Matthias Küß, Michael Heigl, Luis Flacke, Andreas Hörner, Mathias Weiler, Manfred Albrecht, Achim Wixforth
Physical Review Letters **125**, 217203 (2020).

5. **Resonant Nanodiffraction X-Ray Imaging Reveals Role of Magnetic Domains in Complex Oxide Spin Caloritronics**
Paul G. Evans, Samuel D. Marks, Stephan Geprägs, Maxim Dietlein, Yves Joly, Minyi Dai, Jiamian Hu, Laurence Bouchenoire, Paul B. J. Thompson, Tobias U. Schülli, Marie-Ingrid Richard, Rudolf Gross, Dina Carbone, and Danny Mannix
Science Advances **6**, eaba9351 (2020).

6. **Large Spin Hall Magnetoresistance in Antiferromagnetic α-Fe_2O_3/Pt Heterostructures**
Johanna Fischer, Matthias Althammer, Nynke Vlietstra, Hans Huebl, Sebastian T.B. Goennenwein, Rudolf Gross, Stephan Geprägs, Matthias Opel
Physical Review Applied **13**, 014019 (2020).

7. **Quantitative Comparison of Magnon Transport Experiments in Three-Terminal YIG/Pt Nanostructures Acquired via DC and AC Detection Techniques**
J. Gückelhorn, T. Wimmer, S. Geprägs, H. Huebl, R. Gross, and M. Althammer
Applied Physics Letters **117**, 182401 (2020).

8. **Spin Hall Magnetoresistance in Antiferromagnetic Insulators**
Stephan Geprägs, Matthias Opel, Johanna Fischer, Olena Gomonay, Philipp Schwenke, Matthias Althammer, Hans Huebl, Rudolf Gross
Journal of Applied Physics **127**, 243902 (2020).

9. **Effect of Interfacial Oxidation Layer in Spin Pumping Experiments on $Ni_{80}Fe_{20}$/$SrIrO_3$ Heterostructures**
T.S. Suraj, Manuel Müller, Sarah Gelder, Stephan Geprägs, Matthias Opel, Mathias Weiler, K. Sethupathi, Hans Huebl, Rudolf Gross, M.S. Ramachandra Rao, Matthias Althammer
Journal of Applied Physics **128**, 083903 (2020).

10. **Precise Control of $J_{eff} = 1/2$ Magnetic Properties in Sr_2IrO_4 Epitaxial Thin Films by Variation of Strain and Thin Film Thickness**
Stephan Geprägs, Björn Erik Skovdal, Monika Scheufele, Matthias Opel, Didier Wermeille, Paul Thompson, Alessandro Bombardi, Virginie Simonet, Stéphane Grenier, Pascal Lejay, Gilbert Andre Chahine, Diana Quintero Castro, Rudolf Gross, Dan Mannix
Physical Review B **102**, 214402 (2020).

11. **Antiferromagnetic magnon pseudospin: Dynamics and diffusive transport**
Akashdeep Kamra, Tobias Wimmer, Hans Huebl, Matthias Althammer
Physical Review B **102**, 174445 (2020).

12. **Sideband-resolved resonator electromechanics on the single-photon level based on a nonlinear Josephson inductance**
Philip Schmidt, Mohammad T. Amawi, Stefan Pogorzalek, Frank Deppe, Achim Marx, Rudolf Gross, Hans Huebl
Communication Physics **3**, 233 (2020).

13. **Direct evidence for anisotropic three-dimensional magnetic excitations in a hole-doped antiferromagnet**
Rajesh Dutta, Avishek Maity, Anna Marsicano, J. Ross Stewart, Matthias Opel, Werner Paulus
Physical Review B **102**, 165130 (2020).

14. **Thermal transport of helium-3 in a strongly confining channel**
D. Lotnyk, A. Eyal, N. Zhelev, T. S. Abhilash, E. N. Smith, M. Terilli, J. Wilson, E. Mueller, D. Einzel, J. Saunders, J. M. Parpia
Nature Communications **11**, 4843 (2020).

15. **Nonlinear losses in magnon transport due to four-magnon scattering**
Tobias Hula, Katrin Schultheiss, Aleksandr Buzdakov, Lukas Körber, Mauricio Bejarano, Luis Flacke, Lukas Liensberger, Mathias Weiler, Justin M. Shaw, Hans T. Nembach, Jürgen Fassbender, and Helmut Schultheiss
Applied Physics Letters **117**, 042404 (2020).

16. **Bolometer operating at the threshold for circuit quantum electrodynamics**
R. Kokkoniemi, J.-P. Girard, D. Hazra, A. Laitinen, J. Govenius, R. E. Lake, I. Sallinen, V. Vesterinen, M. Partanen, J. Y. Tan, K. W. Chan, K. Y. Tan, P. Hakonen, M. Möttönen
Nature **586**, 47-51 (2020). (2020)

17. **High-Throughput Techniques for Measuring the Spin Hall Effect**
Markus Meinert, Björn Gliniors, Oliver Gueckstock, Tom S. Seifert, Lukas Liensberger, Mathias Weiler, Sebastian Wimmer, Hubert Ebert, and Tobias Kampfrath
Physical Review Applied **14**, 064011 (2020).

18. **Fluctuations and pairing in Fe-based superconductors: Light scattering experiments**
N. Lazarević and R. Hackl
Journal of Physics: Condensed Matter **32**, 413001 (2020).

19. **Measuring the imaginary time dynamics of quantum materials**
S. Lederer, D. Jost, R. Hackl, E. Berg, S.A. Kivelson
Philosophical Magazine B **100**, 2477-2490 (2020).

20. **Cryogenic characterization of a $LiAlO_2$ crystal and new results on spin-dependent dark matter interactions with ordinary matter**
A.H. Abdelhameed et al. (The CRESST Collaboration)
European Physical Journal C **80**, 834 (2020).

21. **Searches for Light Dark Matter with the CRESST-III Experiment**
M. Mancuso, A. H. Abdelhameed et al. (The CRESST Collaboration)
Journal of Low Temperature Physics **199**, 547-555 (2020).

22. **Lithium-Containing Crystals for Light Dark Matter Search Experiments**
E. Bertoldo, A. H. Abdelhameed et al. (The CRESST Collaboration)
Journal of Low Temperature Physics **199**, 510-518 (2020).

23. **Emergence of pseudogap from short-range spin-correlations in electron doped cuprates**
F. Boschini, M. Zonno, E. Razzoli, R. P. Day, M. Michiardi, B. Zwartsenberg, P. Nigge, M. Schneider, E. H. da Silva Neto, A. Erb, S. Zhdanovich, A. K. Mills, G. Levy, C. Giannetti, D. J. Jones, A. Damascelli
npj Quantum Materials **5**, 6 (2020).

24. **Surface distortion of Fe dot-decorated TiO_2 nanotubular templates using time-of-flight grazing incidence small angle scattering**
Neelima Paul, Jean-Francóis Moulin, Gaetano Mangiapia, Armin Kriele, Peter Müller-Buschbaum, Matthias Opel, Amitesh Paul
Scientific Reports **10**, 4038 (2020).

25. **Self-Assembly of Large Magnetic Nanoparticles in Ultrahigh Molecular Weight Linear Diblock Copolymer Films**
Wei Cao, Senlin Xia, Xinyu Jiang, Michael Appold, Matthias Opel, Martina Plank, Roy Schaffrinna, Lucas P. Kreuzer, Shanshan Yin, Markus Gallei, Matthias Schwartzkopf, Stephan V. Roth, Peter Müller-Buschbaum
ACS Applied Materials & Interfaces **12**, 7557 (2020).

© Walther-Meißner-Institute

26. **$La_{1-x}Mn_{1-y}O_{1\pm\delta}$ Buffer Layers on Inclined Substrate Deposited Mgo Templates for Coated Conductors**
Oleksiy Troshyn, Christian Hoffmann, Veit Große, Jens Hänisch, Lucas Becker, Rudolf Gross
Superconducting Science and Technology, accepted for publication (2020), arXiv:2012.01318.

27. **Static magnetic proximity effects and spin Hall magnetoresistance in Pt/$Y_3Fe_5O_{12}$ and inverted $Y_3Fe_5O_{12}$/Pt bilayers**
Stephan Geprägs, Christoph Klewe, Sibylle Meyer, Dominik Graulich, Felix Schade, Marc Schneider, Sonia Francoual, Stephen P. Collins, Katharina Ollefs, Fabrice Wilhelm, Andrei Rogalev, Yves Joly, Sebastian T.B. Goennenwein, Matthias Opel, Timo Kuschel, Rudolf Gross
Physical Review B **102**, 214438 (2020).

28. **Time-resolved tomography of a driven adiabatic quantum simulation**
G. Salis, N. Moll, M. Roth, M. Ganzhorn, S. Filipp
Physical Review A **102**, 062611 (2020).

29. **Benchmarking the noise sensitivity of different parametric two-qubit gates in a single superconducting quantum computing platform**
M. Ganzhorn, G. Salis, D. J. Egger, A. Fuhrer, M. Mergenthaler, C. Müller, P. Müller, S. Paredes, M. Pechal, M. Werninghaus, S. Filipp. Physical Review Research **2** 033447 (2020).

30. **Erste Demonstration von Quantenüberlegenheit**
M. J. Hartmann and F. Deppe
Physik in unserer Zeit **52**, 12-18 (2021).

31. **$La_{1-x}Mn_{1-y}O_{1\pm\delta}$ Buffer Layers on Inclined Substrate Deposited Mgo Templates for Coated Conductors**
Oleksiy Troshyn, Christian Hoffmann, Veit Große, Jens Hänisch, Lucas Becker, Rudolf Gross
Superconducting Science and Technology, accepted for publication (2020), arXiv:2012.01318.

32. **Zeeman spin-orbit coupling and magnetic quantum oscillations in antiferromagnetic conductors**
R. Ramazashvili, P. D. Grigoriev, T. Helm, F. Kollmannsberger, M. Kunz, W. Biberacher, E. Kampert, H. Fujiwara, A. Erb, J. Wosnitza, R. Gross, M. V. Kartsovnik
njp Quantum Matter, accepted for publication (2020), arXiv:1908.01236.

33. **Description of CRESST-III Data**
A.H. Abdelhameed et al. (The CRESST Collaboration)
arXiv:1905.07335, submitted for publication (2019).

34. **Quantum Fourier Transform in Oscillating Modes**
Qi-Ming Chen, Frank Deppe, Re-Bing Wu, Luyan Sun, Yu-xi Liu, Yuki Nojiri, Stefan Pogorzalek, Michael Renger, Matti Partanen, Kirill G. Fedorov, Achim Marx, Rudolf Gross
arXiv:1912.09861, submitted for publication (2019).

35. **Temperature-dependent spin-transport and current-induced torques in superconductor/ferromagnet heterostructures**
Manuel Müller, Lukas Liensberger, Luis Flacke, Hans Huebl, Akashdeep Kamra, Wolfgang Belzig, Rudolf Gross, Mathias Weiler, Matthias Althammer
arXiv:2007.15569, submitted for publication (2020).

36. **Superconducting Wireless Power Transfer Beyond 5 kW at High Power Density for Industrial Applications and Fast Battery Charging**
Christoph Utschick, Cem Som, Ján Šouc, Veit Große, Fedor Gömöry, Rudolf Gross
arXiv:2008.05741, submitted for publication (2020).

37. **In-situ tunable nonlinearity and competing signal paths in coupled superconducting resonators**
Michael Fischer, Qi-Ming Chen, Christian Besson, Peter Eder, Jan Goetz, Stefan Pogorzalek, Michael Renger, Edwar Xie, Michael J. Hartmann, Kirill G. Fedorov, Achim Marx, Frank Deppe, Rudolf Gross
arXiv:2009.13492, submitted for publication (2020).

38. **Temperature independent cuprate pseudogap from planar oxygen NMR**
Jakob Nachtigal, Marija Avramovska, Andreas Erb, Danica Pavicevic, Robin Guehne, Jürgen

Haase
arXiv:2009.09492, submitted for publication (2020).

39. **An integrated tool-set for Control, Calibration and Characterization of quantum devices applied to superconducting qubits**
N. Wittler, F. Roy, K. Pack, M. Werninghaus, A. S. Roy, D. J. Egger, S. Filipp, F. K. Wilhelm, S. Machnes
arXiv:2009.09866, submitted for publication (2020).

40. **Static magnetic proximity effects and spin Hall magnetoresistance in Pt/$Y_3Fe_5O_{12}$ and inverted $Y_3Fe_5O_{12}$/Pt bilayers**
Stephan Geprägs, Christoph Klewe, Sibylle Meyer, Dominik Graulich, Felix Schade, Marc Schneider, Sonia Francoual, Stephen P. Collins, Katharina Ollefs, Fabrice Wilhelm, Andrei Rogalev, Yves Joly, Sebastian T.B. Goennenwein, Matthias Opel, Timo Kuschel, Rudolf Gross
arXiv:2010.03979, submitted for publication (2020).

41. **High-speed calibration and characterization of superconducting quantum processors without qubit reset**
M. Werninghaus, D. Egger, S. Filipp
arXiv:2010.06576, submitted for publication (2020).

42. **Beyond the Standard Quantum Limit of Parametric Amplification**
M. Renger, S. Pogorzalek, Q. Chen, Y. Nojiri, K. Inomata, Y. Nakamura, M. Partanen, A. Marx, R. Gross, F. Deppe, K. G. Fedorov
arXiv:2011.00914, submitted for publication (2020).

43. **Dia- and Adiabatic Dynamics in a Phononic Network**
Daniel Schwienbacher, Thomas Luschmann, Rudolf Gross, Hans Huebl
arXiv:2011.08080, submitted for publication (2020).

44. **Characterization and tomography of a hidden qubit**
M. Pechal, G. Salis, M. Ganzhorn, D. J. Egger, M. Werninghaus, S. Filipp
arXiv:2011.08987, submitted for publication (2020).

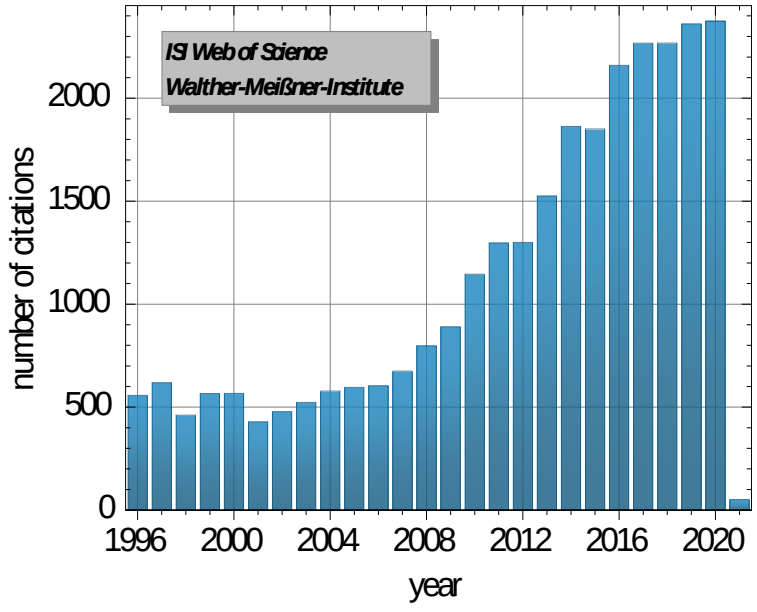

The total number of citations per year of papers published by members of WMI since 1996. This number has about quadrupled within the last twenty years and presently exceeds 2 300.

Bachelor, Master, Doctoral, and Habilitation Theses

A. Completed and Ongoing Habilitation Theses

At present, two postdoctoral researchers – Matthias Althammer and Kirill Fedorov – are passing through the habilitation procedure of the Technical University of Munich. The habilitation serves as the formal assessment tool ascertaining whether or not a candidate is suitable, from an academic and a pedagogical point of view, to be a professor in a particular field at the university level.

In December 2019, Mathias Weiler has successfully completed the habilitation procedure and became a docent in experimental physics at the Physics Department of TUM. Already in October 2020 he started a full (W3) professor position at the TU Kaiserslautern (see page 113). He is an excellent example for the promotion of postdoctoral researcher by WMI making them competitive for professor positions all over the world.

The promotion of highly qualified young scholars is a key concern of WMI. The fostering of young scholars goes hand in hand with equipping them to stand on their own in fields that are very competitive on both the national and international scales.

1. Dr. Matthias Althammer

Matthias Althammer joined WMI in December 2013 after a postdoctoral stay (10/2012 – 11/2013) at the Center for Materials for Information Technology, University of Alabama, Tuscaloosa, USA, where he worked on oxide based spintronics. From 05/2014 to 02/2015 he was on leave from WMI to acquire experience in industry as an Engineering Consultant at Esprit Engineering GmbH, Munich.

Matthias Althammer was accepted as a *"Habilitand"* by the Faculty of Physics of TU Munich in January 2016, with Rudolf Gross (TU Munich), Martin Brandt (TU Munich) and Arunava Gupta (MINT Center, University of Alabama) forming the so-called *Fachmentorat*. The research topic of his habilitation project is the *Experimental Study of Spin-dependent Transport Phenomena*. Regarding teaching, Matthias Althammer was offering the lectures on *Magnetism* and *Spin Electronics* and additionally was organizing the seminar on *Spin Currents and Skyrmionics*.

On 14th June 2018 he successfully passed the intermediate evaluation of his habilitation process. The *Fachmentorat* appreciated that most of the goals fixed in 2016 have been perfectly achieved. The target agreement has been extended for the second two-year phase of the habilitation procedure and the *Fachmentorat* recommended him to finish the habilitation process until autumn 2020. Meanwhile, Matthias Althammer has submitted his habilitation thesis entitled *Pure Spin Currents in Magnetic Insulators*. It will be sent out to international reviewers early in 2021.

2. Dr. Kirill Fedorov

Kirill Fedorov studied physics in Russia (Institute for Physics of Microstructures, Russian Academy of Sciences, Nizhny Novgorod), where he received his master degree in 2008. He

then joined the group of Prof. Alexey Ustinov at the Karlsruhe Institute of Technology as a Ph.D. student. He finished his Ph.D. thesis entitled *Fluxon readout for superconducting flux qubits* in 2013 and then joined Walther-Meißner-Institute as a postdoctoral researcher in December 2013. His key research topic is the realization of seminal quantum experiments based on propagating quantum microwaves. In teaching, he is taking care about the lecture on*Applied Superconductivity: Josephson Effects, Superconducting Electronics and Superconducting Quantum Circuits* and also is co-organizing the seminar on *Superconducting Quantum Circuits*.

Kirill Fedorov was accepted as a *"Habilitand"* by the Faculty of Physics of TU Munich in September 2016. In his case, Rudolf Gross (TU Munich), Jonathan Finley (TU Munich/Walter Schottky Institute) and Enrique Solano (Universidad del País Vasco and Ikerbasque Foundation, Bilbao, Spain) form the *Fachmentorat*. The midterm evaluation of his habilitation process took place on 18th January 2019, when Kirill Fedorov gave a talk within the Colloquium on Solid-State Physics of the Faculty of Physics entitled *Quantum communication with squeezed microwaves*. Kirill Fedorov successfully passed the intermediate evaluation and the *Fachmentorat* extended the target agreement for the second two-year phase of his habilitation.

© Walther-Meißner-Institute

B. Completed and Ongoing Ph.D. Theses

Completed Ph.D. Theses:

1. **Nanomechanical Quantum Systems**
   Philip Ernst Schmidt, Technical University of Munich, February 2020.
2. **Spin Dynamics in Strongly Coupled Spin-Photon Hybrid Systems**
   Stefan Weichselbaumer, Technical University of Munich, March 2020.
3. **Remote State Preparation of Squeezed Microwave States**
   Stefan Pogorzalek, Technical University of Munich, October 2020.

The Ph.D. students of the Walther-Meißner-Institute finishing their Ph.D. theses in 2020.

Ongoing Ph.D. Theses:

1. **Untersuchung des Wärmetransports in expandiertem Perlit zur Entwicklung einer Vakuumpulverisolation für Hochtemperatur-Anwendungen bis 800°C**
   Matthias Johannes Rottmann, Technical University of Munich, Januar 2021.
2. **Chains of Nonlinear and Tunable Superconducting Resonators**
   Michael Fischer, Technical University of Munich, since January 2015.
3. **Nanoelectromechanics: from magnon phonon coupling to circuit quantum bits**
   Daniel Schwienbacher, Technical University of Munich, since October 2015.
4. **Spin Currents in Magnetic Heterostructures**
   Tobias Wimmer, Technical University of Munich, since January 2017.

5. **ReBCO-Schichten auf ISD biaxial texturierten Substraten für supraleitende Bandleiter der 2. Generation**
   Oleksiy Troshyn, Technical University of Munich, since August 2016.
6. **Direct and Inverse Spin-Orbit Torques**
   Lukas Liensberger, Technical University of Munich, since January 2018.
7. **Evaluierung und Neuentwicklung durch Nutzung von Supraleitern in einer zirkularen Anordnung zur quasi verlustfreien kontaktlosen Energieübertragung für sehr hohe Leistungen**
   Christoph Utschick, Technical University of Munich, since June 2018.
8. **Spatially and Momentum Resolved Raman Studies of Unconventional Superconductors**
   Gabriele Rager, Technical University of Munich, since March 2018.
9. **Spin Dynamics of Hybrid Skyrmion-Magnon Solitons**
   Luis Flacke, Technical University of Munich, since September 2018.
10. **Correlation Measurements in Coupled Nonlinear Resonators**
    Qiming Chen, Technical University of Munich, since October 2018.
11. **Quantum Microwave Communication**
    Michael Renger, Technical University of Munich, since November 2018.
12. **Pure Spin Currents in Epitaxial All Oxide Heterostructures**
    Janine Gückelhorn, Technical University of Munich, since March 2019.
13. **Hybride Solid State Quantum Systems**
    Thomas Luschmann, Technical University of Munich, since September 2019.
14. **Coherent Adiabatic Quantum Annealer Based on Superconducting Quantum Circuits**
    Yuki Nojiri, Technical University of Munich, since September 2019.
15. **Spin Phenomena in Superconductor/Ferromagnet Heterostructures**
    Manuel Müller, Technical University of Munich, starting from March 2020.
16. **Fabrication of a High-Coherence Multi-Qubit Superconducting Qubit Platform**
    Leon Koch, Technical University of Munich, since July 2020.
17. **Tailoring the Control of Superconducting Qubits to Efficiently Solve Molecular Chemistry Problems**
    Malay Singh, Technical University of Munich, since October 2020.
18. **Multi-Qubit Gates for the Efficient Exploration of Hilbert Space with Superconducting Circuits**
    Ivan Tsitsilin, Technical University of Munich, since October 2020.
19. **Microwave Photo Detection for a Quantum Radar Receiver**
    Kedar Honasoge, Technical University of Munich, starting from February 2021.
20. **Receiver for Quantum Microwave Radar**
    Fabian Kronowetter, Technical University of Munich, starting from February 2021.
21. **Remote Entanglement of Superconducting Qubits with Two-Mode Squeezing**
    Florian Fesquet, Technical University of Munich, starting from February 2021.

© Walther-Meißner-Institute

C. Completed and Ongoing Bachelor and Master Theses

Completed Master Theses:

1. **A Low Noise Laser System for High Fidelity Rydberg Atom Manipulation**
   Joop Age Harm Adema, Master Thesis, Technical University of Munich, February 2020.
2. **Spin Current Physics in Uniaxial Antiferromagnetic Cr_2O_3/Pt Bilayers**
   Raffael Ferdigg, Master Thesis, Technical University of Munich, March 2020.
3. **Coupled Magnetization Dynamics in Ferrimagnet/Ferromagnet and Chiral Magnet/Ferromagnet Heterostructures**
   Carolina Lüthi, Master Thesis, Technical University of Munich, June 2020.
4. **Quantum Memory mit Optimal Control / Quantum Memory with Optimal Control**
   Stephan Trattnig, Master Thesis, Technical University of Munich, March 2020.
5. **Spin Seebeck Effect: A Powerful Probe for Magnon Properties in Compensated Ferrimagnets**
   Maxim Dietlein, Master Thesis, Technical University of Munich, June 2020.
6. **Experimental Implementation of a Quantum Key Distribution with Squeezed Microwaves**
   Florian Fesquet, Master Thesis, Technical University of Munich, October 2020.
7. **Optimized Geometry for a Compact 3D Quantum Memory**
   Julia Lamprich, Master Thesis, Technical University of Munich, October 2020.

Completed Bachelor Theses:

1. **Superconducting Cables for Quantum Microwave Communication**
   Meike Pfeiffer, Technical University of Munich (2020)
2. **Characterization of Surface Acoustic Wave Devices on Various Material Systems at Room and Cryogenic Temperatures**
   Alexander Jung, Technical University of Munich (2020)
3. **Untersuchung des Spin-Hall-Magnetwiderstands in Spinell-basierten Heterostrukturen**
   Andreas Haslberger, Technical University of Munich (2020)
4. **Spinstromexperimente mit vertikalen Platin | Yttrium-Eisen-Granat Heterostrukturen**
   Christian Mang, Technical University of Munich (2020)
5. **Magnetismus und Phononen in CuMnAs**
   Maria Sigl, Technical University of Munich (2020)
6. **Frequency-Degenerate Josephson Mixer Based on Josephson Parametric Amplifiers**
   Simon Gandorfer, Technical University of Munich (2020)

Ongoing Master Theses:

1. **All-Electrical Magnon Transport and Manipulation in Magnetically Ordered Insulators**
   Emir Karadza, Master Thesis, Technical University of Munich, since November 2019
2. **Improved Fabrication Process for Transmon Qubits**
   Christoph Scheuer, Master Thesis, Technical University of Munich, since November 2019
3. **Tunnel- und Raman-Spektroskopie an Kuprat-Supraleitern / Tunneling- and Raman**

Spectroscopy in Cuprate Superconductors
Minghao Zhang, Master Thesis, Technical University of Munich, since November 2019

4. **Magnetization Dynamics and Chiral Spin Texture in Thin-Film Magnetic Multilayers**
Misbah Yaqoob, Master Thesis, Technical University of Munich, since March 2020
5. **Magnetotransport and Spin Wave Propagation in Synthetic Antiferromagnets**
Elisabeth Meidinger, Master Thesis, Technical University of Munich, since April 2020.
6. **Controlling Magnon Transport**
Korbinian Rubenbauer, Master Thesis, Technical University of Munich, since April 2020.
7. **Quantum Acoustics with Superconducting Qubits**
Christopher Waas, Master Thesis, Technical University of Munich, since June 2020.
8. **Pulse Optimizations of Superconducting Qubit Gates**
Niklas Glaser, Master Thesis, Technical University of Munich, since October 2020.
9. **Characterization and Fabrication of High-Coherence Superconducting Microwave Circuits**
Leonhard Hölscher, Master Thesis, Technical University of Munich, since October 2020.
10. **Characterization and Fabrication of Superconducting Multi-Qubit Devices**
Gerhard Huber, Master Thesis, Technical University of Munich, since October 2020.
11. **High Frequency Superconducting Circuits**
Niklas Bruckmoser, Master Thesis, Technical University of Munich, since October 2020.
12. **Magnetism and Topological Effects in $Co_3Sn_2S_2$**
Ramona Stumberger, Master Thesis, Technical University of Munich, since October 2020.
13. **Durchstimmung der Amplitude des Spin-Hall-Magnetwiderstandes**
Monika Scheufele, Master Thesis, Technical University of Munich, since November 2020.
14. **Oxidische Heterostrukturen für Experimente mit reinen Spinströmen**
Philipp Schwenke, Master Thesis, Technical University of Munich, since November 2020.

Ongoing Bachelor Theses:

1. **Wachstumsoptimierung supraleitender Tantalnitrid (TaN)-Dünnfilme für fortgeschrittene Spinelektronik**
Raphael Hoepfl, Technical University of Munich (2020)
2. **Herstellung von verlustarmen Josephson-Kontakten für Quanten-Bauelemente**
Patrick Missale, Technical University of Munich (2020).

© Walther-Meißner-Institute

Research Projects

A large number of our research projects are benefiting from the collaboration with other research institutions and industry in coordinated research projects, as well as from individual collaborations, exchange programs and visitors. Most collaborations are based on joint projects, which are funded by different funding agencies (see list below). A considerable number of collaborations also exists with universities, other research institutions and industry without direct financial support.

A. German Research Foundation: Excellence Initiative & Strategy

Cluster of Excellence «*Munich Center for Quantum Science and Technology*» *(MCQST)*

The new Cluster of Excellence has been granted in September 2018 within Germany's Excellence Strategy and started in January 2019. Together with Immanuel Bloch of LMU Munich and Ignacio Cirac of Max Planck Institute of Quantum Optics, Rudolf Gross of Walther-Meißner-Institute is one of the three spokespersons of MCQST and coordinator of the Research Unit C on Quantum Computing.

1. Research Unit C: *Quantum Computing*
   Principal Investigators: F. Deppe, S. Filipp, R. Gross
   Contributing Researchers: K. Fedorov, A. Marx, M. Partanen
2. Research Unit D: *Quantum Communication*
   Principal Investigators: F. Deppe, S. Filipp, R. Gross
   Contributing Researchers: K. Fedorov, A. Marx, M. Partanen
3. Research Unit E: *Quantum Sensing*
   Principal Investigators: F. Deppe, H. Hübl, R. Gross
   Contributing Researchers: K. Fedorov, A. Marx
4. Research Unit F: *Quantum Matter*
   Principal Investigators: H. Hübl, R. Gross
   Contributing Researchers: M. Althammer, S. Geprägs, M. Weiler

B. German Research Foundation: Collaborative Research Centers

Transregional Collaborative Research Center TRR 80: ***«From Electronic Correlations to Functionality»***

1. Project A2: *Spatially and Momentum Resolved Raman Studies of Correlated Systems*
   Principal Investigator: R. Hackl

C. German Research Foundation: Priority Programs

1. Spin Dynamics of Hybrid Skyrmion-Magnon Solitons
   within the DFG Priority Program 2137 *Skyrmionics: Topological Spin Phenomena in Real-Space for Applications*
   M. Weiler, R. Gross (Az. WE 5386/5-1)

D. German Research Foundation: Research Projects

1. Project: *Evolution of the Charge Carrier Properties and Electronic Correlations in Layered Organic Metals near the Mott Metal-Insulator Transition*, joint German-Russian project proposal within the RFBR-DFG Cooperation.
   M. Kartsovnik, R. Gross (Az. KA 1652/5-1 and GR 1132/19-1)
2. Project: *Multi-qubit Gates for the Efficient Exploration of Hilbert Space with Superconducting Qubit Systems*
   S. Filipp (Az. FI 2549/1-1)
3. Project: *Fluctuations and Novel Phases in Systems with Spin, Charge and Orbital Correlations*
   R. Hackl (Az. HA 2071/12-1)
4. Project: *Pure Spin Currents in Oxide-Based Epitaxial Heterostructures*
   M. Althammer, R. Gross (Az. AL 2110/12-1)
5. Project: *Direct and Inverse Spin-Orbit Torques*
   M. Weiler (Az. WE 5386/14-1)

E. European Union

1. EU Collaborative Project (call identifier H2020-FETFLAG-2018-2020), project title: *Quantum Microwave Communication and Sensing – QMiCS*
   F. Deppe, K. Fedorov, A. Marx, R. Gross, Grant Agreement No. 820505
   project coordination: Walther-Meißner-Institute, partners: several European Universities, research facilities and companies.
2. EU Collaborative Project (call identifier H2020-FETOPEN-FET H2020-FETOPEN-2018-2020), project title: *Neuromorphic Quantum Computing - Quromorphic*
   S. Filipp, Grant Agreement No. 828826

   partners: several European Universities and research facilities.
3. EU Innovative Training Network (call identifier H2020-MSCA-ITN-2020), project title: *MOlecular Quantum Simulations - MOQS*
   S. Filipp, Grant Agreement No. 955479
   partners: several European Universities and research facilities.
4. EU MSCA Cofund Action (call identifier H2020-MSCA-COFUND-2018), project title: *Quantum Science and Technologies at the European Campus (QUSTEC)*
   S. Filipp, Grant Agreement 847471
   partners: several European Universities and research facilities.
5. EU Collaborative Project (call identifier H2020-FETOPEN-1-2016-2017), project title: *Magnetomechanical Platforms for Quantum Experiments and Quantum Enabled Sensing Technologies – MaQSens*
   H. Huebl, R. Gross, Grant Agreement No. 736943
   partners: several European Universities and research facilities.

F. Bundesminister für Bildung, Wissenschaft, Forschung und Technologie

1. Coordinated Project: *QUAntenRAdarTEam (QUARATE)*, project number: 13N15380,
   project part: *Superconducting Circuits and Quantum Microwaves for Quantum Radar*,
   project coordinator: Rohde & Schwarz GmbH & Co. KG,
   project partners: WMI (F. Deppe with K. Fedorov, S. Filipp, R. Gross, A. Marx), DLR, TUM.

© Walther-Meißner-Institute

2. Coordinated Project: *German Quantum Computer based on Superconducting Qubits (GeQCoS)*, project number: 13N15680
project part: *Scaling and Demonstrator*,
project coordinator: WMI (S. Filipp with F. Deppe, K. Fedorov, R. Gross, A. Marx)
project partners: Forschungszentrum Jülich GmbH, Karlsruher Institut für Technologie, Friedrich-Alexander-Universität Erlangen-Nürnberg, Fraunhofer Gesellschaft zur Forderung der angewandten Forschung e.V, Infineon Technologies AG.

G. Free State of Bavaria

1. International PhD Programme of Excellence *Exploring Quantum Matter (ExQM)* within the Elite Network of Bavaria, Project No. K-NW-2013-231,
R. Gross, A. Marx, F. Deppe, K. Fedorov,
jointly with 12 quantum physics research groups at the TU Munich, the LMU Munich, and the Max Planck Institute of Quantum Optics.

H. Max Planck Society

1. International Max Plank Research School for *Quantum Science and Technology (IMPRS-QST)*, spokesperson: Prof. Dr. J. Ignacio Cirac,
R. Gross, A. Marx, F. Deppe, K. Fedorov,
with several partners from the Max Planck Institute of Quantum Optics, the Ludwig-Maximilians-Universität Munich and the Technical University of Munich.

I. Bavaria California Technology Center (BaCaTeC)

1. Project: *Bypassing the Analytic Continuation: A New Approach to the Analysis of Spectroscopic Data* (No. 21 [2016-2]),
R. Hackl,
Project Partners: Profs. Thomas Devereaux, Steve Kivelson, and Sri Raghu (Stanford University)

J. German Academic Exchange Service

1. Project-based Personnel Exchange Programme (PPP) with Serbia, project 57449106: *Fluctuations, Magnetic Frustration, and Sub-Dominant Pairing in Fe-Based Compounds*, collaboration with the Institute of Physics, University of Belgrade (Dr. Z. V. Popovic),
R. Hackl
2. Project-based Personnel Exchange Programme (PPP) with India, project 57452943: *Spin Current Transport Across Antiferromagnetic/Metallic Oxide Interfaces*, collaboration with the IIT Madras, Chennai (Prof. Dr. M. S. Ramachandra Rao),
R. Gross

K. Scientific Instrumentation

1. UHV PLD-MBE System, DCA Instruments,
(R. Gross, DFG, Excellence Strategy, EXC-2111-390814868)
2. Tieftemperatur-Mikrowellenmessapparatur für schnellen Probenaustausch
(S. Filipp, DFG-GZ: INST 95/1636-1 FUGG)

3. Heliumverflüssigungsanlage, Vorbuchner VL 100
   (R. Gross, DFG-GZ: INST 95/1637-1 LAGG)
4. Cryogen-Free Dilution Refrigerator System with Microwave Measurement Systems, Bluefors Model BF-XLD 400,
   (S. Filipp, DFG-GZ: INST 95/1623-1 FUGG)
5. UHV Electron Beam Deposition System including Sputter Deposition Chamber, Plassys MEB 550S4-I,
   (R. Gross, DFG, Excellence Strategy, EXC-2111-390814868)
6. Cryogen-Free Dilution Refrigerator System, Bluefors Model BF-XLD 1000,
   (R. Gross, DFG, Excellence Strategy, EXC-2111-390814868)

© Walther-Meißner-Institute

Conferences, Workshops, Public Engagement

The Walther-Meißner-Institute usually organizes/co-organizes several conferences, workshops and symposia every year. It also participates in several public outreach events aiming at making science accessible to the public. Unfortunately, the year 2020 was quite unusual as due to the Covid-19 pandemic many conferences, workshops and other events had to be either turned into virtual events or postponed. For example, the *CENS-MCQST Workshop on Quantum Science and Nanotechnology*, co-organized by Hans Hübl, has been postponed to 2021 in the same way as the *International Workshop on Novel Superconductors: Methods, Models and Perspectives*, organized by Rudi Hackl. Several events such as the annual day of open house or the Ferienakademie had to be cancelled.

A. 710. WE-Heraeus-Seminar «Spin Transport in Complex Magnetic Structures» (08 – 10 January 2020, Physikzentrum Bad Honnef, Germany)

The **710th WE-Heraeus-Seminar** was organized by Matthias Althammer (WMI) and Henning Ulrichs (University of Göttingen). It was addressing spin-dependent transport phenomena in complex magnetic materials, which are at the heart of many established and currently investigated spintronic applications. Spin transport is a major driver behind the tremendous increase of information storage capabilities taking place over the last decades. As such, it has shaped the transformation into a knowledge society. To continue this success story and contribute to global trends like digitalization and artificial intelligence, new materials, new me in spa an int In pa ial ap

The key goal of the 710th WE-Heraeus-Seminar was to bring together researchers working at the forefront of material research, and others who develop and apply novel methods to image magnetic properties in such materials, with the scientists who directly investigate spin transport physics on a fundamental level and for applications.

B. Deutsche Kristallzüchtungstagung (DKT 2020) (11 – 13 March 2020, Physics Department, TUM, Germany

The annual meeting of the **German Association for Crystal Growth** (Deutsche Gesellschaft für Kristallzüchtung und Kristallwachstum, DGKK) was organized by Andreas Erb of WMI. During this particular conference the DGKK also celebrated its 50th anniversary.

Even though about one third of the participants could not attend the conference in person because of the beginning of the Covid 19 pandemic, more than 100 scientists were present and about 15 companies were contributing with information booths. The scientific program was broad, but contained focused sessions with renowned invited speakers in the fields of energy storage, diamond synthesis, super alloys, digital materials, laser materials and detector crystals for particle physics. While for many years the importance of crystal growth was largely focussed on silicon because of its importance in semiconductor and computer industry, the use of single crystals is nowadays prevalent in many fields and especially oxide crystals have an enormous technological potential. At the DKT 2020 meeting, the leading experts in the field of on crystal growth could meet once again and exchange valuable information on growth techniques and ongoing research activities. During the meeting it became evident that knowledge about crystal growth not only is of key relevance for many research fields but also has significant economic impact.

C. Munich Conference on «Quantum Science and Technology (MCQST 2020) » (06 – 08 July 2020, Germany)

The worldwide Covid-19 pandemic has affected all our lives and dramatically changed the status-quo, including how scientific events are organized. It is not surprising that also the second **Munich Conference on Quantum Science and Technology (MCQST 2020)** had to take place as a virtual event. This annual conference is organized by the Cluster of Excellence *Munich Center for Quantum Science and Technology* and aims at bringing together its scientific community from all career-stages with international guests in academia and industry to strengthen the exchange of ideas and discuss the latest advancements in all fields of quantum science and technology. Covered topics at the virtual MCQST 2020 conference included: Quantum Information Theory, Quantum Simulation, Quantum Computing, Quantum Communication, Quantum Metrology & Sensing, Quantum Matter, and Explorative Directions. Despite the new online format, with about 560 participants and more than 350 guests the conference was a big success.

© Walther-Meißner-Institute

The online conference was implemented within a virtual 3D auditorium, where all scientific talks were streamed within Zoom webinars, with additional engaging live Q&A sessions. On the virtual main stage, about 30 invited speakers were presenting their exciting talks and 14 companies were participating in the Science-meets-Industry Sessions. For the poster session, virtual galleries with innovative presenting solutions were used, making the poster session a special event. More than 100 scientific posters were presented in a 3D poster show, including video chat functionality. The virtual conference site also provided a networking area for virtual coffee breaks, industry roundtables, and spontaneous meetings with easy table hopping. The virtual tables were extensively used for discussions or for exchanging ideas via video chats. Moreover, a parallel Twitter campaign further raised engagement and outreach.

Cooperations

The Walther-Meißner-Institute is involved in many collaborations also without any direct project funding. In the following we list the most relevant collaboration partners:

- IBM Research - Zurich, Zurich, Switzerland (A. Fuhrer, D. Egger, G. Salis)
- Green Innovation Research Laboratories, NEC Corporation, Japan (J.S. Tsai, K. Inomata, T. Yamamoto)
- Forschungszentrum Jülich (P. Bushev, F.K. Wilhelm-Mauch, D. DiVincenzo)
- University of Tokyo, Tokyo, Japan (Y. Nakamura)
- ETH-Zurich, Switzerland (C. Eichler, A. Wallraff, L. Degiorgi, R. Monnier, Dr. M. Lavagnini)
- Chalmers University of Technology Gothenburg, Sweden (J. Bylander, P. Delsing, G. Wendin)
- Stanford University, Stanford, USA (T.P. Devereaux, I. Fisher, B. Moritz, H.N. Ruiz, S.A. Kivelson)
- Universidad del País Vasco and Ikerbasque Foundation, Bilbao, Spain (E. Solano, M. Sanz, L. Lamata)
- Instituto de Física Fundamental, CSIC, Madrid, Spain (J.J. Garcia-Ripoll)
- Instituto de Ciencia de Materials de Barcelona, CSIC, Spain (E. Canadell)
- University of Tohoku, Sendai, Japan (G.E.W. Bauer, E. Saitoh, J. Barker)
- Japan Science and Technology Agency, Sendai, Japan (H. Adachi, S. Maekawa)
- Osaka Prefecture University, Osaka, Japan (H. Fujiwara)
- University of Chinese Academy of Science, Beijing, China (D. Li, P.P. Shen, X.L. Dong, Z.X. Zhao)
- European Synchrotron Radiation Facility (ESRF), Grenoble (H. Müller, F. Wilhelm, K. Ollefs, A. Rogalev)
- Lund University, Lund, Sweden (D. Mannix)
- Materials Science Research Centre, IIT Madras, India (M.S. Ramachandra Rao, J. Mukherjee, T.S. Suraj)
- University of Geneva, Geneva, Switzerland (I. Maggio-Aprile)
- University of Alabama, MINT Center, Tuscaloosa, USA (A. Gupta)
- Helsinki University of Technology, Materials Physics Laboratory, Finland (T. Heikkilä)
- Delft University of Technology, Kavli Institute of NanoScience, Delft, The Netherlands (T.M. Klapwijk, G.E.W. Bauer)
- B. Verkin Institute for Low Temperature Research and Engineering, Kharkov, Ukraine (V.G. Peschansky)
- Landau Institute for Theoretical Physics, Chernogolovka, Russia (P. Grigoriev)
- University of Oxford, Clarendon Laboratory, England (A. Karenowska)
- Institute of Solid State Physics, Chernogolovka, Russia (V. Zverev)
- Russian Academy of Sciences, Chernogolovka, Russia (N. Kushch, E. Yagubskii)
- High Magnetic Field Laboratory, Dresden (E. Kampert, J. Wosnitza, T. Helm)
- High-Magnetic-Field Laboratory, Grenoble, France (I. Sheikin, D. LeBoeuf)
- High Magnetic Field Laboratory, Toulouse, France (C. Proust, D. Vignolles)
- National High Magnetic Field Laboratory, Tallahassee, USA (J. Brooks)

© Walther-Meißner-Institute

- University of British Columbia, Vancouver, Canada (D. Bonn, A. Damascelli)
- Université de Toulouse, Laboratoire de Physique Théorique, Toulouse, France (R. Ramazashvili)
- Lawrence Berkeley National Laboratory, Berkeley, USA (A. F. Kemper)
- University of Belgrade, Belgrade, Serbia (Z. Popovic, N. Lazarevic, D. U. Ralevic, R. Gajic)
- University of Aveiro, Portugal (N. A. Sobolev)
- Macquarie University, MQ Research Centre for Quantum Science and Technology, Australia (J. Twamley)
- Hungarian Academy of Sciences, Research Institute for Solid State Physics and Optics, Budapest, Hungary (I. Tüttö)
- University of Rome "La Sapienza", Rome, Italy (S. Caprara, C. Di Castro, M. Grilli)
- Budapest University of Technology and Economics, Budapest, Hungary (A. Virosztek, G. Mihály)
- EPFL Lausanne, Switzerland (T. Kippenberg, H. Ronnov)
- University of New South Wales, Sydney, Australia (M. Simmons, A. Morello, J. Pla)
- McMaster University, Hamilton, Canada (J.P. Carbotte)
- Technical University of Graz, Austria (E. Schachinger)
- University of Vienna, Austria (M. Aspelmeyer, S. Rotter)
- University of Innsbruck, Austria (G. Kirchmair)
- Johannes-Kepler University of Linz, Institute for Semiconductor and Solid State Physics, Austria (A. Ney)
- National Institute of Standards and Technology, Boulder, USA (H. Nembach, J. Shaw, T.J. Silva, E. Edwards)
- University of Florida, Gainesville, Florida, USA (P.J. Hirschfeld, S. Maiti)
- University of California, Santa Barbara, USA (D.J. Scalapino)
- University of Manitoba, Winnipeg, Canada (C.-M. Hu)
- Kyoto University, Japan (M. Shiraishi)
- Norwegian University of Science and Technology, Trondheim, Norway (A. Kamra)
- Universität Erlangen-Nürnberg (M. Hartmann, F. Marquardt)
- Universidad Nacional de Colombia, Colombia (O. Moran)
- University of Birmingham, UK (E.M. Forgan)
- University of Groningen, The Netherlands (T. Palstra, M. Mostovoy, A. Aqeel)
- IFW Dresden, Germany (B. Büchner, J. Fink, S.V. Borisenko, M. Knupfer, A. Thomas)
- Max-Planck-Institut für Festkörperforschung, Stuttgart (B. Keimer, L. Boeri)
- Max-Planck-Institute for the Science of Light, Erlangen (S. Viola-Kusminsky)
- University of Tübingen, Germany (R. Kleiner, D. Kölle)
- University of Würzburg, Germany (W. Hanke, R. Thomale)
- University of Augsburg, Germany (P. Hänggi, A. Wixforth, A. Kampf, A. Loidl, J. Deisenhofer, V. Tsurkan)
- University of Leipzig, Germany (J. Haase)
- University of Ulm, Abt. Halbleiterphysik, Germany (W. Limmer, M. Abdi)
- Ernst-Moritz-Arndt Universität Greifswald, Germany (M. Münzenberg)
- Martin-Luther-Universität Halle, Germany (G. Woltersdorf, G. Schmidt)

- Universität Bielefeld, Germany (G. Reiss, T. Kuschel M. Meinert)
- Free University of Berlin, Berlin, Germany (R. Di Candia)
- Technical University of Munich, Physics Department, Germany (Ch. Back, P. Böni, Ch. Pfleiderer, M. Poot, F.C. Simmel, P. Müller-Buschbaum)
- Technical University of Munich, Walter Schottky Institute, Germany (M. Stutzmann, J. Finley, M. Brandt, A. Holleitner)
- Technical University of Munich, Electrical Engineering (M. Becherer)
- LMU Munich, Physics Department, Germany (J. von Delft, E. Frey, J. Rädler, A. Högele)
- LMU Munich, Chemistry Department, Germany (H. Ebert, D. Ködderitzsch)
- University of Konstanz (A. Leitenstorfer, E. Weig, J. Demsar, A. Pashkin, W. Belzig)
- Jülich Centre for Neutron Science JCNS, Garching, Germany (S. Pütter)
- Goethe University, Frankfurt, Germany (S. Winter, M. Lang)
- Technical University of Braunschweig, Germany (D. Menzel, S. Süllow)
- Technical University of Dresden, Germany (S.T.B. Gönnenwein)
- Fritz Haber Institut Berlin, Germany (T. Seifert, T. Kampfrath)
- Technical University of Dortmund, Germany (M. Müller)
- Johannes-Gutenberg University, Mainz, Germany (C. Cramer, M. Kläui, O. Gomomay)
- Universität Potsdam, Potsdam, Germany (A.v. Reppert, M. Bargheer)
- Innovent Technologieentwicklung Jena, Germany (C. Dubs, O. Surzhenko)
- BMW Group, Munich, Germany (J. Schnagl, W. Stadlbauer, G. Steinhoff)
- Attocube, Munich, Germany (K. Karrai, D. Andres, E. Hoffmann)
- THEVA Dünnschichttechnik, Ismaning, Germany (W. Prusseit)

© Walther-Meißner-Institute

Stays abroad

Extended visits of members of the Walther-Meißner-Institute at foreign research laboratories have been restricted to the beginning of 2020. Later on, such stays have to be cancelled due to the Covid-19 pandemic.

1. **Matthias Opel**
   Materials Science Research Centre, Indian Institute of Technology (IIT) Madras, Chennai, India
   03. 02. - 15. 02. 2020

© Walther-Meißner-Institute

Conference Talks and Seminar Lectures

Matthias Althammer

1. **Spin transport in complex magnetic materials**
   Organization of the 710th WE Heraeus Seminar, Bad Honnef, Germany
   08. - 10. 01. 2020

Frank Deppe

1. **Beyond the standard quantum limit of parametric amplification**
   Invited Online Talk, Institute for Basic Science, Center for Theoretical Physics of Complex Systems, Daejeon, South Korea.
   27. 10. 2020
2. **Quantum Microwaves for Communication and Sensing (QMiCS)**
   Invited Online Talk, European Quantum Week, Flagship Project presentations.
   03. 11. 2020
3. **Microwave Quantum LAN and Quantum Radar**
   Invited Online Talk, European Quantum Week, QT Use Case Session.
   05. 11. 2020

Stefan Filipp

1. **Quantensimulation & -computing: Quantum Chemistry**
   Invited Online Talk, *Münchener Kreis - Quantenanwendungen*.
   18. 11. 2020
2. **Quantenbits: Können wir damit rechnen?**
   Public Lecture at the *DPG Münchener Schülertagung*.
   12. 9. 2020
3. **Tailored quantum gates for chemistry calculations on superconducting quantum devices**
   Invited Online Talk, Munich Conference on *Quantum Science & Technology (MCQST 2020)*.
   07. 07. 2020
4. **Quantenbits: Können wir damit rechnen?**
   Public Lecture at the Saarland University.
   08. 02. 2020

Rudolf Gross

1. **Quantencomputing – Grundlagen, Status und Zukunftschancen**
   Public Evening Talk, Online, organized by VDE Südbayern.
   24. 09. 2020
2. **Superconducting Quantum Circuits and Quantum Computing at WMI**
   BMW-TUM Workshop on *Quantum Computing*, BMW ITZ, Munich, Germany.
   23. 10. 2020
3. **Quantum Computing in Bavaria – Status, Competences, Perspectives**
   Invited Online Talk, Roundtable *QuantenTech Vision Bayern* organized by the Bavarian State Ministries of Economic Affairs, Regional Development and Energy, of Digital Affairs, as well as of Science and Arts.
   27. 10. 2020

Rudolf Hackl

1. **Open spectroscopic problems in quantum materials**
   Invited Talk, Winter School on Quantum Materials, Aspen, USA.
   06. - 15. 03. 2020

Hans Hübl

1. **Controlling magnon transport in ferrimagnetic insulators**
   Invited Talk, 710th WE Heraeus Seminar on Spin Transport in Complex Magnetic Structures, Bad Honnef, Germany.
   08. - 10. 01. 2020

2. **Large Electromechanical Coupling in Inductively Coupled Electromechanics**
   Invited Talk, Mikromechanik Konferenz, Obergurgl, Austria.
   09. - 14. 02. 2020
3. **Dynamics of Excitations in Strongly Coupled Spin-Microwave Hybrid Systems**
   Invited Talk, Universidad del Pais Vasco, San Sebastian, Spain.
   12. 03. 2020
4. **Hybrid Systems: Spins, Strings and Superconducting circuits**
   Invited Talk, Online, PGI-Seminar, Forschungszentrum Jülich, Germany.
   04. 06. 2020
5. **Inductively coupled nano-electromechanics: a pathway towards strong coupling**
   Invited Talk, Online, MCQST 2020 Conference.
   06. - 08. 07. 2020

Mark Kartsovnik

1. **Magnetic quantum oscillations: a tool for probing electronic properties of conducting materials**
   Invited Talk, 9^{th} Meeting of jDGKK, Munich, Germany.
   10. 03. 2020

Matthias Opel

1. **Spin Hall Magnetoresistance (SMR) in Antiferromagnetic Insulators**
   Invited Talk, Indian Institute of Technology (IIT) Madras, Chennai, India.
   13. 02. 2020
2. **Spin Hall magnetoresistance in antiferromagnetic insulators**
   Invited Online Talk, Joint European Magnetic Symposia, Lisbon, Portugal.
   10. 12. 2020

© Walther-Meißner-Institute

Appointments

A. Mathias Weiler was appointed W3 professor at TU Kaiserslautern

President Prof. Dr. Arnd Poetzsch-Heffter (right) and Prof. Dr. Herwig Ott, Dean of the Faculty of Physics (left), welcome Prof. Mathias Weiler at the TU Kaiserslautern (photo: TUK/Koziel).

Priv.-Doz. Dr. Mathias Weiler (born 1983) received an offer for a W3-professorship for solid state physics from the Technical University of Kaiserslautern. He accepted the offer and moved to Kaiserslautern in October 2020. At TU Kaiserslautern, he is focussing on the experimental study and engineering of solid-state spin systems. Besides the **Landesforschungszentrum OPTIMAS** with focus on optics and materials science, the TU Kaiserslautern established a new **Laboratory for Advanced Spin Engineering (LASE)**, with a new research building that will be ready in 2021. Mathias Weiler will be part of LASE and will play a central role in the interdisciplinary research on complex spin systems at Kaiserslautern. On the one hand, we are very happy about the promotion of Mathias Weiler and congratulate him to his new full professor position. On the other hand, we are of course sad about loosing an excellent scientist and a very nice colleague. We hope to see him often at WMI in future and are looking forward to a fruitful collaboration.

Mathias Weiler joined WMI in December 2006 for his master thesis entitled *Magnetization Control in Multiferroic Heterostructures*. He then continued with his PhD on *Magnon-Phonon Interactions in Ferromagnetic Thin Films*, which he finished in May 2012. After a two-year postdoctoral stay at NIST, Boulder, Colorado, USA, where he worked on spin current transport, he joined WMI again in December 2014. Besides his successful research work, he took over the lectures on *Magnetism* (winter semester 2015/2016, 2017/2018, and 2019/2020) and *Spin Electronics* (summer semester 2016 and 2018), and actively contributed to several WMI seminars. His lectures attracted a large number of students and received very good marks from the students. In winter semester 2018/19, he received the ***Supervisory Award*** of the TUM Physics Department. This award was presented to Mathias Weiler by the PhD students of the Faculty Graduate Center for his outstanding performance in advising PhD students. During his postdoctoral stay at WMI, Mathias Weiler started the habilitation process at TUM in June 2015, which he successfully completed in December 2019.

For more than 10 years Mathias Weiler not only was doing excellent research at WMI, but also setting up several experimental facilities e.g. for broadband FMR and frequency-resolved MOKE. He did an excellent job in every respect and was one of key players at WMI. In the past years, he was principal investigator within the **DFG Priority Programm 2137 Skyrmionics – Topological Spin Phenomena in Real-Space for Application** and was providing important contributions to the excellence clusters Nanosystems Inititive Munich and Munich Center for Quantum Science and Technology. At present, his impressive publication record includes more than 50 publications in refereed journals with more than 3 5000 citations (h-index: 28, according to Google scholar). In many invited talks on conference and workshops, he contribute to the international visibility of WMI. Mathias Weiler certainly is an excellent example for the successful fostering of young talents at WMI.

Honors and Awards

A. Best Presentation and Poster Awards

Most of our Ph.D. and master students give several oral and poster presentations at national and international conferences over the year. We are very happy that they are regularly receiving awards for their presentations. In 2020, Louis Flacke of WMI was particularly successful in this respect by collecting two best presentation awards.

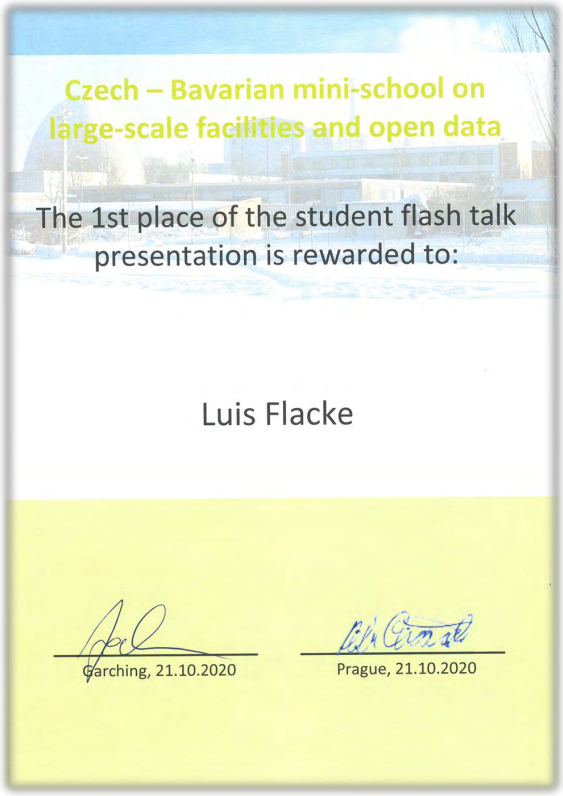

B. Rudolf Gross has been elected member of acatech

acatech
DEUTSCHE AKADEMIE DER TECHNIKWISSENSCHAFTEN

In October 2020, Rudolf Gross has been elected member of the **National Academy of Science and Engineering** (Deutsche Akademie der Technikwissenschaften e.V, acatech). Funded by the Federal Government and the Länder, acatech is the voice of the technological sciences at home and abroad. It provides advice on strategic engineering and technology policy issues to policymakers and the public. Thereby, it fulfils its mandate to provide independent, evidence-based advice that is in the public interest.

Acatech brings together science, industry and civil society. The Academy's Members are scientists from the fields of engineering, the natural sciences and medicine, as well as the humanities and social sciences. The Senate is made up of leading figures from technology companies and organisations and the major science organisations.

C. Rudolf Gross has been awarded the «Goldene Kreide»

Rudolf Gross was awarded the so-called «Golden Chalk» for his lectures on Condensed Matter Physics I and II within the bachelor course of the Faculty of Physics of TUM. The «Golden Chalks» are presented annually by the student body of the faculty to honor excellent teaching in experimental and theoretical physics within the bachelor and master course, as well as to award the best tutor exercise and the best "import" lecture given by a docent from another faculty.

Since long the exercise groups to the lectures on Condensed Matter Physics I and II are organized by Stephan Geprägs and his team of Ph.D. students. They are also evaluated by the students and regularly receive excellent marks. Therefore, a significant part of the Golden Chalk belongs to Stephan and his team.

D. Rudolf Hackl has been appointed extraordinary professor at TUM


Technische Universität München

URKUNDE

Die Technische Universität München bestellt

den Privatdozenten

Herrn Dr. habil. (TU Budapest)

Rudolf Hackl

auf Grundlage des Bayerischen Hochschulpersonalgesetzes

zum außerplanmäßigen Professor.

München, 23. Januar 2020

Thomas F. Hofmann
Präsident

In January 2020, Rudolf Hackl has been appointed extraordinary professor in experimental physics at the Technical University of Munich. We congratulate Rudolf Hackl to this appointment, recognizing his long-standing excellent contributions in both research and teaching.

Membership in Advisory Boards, Committees, etc.

1. **Frank Deppe** is Coordinator of the European Quantum Technology Flagship Project *Quantum Microwaves for Communication and Sensing (QMiCS)*.
2. **Frank Deppe** is associate member of the Cluster of Excellence *Nanosystems Initiative Munich (NIM)*.
3. **Frank Deppe** is member and principal investigator of the Cluster of Excellence *Munich Center for Quantum Science and Technology (MCQST)*.
4. **Andreas Erb** is spokesmen of the *Arbeitskreis Intermetallische und oxydische Systeme mit Spin- und Ladungskorrelationen* of the *Deutsche Gesellschaft für Kristallzüchtung und Kristallwachstum (DGKK)*.
5. **Stefan Filipp** is chairman of the *Expertenrat zur Erarbeitung einer nationalen Roadmap Quantencomputing* established in response to the demand of Federal Minister Helge Braun.
6. **Stefan Filipp** is advisory board member of the *International AIQT Foundation*.
7. **Stefan Filipp** is member of the *BMBF Programmausschuss Quantensysteme*.
8. **Stefan Filipp** is member of the scientific advisory board of the EU FET Open project *AVAQUS - Annealing based Variational Quantum Processors*.
9. **Stefan Filipp** is member of the scientific advisory board of the *Wallenberg Center for Quantum Technology*.
10. **Stefan Filipp** is editorial board member of the IOP multidisciplinary journal *Materials for Quantum Technology*.
11. **Stefan Filipp** is member and principal investigator of the Cluster of Excellence *Munich Center for Quantum Science and Technology (MCQST)*.
12. **Stefan Filipp** is adjoint Member of the Special Research Fund (SFB) *BeyondC* funded by the Austria Science Fund (FWF).
13. **Stefan Filipp** is member of the *Munich Quantum Center (MQC)*.
14. **Rudolf Gross** is spokesperson (together with Immanuel Bloch and Ignacio Cirac) of the Cluster of Excellence *Munich Center for Quantum Science and Technology (MCQST)* and coordinator of the Research Unit C on *Quantum Computing*.
15. **Rudolf Gross** is member of the *Deutsche Akademie der Technikwissenschaften e.V. (acatech)*.
16. **Rudolf Gross** is member of the Advisory Board of the permanent exhibition on *Matter and Light* of the German Science Museum.
17. **Rudolf Gross** is member of the *Committee for the allocation of Alexander von Humboldt Foundation Research Awards*.
18. **Rudolf Gross** is member of the *Appointment and Tenure Board* of the Technical University of Munich.
19. **Rudolf Gross** is member of the *Munich Quantum Center (MQC)*.

© Walther-Meißner-Institute

20. **Rudolf Gross** is member of the *Scientific Advisory Board of the Bayerisches Geoinstitut*, Bayreuth, Germany.

21. **Rudolf Gross** is member of the *Scientific Advisory Board of the Institut de Ciència de Materials de Barcelona*, Spain.

22. **Rudolf Gross** is course leader at the *Ferienakademie of the Universities Munich (TU), Stuttgart and Erlangen-Nürnberg* since 2005.

23. **Rudolf Hackl** is member of the *Evaluation Board of the neutron source Heinz Maier-Leibnitz (FRM II)*.

24. **Hans Hübl** is member and principal investigator of the Cluster of Excellence *Munich Center for Quantum Science and Technology (MCQST)*.

25. **Mark Kartsovnik** is member of the *Selection Committee of EMFL* (European Magnetic Field Laboratories).

26. **Mark Kartsovnik** is member of the *International Advisory Committee of the 14^{th} International Symposium on Crystalline Organic Metals Superconductors and Ferromagnets (ISCOM 2021)*.

27. **Matthias Opel** is one of the four elected members of the *Speaker Council* for the scientists of the Bavarian Academy of Sciences and Humanities.

28. **Mathias Weiler** is member of the *Editorial Review Board of IEEE Magnetics Letters*.

© Walther-Meißner-Institute

Teaching

Lectures, Courses and other Teaching Activities

Several members of the Walther-Meißner-Institute give lectures and seminars at the Technical University of Munich.

Matthias Althammer

WS 2019/2020	• Seminar: Spin Currents and Skyrmionics (with H. Huebl, M. Weiler) • Seminar: Advances in Solid-State Physics (with R. Gross, H. Hübl, A. Marx, M. Opel) • Seminar: Topical Issues in Magneto- and Spin Electronics (with H. Hübl, M. S. Brandt, M. Weiler)
SS 2020	• Seminar: Spin Currents and Skyrmionics (with H. Huebl, M. Weiler) • Seminar: Advances in Solid-State Physics (with R. Gross, H. Hübl, A. Marx, M. Opel) • Seminar: Topical Issues in Magneto- and Spin Electronics (with H. Hübl, M. S. Brandt, M. Weiler)
WS 2020/2021	• Seminar: Spin Currents and Skyrmionics (with H. Huebl, M. Weiler) • Seminar: Advances in Solid-State Physics (with R. Gross, H. Hübl, A. Marx, M. Opel) • Seminar: Topical Issues in Magneto- and Spin Electronics (with H. Hübl, M. S. Brandt, M. Weiler)

Frank Deppe

WS 2019/2020	• Seminar: Superconducting Quantum Circuits (with R. Gross, A. Marx, K. Fedorov)
SS 2020	• Seminar: Superconducting Quantum Circuits (with R. Gross, A. Marx, K. Fedorov) • WMI Seminar on Current Topics of Low Temperature Solid-State Physics (with M. Althammer, K. Fedorov, R. Gross, R. Hackl, H. Hübl, A. Marx, M. Opel, M. Weiler)
WS 2020/2021	• Supraleitung und Tieftemperaturphysik I (Superconductivity and Low Temperature Physics I) • Übungen zu Supraleitung und Tieftemperaturphysik I (Superconductivity and Low Temperature Physics I, Problem Sessions) • Seminar: Superconducting Quantum Circuits (with R. Gross, A. Marx, K. Fedorov, S.Filipp)

Dietrich Einzel

WS 2019/2020	• Mathematische Methoden der Physik I (Mathematical Methods of Physics I) • Übungen zu Mathematische Methoden der Physik I (Mathematical Methods of Physics I, Problem Sessions)
SS 2020	• Mathematische Methoden der Physik II (Mathematical Methods of Physics II) • Übungen zu Mathematische Methoden der Physik II (Mathematical Methods of Physics II, Problem Sessions)
WS 2020/2021	• Mathematische Methoden der Physik I (Mathematical Methods of Physics I)

- Übungen zu Mathematische Methoden der Physik I (Mathematical Methods of Physics I, Problem Sessions)

Kirill Fedorov

WS 2019/2020
- Seminar: Superconducting Quantum Circuits (with F. Deppe, R. Gross, A. Marx)

SS 2020
- Angewandte Supraleitung: Josephson Effekte, supraleitende Elektronik und supraleitende Quantenschaltkreise (Applied Superconductivity: Josephson Effects, Superconducting Electronics and Superconducting Quantum Circuits, with R. Gross)
- Seminar: Superconducting Quantum Circuits (with F. Deppe, R. Gross, A. Marx)

WS 2020/2021
- Seminar: Superconducting Quantum Circuits (with F. Deppe, S. Filipp, R. Gross, A. Marx)

Stefan Filipp

WS 2020/2021
- Physik der Kondensierten Materie I (Condensed Matter Physics I, with R. Gross)
- Übungen zu Physik der Kondensierten Materie I (Condensed Matter Physics I, Problem Sessions, with R. Gross, S. Geprägs)
- Quanten-Computing mit supraleitenden Qubits: Architektur und Algorithmen (Quantum Computing with Superconducting Qubits: Architecture and Algorithms)
- Übungen zu Quanten-Computing mit supraleitenden Qubits: Architektur und Algorithmen (Quantum Computing with Superconducting Qubits: Architecture and Algorithms, Problem Sessions)
- Seminar: Superconducting Quantum Circuits (with F. Deppe, R. Gross, A. Marx, K. Fedorov)
- WMI Seminar on Modern Topics of Low Temperature Solid-State Physics (with M. Althammer, F. Deppe, K. Fedorov, R. Gross, R. Hackl, H. Hübl, A. Marx, M. Opel, M. Weiler)
- Seminar: Quanten-Entrepreneurship-Labor (with Ch. Mendl, F. Pollmann)

Rudolf Gross

WS 2019/2020
- Physik der Kondensierten Materie I (Condensed Matter Physics I)
- Übungen zu Physik der Kondensierten Materie I (Condensed Matter Physics I, Problem Sessions, with S. Geprägs)
- WMI Seminar on Modern Topics of Low Temperature Solid-State Physics (with M. Althammer, F. Deppe, K. Fedorov, R. Hackl, H. Hübl, A. Marx, M. Opel, M. Weiler)
- Seminar: Advances in Solid-State Physics (with H. Hübl, A. Marx, M. Opel)
- Seminar: Superconducting Quantum Circuits (with F. Deppe, K. Fedorov, A. Marx)
- Festkörperkolloquium (Colloquium on Solid-State Physics, with D. Einzel)

SS 2020
- Physik der Kondensierten Materie II (Condensed Matter Physics II)
- Übungen zu Physik der Kondensierten Materie II (Condensed Matter Physics II, Problem Sessions, with S. Geprägs)
- Seminar: Advances in Solid-State Physics (with H. Hübl, A. Marx, M. Opel)
- WMI Seminar on Modern Topics of Low Temperature Solid-State Physics (with M. Althammer, F. Deppe, K. Fedorov, S. Filipp, R. Hackl, H. Hübl, A. Marx, M. Opel, M. Weiler)

© Walther-Meißner-Institute

- Seminar: Superconducting Quantum Circuits (with F. Deppe, K. Fedorov, S. Filipp, A. Marx)
- Festkörperkolloquium (Colloquium on Solid-State Physics, with D. Einzel)
- Ferienakademie: Course 3 «Physics and Electronics in Everyday Life»

WS 2020/2021

- Physik der Kondensierten Materie I (Condensed Matter Physics I, with S. Filipp)
- Übungen zu Physik der Kondensierten Materie I (Condensed Matter Physics I, Problem Sessions, with S. Filipp, S. Geprägs)
- WMI Seminar on Modern Topics of Low Temperature Solid-State Physics (with M. Althammer, F. Deppe, K. Fedorov, S. Filipp, R. Hackl, H. Hübl, A. Marx, M. Opel, M. Weiler)
- Seminar: Advances in Solid-State Physics (with H. Hübl, A. Marx, M. Opel)
- Seminar: Superconducting Quantum Circuits (with F. Deppe, K. Fedorov, S. Filipp, A. Marx)
- Festkörperkolloquium (Colloquium on Solid-State Physics, with D. Einzel)

Rudi Hackl

WS 2019/2020

- Supraleitung und Tieftemperaturphysik I (Superconductivity and Low Temperature Physics I)
- Übungen zu Supraleitung und Tieftemperaturphysik I (Superconductivity and Low Temperature Physics I, Problem Sessions)
- Seminar: Advances in Solid-State Physics (with R. Gross, H. Hübl, A. Marx, M. Opel)
- WMI Seminar on Current Topics of Low Temperature Solid-State Physics (with M. Althammer, F. Deppe, K. Fedorov, R. Gross, H. Hübl, A. Marx, M. Opel, M. Weiler)

SS 2020

- Supraleitung und Tieftemperaturphysik I (Superconductivity and Low Temperature Physics I)
- Übungen zu Supraleitung und Tieftemperaturphysik I (Superconductivity and Low Temperature Physics I, Problem Sessions)
- WMI Seminar on Current Topics of Low Temperature Solid-State Physics (with M. Althammer, F. Deppe, K. Fedorov, S. Filipp, R. Gross, H. Hübl, A. Marx, M. Opel, M. Weiler)

WS 2020/2021

- WMI Seminar on Current Topics of Low Temperature Solid-State Physics (with M. Althammer, F. Deppe, K. Fedorov, S. Filipp, R. Gross, H. Hübl, A. Marx, M. Opel, M. Weiler)

Hans Hübl

WS 2019/2020

- Seminar: Spin Currents and Skyrmionics (with M. Althammer, M. Weiler, M. Opel, S. Geprägs)
- Seminar: Advances in Solid-State Physics (with R. Gross, A. Marx, M. Opel)
- WMI Seminar on Current Topics of Low Temperature Solid State Physics (with M. Althammer, F. Deppe, K. Fedorov, R. Gross, R. Hackl, A. Marx, M. Opel, M. Weiler)
- Seminar: Topical Issues in Magneto- and Spin Electronics (with M. S. Brandt, M. Althammer, M. Weiler, S. Geprägs)

SS 2020

- Seminar: Spin Currents and Skyrmionics (with M. Althammer, M. Weiler, M. Opel, S. Geprägs)
- Seminar: Advances in Solid-State Physics (with R. Gross, A. Marx, M. Opel)
- WMI Seminar on Current Topics of Low Temperature Solid State Physics (with M. Althammer, F. Deppe, K. Fedorov, S. Filipp, R. Gross, R. Hackl, A. Marx, M. Opel, M. Weiler)

- Seminar: Topical Issues in Magneto- and Spin Electronics (with M. S. Brandt, M. Althammer, M. Weiler, S. Geprägs)

WS 2020/2021

- Magnetismus (Magnetism)
- Übungen zu Magnetismus (Magnetism, Problem Sessions)
- Seminar: Spin Caloritronics and Spin Pumping (with M. Althammer, M. Weiler)
- Seminar: Advances in Solid-State Physics (with R. Gross, A. Marx, M. Opel)
- WMI Seminar on Current Topics of Low Temperature Solid State Physics (with M. Althammer, F. Deppe, K. Fedorov, S. Filipp, R. Gross, R. Hackl, A. Marx, M. Opel, M. Weiler)
- Seminar: Topical Issues in Magneto- and Spin Electronics (with M. S. Brandt, M. Althammer, M. Weiler, S. Geprägs)

Mathias Weiler

WS 2019/2020

- Magnetismus (Magnetism)
- Übungen zu Magnetismus (Magnetism, Problem Sessions)
- Seminar: Spin Currents and Skyrmionics (with M. Althammer, H. Hübl)
- Seminar: Topical Issues in Magneto- and Spin Electronics (with M. Althammer, H. Hübl, M. S. Brandt)

© Walther-Meißner-Institute

Seminars and Colloquia

A. Walther-Meißner-Seminar on Modern Topics in Low Temperature Physics WS 2019/2020, SS 2020 and WS 2020/2021

WS 2019/2020:

1. **Transport Studies in Iridate-Manganite ($SrIrO_3$/$LaMnO_3$) heterostructures**
   T.S. Suraj, Indian Institute of Technology Madras, Chennai, India
   18. 10. 2019
2. **Theory of Higgs spectroscopy of superconductors in non-equilibrium**
   Prof. Dirk Manske, Max Planck Institute for Solid State Research, Stuttgart, Germany
   08. 11. 2019
3. **Strongly correlated spin charge dynamics govern the few-femtosecond magnetic response of ferromagnetic materials**
   Dr. Phoebe Tengdin, Laboratory for Ultrafast Microscopy and Electron Scattering, EPFL, Lausanne, Switzerland
   22. 11. 2019
4. **Superconducting triplet spintronics: why, how and what next**
   Dr. Sol H. Jacobson, Norwegian University of Science and Technology, Trondheim, Norway
   06. 12. 2019
5. **Investigating defects in superconducting qubits with strain and electric fields**
   Dr. Jürgen Lisenfeld, Institute of Technology, Karlsruhe, Germany
   13. 12. 2019
6. **Moderne Fernerkundung mit Mikrowellen – ein nützliches Werkzeug für viele Anwendungen**
   Dr. Markus Peichl, DLR, Institut für Hochfrequenztechnik und Radarsysteme, Wessling, Germany
   15. 01. 2020
7. **Testing of quantum gravity with macroscopic mechanical oscillators and pendulums**
   Prof. Dr. P. Bushev, JARA-Institute for Quantum Information, Forschungszentrum Jülich, Germany
   24. 01. 2020
8. **Measurement and simulation of ultrafast optical phase-controlled 2-coloured coherent electron interference in monolayer graphene**
   Timo Eckstein, Institut für Physik der Kondensierten Materie, FAU Erlangen-Nürnberg, Germany
   20. 02. 2020
9. **Effective Thermal Conductivity of Evacuated, Expanded Perlite between 20°C and 800°C**
   Matthias Rottmann, ZAE Bayern, Bereich Energiespeicherung, Garching, Germany
   28. 02. 2020
10. **Spins in Low-dimensional Materials Systems: Transport, Gate Control and Conversion**
    Prof. Dr. Masashi Shiraishi, Kyoto University, Kyoto, Japan
    10. 03. 2020

SS 2020:

11. **Positioning and Investigation of Magnetic Nanoparticles**
    Leon Koch, Universität Tübingen, Tübingen, Germany
    16. 04. 2020
12. **TLS and circulators – Challenges and opportunities for quantum technology**
    Dr. Clemens Müller, IBM Research Zurich, Switzerland
    15. 05. 2020
13. **Error mitigation via symmetry verification in a variational quantum eigensolver**
    Malay Singh, Delft University of Technology, Delft, The Netherlands
    04. 06. 2020

14. **Backaction and Exchange Interaction Effects in Electron Spin Qubits in GaAs**
Patrick Bethke, RWTH Aachen, Aachen, Germany
05. 06. 2020
15. **Topology development, calibration and research of circuits on transmons**
Ivan Tsitsilin, Moscow Institute of Physics and Technology, Moscow, Russia
18. 06. 2020
16. **Collective dynamics of a five-transmon chain**
Elena Egorova, Moscow Institute of Physics and Technology, Moscow, Russia
19. 06. 2020
17. **Coherent electrical control of a high spin nucleus in silicon**
Vincent Mourik, University of New South Wales, Australia
24. 07. 2020
18. **Quantum Rifling – protecting a qubit from measurement back-action**
Dr. Clemens Müller, IBM Research, Zurich, Switzerland
14. 09. 2020

WS 2020/2021:

19. **Temporal Coherence of the Excitronic Emission in TMDC Heterostructures**
Fabian Kronowetter, Rohde & Schwarz GmbH, München, Germany
04. 12. 2020

B. Topical Seminar on Advances in Solid State Physics WS 2019/2020, SS 2020 and WS 2020/2021

WS 2019/2020:

1. **Preliminary discussion and assignment of topics**
R. Gross, Walther-Meißner-Institute, BAdW, and Chair of Technical Physics (E23), Technical University of Munich
15. 10. 2019 and 22. 10. 2019
2. **Spin colossal magnetoresistance in an antiferromagnetic insulator**
Pham Thai Phi-Long, Technical University of Munich
26. 11. 2019
3. **Superconducting cables for quantum microwave communication**
Meike Pfeiffer, Technical University of Munich
03. 12. 2019
4. **Magnetic Skyrmion field effect transistors**
Alexander Jung, Technical University of Munich
10. 12. 2019
5. **Observation of anisotropic magneto-Peltier effect in nickel**
Elisabeth Meidinger, Technical University of Munich
17. 12. 2019
6. **Gated Conditional Displacement Readout of Superconducting Qubits**
Kexun Luo, Technical University of Munich
04. 02. 2020

SS 2020:

7. **Preliminary discussion and assignment of topics**
R. Gross, Walther-Meißner-Institute, BAdW, and Chair of Technical Physics (E23), Technical University of Munich
21. 04. 2020 and 28. 04. 2020
8. **Coherent spin-photon coupling using a resonant exchange qubit**
Karin Thalmann, Technical University of Munich
26. 05. 2020

© Walther-Meißner-Institute

9. **Mutual control of coherent spin waves and magnetic domain walls in a magnonic device**
   Maria Sigl, Technical University of Munich
   16. 06. 2020
10. **Bismuthene on a SiC substrate: A candidate for a high-temperature quantum spin Hall material**
    Pauline Fichter, Technical University of Munich
    23. 06. 2020
11. **Observation of second sound in graphite at temperatures above 100 K**
    Stefan Böhm, Technical University of Munich
    14. 07. 2020
12. **Superconductivity in an infinite-layer nickelate**
    Nina Miller, Technical University of Munich
    28. 07. 2020

WS 2020/2021:

13. **Preliminary discussion and assignment of topics**
    R. Gross, Walther-Meißner-Institute, BAdW, and Chair of Technical Physics (E23), Technical University of Munich
    03. 11. 2020 and 10. 11. 2020
14. **Sensitivity optimization for NV-diamond magnetometry**
    Adrian Misselwitz, Technical University of Munich
    24. 11. 2020
15. **Quantum-critical phase from frustrated magnetism in a strongly correlated metal**
    Malte Bieringer, Technical University of Munich
    08. 12. 2020
16. **Violating Bell's inequality with remotely connected superconducting qubits**
    Johannes Arceri, Technical University of Munich
    15. 12. 2020
17. **Nonlinear Planar Hall Effect**
    Safwan Uddin Ahmed, Technical University of Munich
    22. 12. 2020
18. **Qubit Measurement by Multichannel Driving**
    Arthur Butorev, Technical University of Munich
    12. 01. 2021
19. **The Remarkable Underlying Ground States of Cuprate Superconductors**
    Aristo Kevin, Technical University of Munich
    19. 01. 2021
20. **Evidence of high-temperature exciton condensation in two-dimensional atomic double layers**
    Johannes Kowalewicz, Technical University of Munich
    26. 01. 2021
21. **Giant topological Hall effect in correlated oxide thin films**
    Tobias Konrad, Technical University of Munich
    02. 02. 2021
22. **Waveguide quantum electrodynamics with superconducting artificial giant atoms**
    Fanjun Xu, Technical University of Munich
    09. 02. 2021

C. Topical Seminar: Spin current and Skyrmionics WS 2019/2020, SS 2020 and WS 2020/2021

WS 2019/2020:

1. **Preliminary discussion and assignment of topics**
   M. Weiler, M. Althammer, S. Geprägs, H. Hübl, Walther-Meißner-Institute, BAdW, and Chair of

Technical Physics (E23), Technical University of Munich
17. 10. 2019 and 24. 10. 2019

2. **Spin orbit torque**
Mathias Weiler, Walther-Meißner-Institute, BAdW
14. 11. 2019

3. **Magnetization dynamics in magnetic bilayers**
Carolina Lüthi, Walther-Meißner-Institute, BAdW and Technical University of Munich
21. 11. 2019

4. **Revealing the origin of the spin Seebeck effect**
Maxim Dietlein, Walther-Meißner-Institute, BAdW and Technical University of Munich
28. 11. 2019

5. **Magnon transport in magnetic insulators**
Janine Gückelhorn, Walther-Meißner-Institute, BAdW and Technical University of Munich
05. 12. 2019

6. **Modulation of magnon spin transport in a magnetic gate transistor**
Matthias Grammer, Technical University of Munich
12. 12. 2019

7. **Magnetization dynamics in metallic heterostructures**
Manuel Müller, Walther-Meißner-Institute, BAdW and Technical University of Munich
16. 01. 2020

8. **Nonlinear response in magnetization dynamics**
Tobias Wimmer, Walther-Meißner-Institute, BAdW and Technical University of Munich
23. 01. 2020

9. **Magnetic multilayers**
Luis Flacke, Walther-Meißner-Institute, BAdW and Technical University of Munich
30. 01. 2020

SS 2020:

10. **Preliminary discussion and assignment of topics**
M. Weiler, M. Althammer, S. Geprägs, H. Hübl, Walther-Meißner-Institute, BAdW, and Chair of Technical Physics (E23), Technical University of Munich
23. 04. 2020 and 30. 04. 2020

11. **Magnetostatic twists in room-temperature skyrmions explored by nitrogen-vacancy center spin texture reconstruction**
Tobias Hochreiter, Technical University of Munich
07. 05. 2020

12. **Hybrid magnetization dynamics**
Carolina Lüthi, Walther-Meißner-Institute, BAdW and Technical University of Munich
26. 05. 2020

13. **Multilayer systems**
Luis Flacke, Walther-Meißner-Institute, BAdW and Technical University of Munich
23. 07. 2020

14. **Spinstrom-Experimente mit vertikalen Heterostructuren**
Christian Mang, Technical University of Munich
30. 07. 2020

WS 2020/2021:

15. **Preliminary discussion and assignment of topics**
M. Althammer, S. Geprägs, H. Hübl, Walther-Meißner-Institute, BAdW, and Chair of Technical Physics (E23), Technical University of Munich
05. 11. 2020 and 12. 11. 2020

16. **Multilayers for topological spin textures**
Misbah Yaqoob, Walther-Meißner-Institute, BAdW and Technical University of Munich

19. 11. 2020

17. **Microwave control of magnon transport**
Korbinian Rubenbauer, Walther-Meißner-Institute, BAdW and Technical University of Munich
26. 11. 2020

18. **Spin and charge transport in multilayers with interfacial Dzyaloshinskii Moriya Interaction**
Elisabeth Meidinger, Walther-Meißner-Institute, BAdW and Technical University of Munich
10. 12. 2020

19. **Propagation Length of Antiferromagnetic Magnons Governed by Domain Configurations**
Matthias Grammer, Technical University of Munich
17. 12. 2020

20. **Fast current-driven domain walls and small skyrmions in a compensated ferrimagnet**
Joris Thiel, Technical University of Munich
14. 01. 2021

21. **Constrained yttrium iron garnet trilayers**
Philipp Schwenke, Walther-Meißner-Institute, BAdW and Technical University of Munich
21. 01. 2021

22. **Spin Hall Magnetoresistance in antiferromagnets**
Monika Scheufele, Walther-Meißner-Institute, BAdW and Technical University of Munich
28. 01. 2021

23. **Chiral Spin-Wave Velocities Induced by All-Garnet Interfacial Dzyaloshinskii-Moriya Interaction in Ultrathin Yttrium Iron Garnet Films**
Daryoush Nosraty Alamdary, Walther-Meißner-Institute, BAdW and Technical University of Munich
11. 02. 2021

D. Topical Seminar on Superconducting Quantum Circuits WS 2019/2020, SS 2020 and WS 2020/2021

WS 2019/2020:

1. **Preliminary discussion and assignment of topics**
F. Deppe, A. Marx, R. Gross, Walther-Meißner-Institute, BAdW, and Chair of Technical Physics (E23), Technical University of Munich
15. 10. 2019 and 22. 10. 2019

2. **To catch and reverse a quantum jump mid-flight**
Qiming Chen, Walther-Meißner-Institute, BAdW and Technical University of Munich
29. 10. 2019

3. **Midterm report: Optimal control of 3D quantum memory**
Stefan Trattnig, Walther-Meißner-Institute, BAdW and Technical University of Munich
05. 11. 2019

4. **Stabilizing Rabi oscillations in a superconducting qubit using quantum feedback**
Yuki Nojiri, Walther-Meißner-Institute, BAdW and Technical University of Munich
12. 11. 2019

5. **Phonon-mediated quantum state transfer and remote qubit entanglement**
Gerhard Huber, Technical University of Munich
19. 11. 2019

6. **High-Efficiency Measurement of an Artificial Atom Embedded in a Parametric Amplifier**
Tammo Sievers, Technical University of Munich
26. 11. 2019

7. **Coupling microwave photons to a mechanical resonator using quantum interference**
Philip Schmidt, Walther-Meißner-Institute, BAdW and Technical University of Munich
03. 12. 2019

8. **Violating Bell's inequality with remotely connected superconducting qubits**
Michael Renger, Walther-Meißner-Institute, BAdW and Technical University of Munich

14. 01. 2020

9. **Multiphonon interactions between nitrogen-vacancy centers and nanomechanical resonators**
Daniel Schwienbacher, Walther-Meißner-Institute, BAdW and Technical University of Munich
28. 01. 2020

10. **Solid-state electron spin lifetime limited by phononic vacuum modes**
Stefan Weichselbaumer, Walther-Meißner-Institute, BAdW and Technical University of Munich

SS 2020:

11. **Preliminary discussion and assignment of topics**
F. Deppe, A. Marx, R. Gross, Walther-Meißner-Institute, BAdW, and Chair of Technical Physics (E23), Technical University of Munich
21. 04. 2020 and 28. 04. 2020

12. **Quantum supremacy using a programmable superconducting processor**
Philipp Krüger, Technical University of Munich
19. 05. 2020

13. **Collective dynamics of strain-coupled nanomechanical pillar resonators**
Jasper Ebel, Technical University of Munich
26. 05. 2020

14. **Resolving the energy levels of a nanomechanical oscillator**
Karl Miklautz, Technical University of Munich
02. 06. 2020

15. **Generation of multicomponent atomic Schrödinger cat states of up the 20 qubits**
Yu Wang, Technical University of Munich
09. 06. 2020

16. **A unidirectional on-chip photonic interface for superconducting circuits**
Max-Emanuel Kern, Technical University of Munich
16. 06. 2020

17. **Measurement of Motion beyond the Quantum Limit by Transient Amplification**
Simone Spedicato, Technical University of Munich
23. 06. 2020

WS 2020/2021:

18. **Preliminary discussion and assignment of topics**
F. Deppe, A. Marx, R. Gross, Walther-Meißner-Institute, BAdW, and Chair of Technical Physics (E23), Technical University of Munich
03. 11. 2020 and 10. 11. 2020

19. **Challenges and results on the way to quantum acoustodynamics**
Christopher Waas, Walther-Meißner-Institute, BAdW and Technical University of Munich
01. 12. 2020

20. **Teleportation-based collective attacks in Gaussian quantum key distribution**
Daniel Prelipcean, Technical University of Munich
08. 12. 2020

21. **Solid-state qubits integrated with superconducting through-silicon vias**
Yuyang Huang, Technical University of Munich
15. 12. 2020

22. **The superconducting quasicharge qubit**
Jonas Schmitt, Technical University of Munich
12. 01. 2021

23. **Breaking the trade-off between fast control and long lifetime of a superconducting qubit**
Niklas Bruckmoser, Technical University of Munich
19. 01. 2021

24. **A quantum memory at telecom wavelengths**

© Walther-Meißner-Institute

Patrick Missale, Technical University of Munich
26. 01. 2021

25. **Automated discovery of superconducting circuits and its application topological coupler design**
Nicolas Gosling, Technical University of Munich
02. 02. 2021

26. **Tunable Coupler for Realizing a Controlled-Phase Gate with Dynamically Decoupled Regime in a Superconducting Circuit**
Malay Singh, Walther-Meißner-Institute, BAdW and Technical University of Munich
09. 02. 2021

E. Solid State Colloquium

The WMI has organized the Solid-State Colloquium of the Faculty of Physics in WS 2019/2020, SS 2020 and WS 2020/2021. The detailed program can be found on the WMI webpage: http://www.wmi.badw-muenchen.de/teaching/Seminars/fkkoll.html.

© Walther-Meißner-Institute

Staff

Staff of the Walther-Meißner-Institute

Scientific Directors
Prof. Dr. Stefan Filipp
Prof. Dr. Rudolf Gross (managing director)

Deputy Director
Priv.-Doz. Dr. habil. Hans Hübl

Technical Director
Dr. Achim Marx

The deputy director, the technical director and the elected representative of the scientific staff (Dr. Matthias Opel) are members of the WMI Executive Committee and support the scientific directors in the management of WMI.

Administration/Secretary's Office
Andrea Person
Carola Siegmayer
Emel Dönertas
Martina Meven

Scientific Staff
Dr. Matthias Althammer
Dr. Andreas Baum
Priv.-Doz. Dr. habil. Frank Deppe
Prof. Dr. Andreas Erb
Dr. Kirill Fedorov
Dr. Stephan Geprägs
Prof. (apl.) Dr. habil. Rudolf Hackl
Dr. Mark Kartsovnik
Dr. Nadezhda Kukharchyk
Dr. Matthias Opel
Dr. Matti Partanen
Dr. Stefan Pogorzalek
Dr. Stefan Weichselbaumer
Priv.-Doz. Dr. habil. Mathias Weiler
M. Sc. Qiming Chen
M. Sc. Peter Eder
M. Sc. Michael Fischer
M. Sc. Luis Flacke
M. Sc. Janine Gückelhorn
M. Sc. Daniel Jost
M. Sc. Leon Koch
M. Sc. Lukas Liensberger
M. Sc. Thomas Luschmann
M. Sc. Yuki Nojiri
M. Sc. Gabriele Rager
M. Sc. Michael Renger
M. Sc. Daniel Schwienbacher
M. Sc. Malay Singh
M. Sc. Ivan Tsitsilin
M. Sc. Tobias Wimmer

Technical Staff
Peter Binkert
Thomas Brenninger, M.Sc.
Dieter Guratzsch
Astrid Habel
Dipl.-Ing. (FH) Josef Höss
Sebastian Kammerer
Jan Naundorf
Georg Nitschke
Mario Nodes
Christian Reichlmeier
Alexander Rössl
Andreas Russo
Harald Schwaiger

Assistants
Sybilla Plöderl
Maria Botta

Permanent Guests

Dr. Werner Biberacher
Prof. Dr. Dietrich Einzel
Prof. Dr. B.S. Chandrasekhar
Dr. Kurt Uhlig

© Walther-Meißner-Institute

Guest Researchers

1. Dr. Werner Biberacher
   permanent guest
2. Prof. Dr. B.S. Chandrasekhar
   permanent guest
3. Prof. Dr. Dietrich Einzel
   permanent guest
4. Dr. Kurt Uhlig
   permanent guest
5. Dr. Akashdeep Kamra, Norwegian University of Science and Technology, Trondheim, Norway.
   03. 08. - 07. 08. 2020
6. Mayank Sharma, Indian Institute of Technology (IIT), Madras, Chennai, India.
   16. 10.2020 - 31. 03. 2021
7. Dr. Johanna Fischer, Unite Mixte de Physique CNRS/Thales, Palaiseau, France.
   04. 12. - 18. 12. 2020

© Walther-Meißner-Institute

Scientific Advisory Board & Executive Committee

Scientific Advisory Board

According to the statutes of the Bavarian Academy of Sciences and Humanities (BAdW) the Scientific Advisory Board evaluates the quality of the scientific work of Walther-Meißner-Institute (WMI) and gives advice to its Executive Committee to provide scientific quality assurance. The Scientific Advisory Board regularly reports to the Research Committee of BAdW.

The members of the Scientific Advisory Board include members of BAdW with appropriate scientific background, representatives of the two Munich universities (TUM and LMU), as well as leading national and international scientists. They are appointed by the Section III "Naturwissenschaften, Mathematik, Technikwissenschaften" of BAdW for five years. The managing director of WMI is a consultive member of the WMI Scientific Advisory Board. The Scientific Advisory Board is headed by a chairperson and deputy chairperson. They are elected by the Section III "Naturwissenschaften, Mathematik, Technikwissenschaften" of BAdW for five years at the suggestion of the members of the WMI Scientific Advisory Board. The chairperson of the Scientific Advisory Board must be a member of BAdW.

The present members of the WMI Scientific Advisory Board are:

- **Vollhardt, Dieter**, chairman (BAdW, University of Augsburg)
- **Abstreiter, Gerhard**, deputy chairman (BAdW, Technical University of Munich)
- **Bloch, Immanuel** (BAdW, LMU Munich and Max-Planck-Institute of Quantum Optics)
- **Bühler-Paschen, Silke** (Technical University of Vienna)
- **Finley, Jonathan** (Technical University of Munich)
- **Gross, Rudolf**, consultive member (BAdW, Technical University of Munich)
- **Hänsch, Theodor** (BAdW, LMU Munich and Max-Planck-Institute of Quantum Optics)
- **Michael Hartmann** (FAU Erlangen-Nuremberg)
- **Laurens Molenkamp** (BAdW and University of Würzburg)
- **Wallraff, Andreas** (ETH Zurich)
- **Weiss, Dieter** (University of Regensburg)

Executive Committee

The Walther-Meißner-Institute is headed by the board of scientific directors which is responsible for the development and implementation of the research program. The scientific directors hold a full professor position at one of the Munich universities (TUM or LMU). They are appointed in a joint process of the respective university and BAdW. The scientific directors are supported by the deputy director, the technical director and an elected representative of the scientific staff. They are appointed by the Section III "Naturwissenschaften, Mathematik, Technikwissenschaften" of BAdW for five years at the suggestion of the members of the WMI Scientific Advisory Board.

The present members of the WMI Executive Committee are:

- **Filipp, Stefan**, scientific director
- **Gross, Rudolf**, scientific director (managing director)
- **Hübl, Hans**, deputy director
- **Marx, Achim**, technical director
- **Opel, Matthias**, representative of the scientific staff

© Walther-Meißner-Institute

Contact:

Walther–Meißner–Institut
Bayerische Akademie der Wissenschaften
Walther–Meißner–Str. 8
D - 85748 Garching
GERMANY

Phone: +49 – (0)89 289 14202
Fax: +49 – (0)89 289 14206
E–mail: Sekretariat@wmi.badw.de

www.wmi.badw.de

Published by:

Walther–Meißner–Institut
Walther–Meißner–Str. 8, D - 85748 Garching
December 2020